Novel Sensory Pathways for Thermosensation and Pain Under Physiological and Pathological Conditions

by

Lorraine Horwitz

A dissertation submitted in partial fulfillment
of the requirements for the degree of
Doctor of Philosophy
(Neuroscience)
In the University of Michigan
2022

Doctoral Committee:
Assistant Professor Bo Duan, Co-Chair
Professor Susan Shore, Co-Chair
Associate Professor Dawen Cai
Associate Professor Catherine Collins
Professor Gabriel Corfas

Lorraine Raquel Horwitz

lrhorw@umich.edu

ORCID: 0000-0002-9715-0026

Dedication

To mom, dad, Natalie, Nathan, mami, and the entire family. You have wanted nothing but the best for me, and I love you. To Elizabeth, you are my sister and my best friend. To Fred, my love, you are my rock. Without each of you, this body of work could not have come to fruition. And to you dear reader, may this work aid you in your scientific exploration.

Acknowledgments

I owe a great deal of thanks to many members of my community who have made this thesis possible. First, I acknowledge my mentor Dr. Bo Duan who always considered me a member of his lab, even before I joined. It has been indescribable to be your first graduate student. My scientific journey is a reflection of your mentorship, and I have deeply enjoyed seeing us both grow in each role. Your belief that hard work can overcome any difficulty has kept me pushing through the hardest moments. I wish to thank my co-mentor, Dr. Susan Shore, for welcoming me into your lab with open arms. Your mentorship and guidance is greatly appreciated. To my previous mentors, Drs. Monica Dus and Wendy Saltzman, for introducing me to the world of science and academia. Thank you to my committee members, Drs. Dawen Cai, Catherine Collins, and Gabriel Corfas for their thoughts and insights on my work and experiences. I wish to thank every member of the Duan and Shore labs, with special thanks to Calvin Wu and Mahar Fatima for not only teaching me any and every technique they could, but for the scientific discussions, unconditional support, and comradery. An additional thank you to Calvin, for taking excellent care of Speckles and Bertie without fail every single time asked, and for telling me to use the good tape.

I generated this dissertation data in collaboration with several others including Hanky Lee, Chia Chun Hor (Victor), Fred Shen, Wei Cai, Emily Pai, David Martel, Chen Li, Adam Hockley, Calvin Wu, and Lingchao Ji. I thank my mentees, Ilma Rovcanin, Tin Long Rex Fung, Danyal Raza, Mitchel Cin, Niketh Chopra, and Katherine Thorne, for

scientific assistance and allowing me to develop as a mentor. Thank you to collaborators Drs. Dawen Cai, Gabriel Corfas, Shawn Xu, and Kevin Pipe for providing intellectual, technical, and monetary support for this work. The University of Michigan has been an exemplary training environment, and I could not have asked for a better group of peers to share this journey with, including Dalia Murra, Sarah Pizzano, Amanda White, Shannon Wright, Alexa Faulkner, Dan (D.J.) Doyle, Ahmed Malik, Anthony Nastase, Jeff Zwicker, Christina May, Jenna Persons, Marina Silveira, Marie Walicki, Lauren Rystak, Alexis Vegas, Michael Selesko, Travis Riffle, Gerilyn Jones, Christina Maria Rios, Carina Castellanos, Ashley Cotes Hernandez, Jean Carlos Rodriguez Diaz and many many more. I have had the amazing opportunity to be a part of the Neuroscience Graduate Program (NGP), Kresge Hearing Research Institute (KHRI), and Molecular Cellular Developmental Biology (MCDB) department where I have developed as a scientist. David Goyer and Calvin Wu guided me in establishing stereotaxic mouse surgeries in the Duan lab; Luis Cassinoti and Lingchao Ji taught me Auditory Brainstem Response data collection and analysis; Adam Hockley, David Martel, and Deepak Dileepkumar provided technical expertise in developing the animal behavior model of hyperacusis. Thank you to the NGP, KHRI, and MCDB administrative staff: Valerie Smith, Rachel Harbach, Vicky Martin, Stella Bublitz, and Jackie Blake. The NGP has consistently evolved throughout my time at the University of Michigan and I acknowledge our current and past directors, Drs. Ed Stuenkel, Audrey Seasholtz, Leslie Satin, Arun Anantharam, and Carol Elias; as well as affiliated faculty who have always tried to improve the student experience, Drs. Shelly Flagel, Michael Roberts, Victoria Booth, Keith Duncan, and Sara Aton. Diversity, Equity, and Inclusion is vital to cultivate

a welcoming learning environment and I would like to thank each member of the Outreach and Activism DEI Task force. It was a pleasure working with you all.

Without my support system outside of the laboratory environment, this thesis would not have been possible. Thank you to Carmela Magot, Gurjot Walia, Michael Okoreeh, and Hayllens Hernandez whose friendship knows no bounds. Elizabeth Nguyen and Natalie Horwitz, my sisters, I deeply appreciate the late-night pep talks, support, and guidance you have provided over the years. Mom, dad, Nathan, mami, and my entire family, I love you forever and always. Lastly, I thank my fiancé, Fred Shen. I'm not sure how it's possible but I love you more and more each day. Thank you for returning to the lab to teach me expansion microscopy, and believing in me when I didn't believe in myself. Your steady support throughout this thesis and graduate school was a fundamental part of my experience, and the thought of starting this next chapter together is what has fueled the final push to complete this work.

Table of Contents

List of Figures

Abstract:

For this dissertation, I studied the basic coding mechanisms of a sensory system to then understand how dysregulation of sensory systems can lead to activation of nociceptive pathways even in innocuous situations. First I explored the thermosensory system under physiological conditions to appreciate the basic mechanisms for sensory transmission underlying a specific neural circuit. Specifically, I identified a population of excitatory interneurons co-expressing Caldinin1 and Lbx1 in the dorsal spinal cord that receives monosynaptic connections from TRPM8^{+} primary sensory neurons and plays a key role in the transmission of innocuous cool sensations. Next, I studied the interactions between the auditory and nociceptive systems under pathological conditions. Loud noise exposure can lead to dysregulation of the auditory system resulting is several auditory disorders such as tinnitus, hearing loss, and hyperacusis. Hyperacusis is a particularly debilitating disorder that can be classified into loudness and affective types, therefore it is important to use the appropriate animal model for each subtype of hyperacusis. Currently there are few animal models for affective hyperacusis, therefore I developed several novel animal models of affective hyperacusis. Furthermore, hyperacusis is often co-morbid with somatosensory disorders. I tested the hypothesis that the auditory system interacts with the somatosensory system and found that all mice regardless of hyperacusis status developed mechanical allodynia. These results suggests that a single auditory insult

can result in chronic changes to not just the auditory but also the somatosensory systems. Taken together, these projects aid in our understanding of sensory coding mechanisms and the role of multisensory integration in the generation of chronic pain.

Chapter 1

From the Skin to the Brain: Thermosensation Under Physiological Conditions

1.1 Introduction

Distinct sensory stimuli are precisely processed in the nervous system. Sensory organs such as the skin, tongue, ears, eyes, and nose contain specialized sensory receptors that are capable of sensing and distinguishing external stimuli. Peripheral sensory neurons transmit these external stimuli to primary relay stations in the central nervous systems for integration, then key signals are sent to higher-order brain regions for further processing. While progress has been made in identifying molecular receptors, such as thermosensors, in the periphery, the neural circuits that process somatosensory information in the central nervous system are less well defined.

The primary cells that contain sensory receptors are integral components of the sensory system, however they are often exposed to the external environment leading to cell death and loss of sensation. Nociception is a distressing feeling caused by intense or damaging stimuli which motivates the individual to withdraw from a dangerous situation, protect a damaged body part while it heals, and/or to avoid similar experiences in the future. Under physiological conditions, nociception is a critical mechanism to protect against injury. However, under pathological conditions, noxious signals are transmitted even in innocuous states.

1.2 Thermosensation is necessary for life

1.2.1 Temperature Scales

The thermodynamic definition of heat is energy transfer to or from a thermodynamic system. The common definition of heat refers to the perception of either thermal energy or temperature, which can instead be referred to as thermoception (or thermosensation). Whether the perception of temperature or the transfer of energy, it is difficult to measure heat. Robert Hooke in 1664 first proposed the freezing point of water as a zero point from which temperatures could be measured against. Ole Roemer expanded upon Hooke's freezing point by including a second reference point, the boiling point of water, to allow for two fixed points as references that could be interpolated between. These references allow us to begin to describe how "hot" or "cold" a body or material is. Throughout history, new devices have been developed to measure changes in temperatures. From the thermometer invented in 1612 by Santori Santorii, to the identification of absolute zero by Gay-Lussac and colleagues during the 19th century, our ability to measure energy transfer has greatly improved throughout the centuries (Oyebola and Odueso, 2017). However, our understanding of the neurobiological underpinnings that are responsible for the perception of heat has been less well studied.

The establishment of temperature scales was an important advancement towards investigating our perception of diverse temperature ranges. In 1714, Daniel Gabriel Fahrenheit invented the first widely used, practical, and accurate thermometer, the mercury-in-glass thermometer. During this time, Fahrenheit realized the necessity of a temperature scale and developed the first standardized temperature scale to be

widely used, the Fahrenheit scale. For this scale, the freezing point of pure water was set at 32 degrees Fahrenheit (°F) and the boiling point of pure water was set at 212 °F at sea-level atmospheric pressure. In 1742, the Swedish physicist Anders Celsius proposed the Centigrade temperature scale, which defined the freezing point of water as 0 °C and the boiling point of water as 100 °C. This 100-degree interval “centigrade scale” is currently used most often around the world. Expanding upon the centigrade scale, the Kelvin scale developed by William Thomson and Lord Kelvin, uses absolute zero as the starting point and is often used in the field of physical science (Oyebola and Odueso, 2017). The introduction of these various temperature scales continues to be expanded upon, and are fundamental in our study of thermoception.

Thermoception begins when an organism receives a temperature stimulus which is transduced by thermosensors into electrical signals that are then transmitted to the brain for further processing. The introduction of temperature scales allowed for the standardization of distinct thermosensory perceptions in relation to temperature intensity. In humans, when the skin is cooled to temperatures ranging from 15-20 °C the sensation is described as ‘cool’ (referred to as innocuous cool) (Chen et al. 1996; Croze and Duclaux 1978; Stevens 1979; Greenspan et al. 1993). Further temperature reduction can evoke a painful sensation described as ‘pricking’, ‘burning’, or ‘aching’ (referred to as noxious cold) (Chen et al. 1996; Wolf and Hardy 1941; Kunkle 1949; Chery-Croze and Duclaux 1980; Chery-Croze 1983; Yarnitsky and Ochoa 1990; Morin et al. 1994). Warm sensations generally fall between 35-43 °C (referred to as innocuous warmth) (Palkar et al., 2015; Green 2009, Nagy and Rang 1999; Treede et al., 1995), although some studies attribute warm temperature sensations up to 45 °C (Craig et al.,

2001). Temperatures above 45 °C are reported as painful (referred to as noxious heat) (Hallin et al., 1981). Noxious cold, innocuous cool, and thermal heat sensing are distinct evolutionarily-conserved sensory modalities that work together to maintain homeostasis, with noxious cold and noxious heat playing an additional role to protect against tissue damage and future injury.

1.2.2 The Role of Thermoception in Thermoregulation

Thermoception is an essential component of thermoregulation, the tightly controlled self-regulation mechanism by which mammals maintain their core internal body temperature (homeostasis). Although the body can sense and detect stimuli across the temperature spectrum, a healthy internal body temperature lies within a very select temperature window. Humans for example have an average body temperature that falls between 37.0-37.8 °C. Unlike ectotherms which do not have an internal body temperature regulation mechanism, endotherms such as mammals do not dependent upon the external environmental temperature for homeostasis. However, body temperature regulation in mammals is still affected by several factors including the external environmental temperature, circadian rhythm, and menses. For example, an extremely cold or extremely hot environment will disrupt the body's ability to thermoregulate leading to hypothermia (being too cold) or hyperthermia (overheating) respectively. Although mammals can survive at temperatures outside of the ideal internal body temperature zone, the biological function of the organism is greatly affected and will eventually lead to detrimental (brain damage, internal organ failure, etc) and eventually fatal outcomes. Therefore, the ability to accurately detect and

appropriately respond to external environmental stimuli is an essential component of thermoregulation and life.

Thermoregulation has three central components: thermoception (afferent sensing), central control (integration with the current biological status of the animal), and efferent responses to produce appropriate behavioral outputs. Thermosensors for heat and cold are distributed throughout the body to determine if the core body temperature is too hot or too cold. While the central control component of thermoregulation in the brain and peripheral nervous system has been well studied, the detection and integration of external sensory signals in the spinal cord is not well understood. In this introductory chapter to thermosensation under physiological conditions, I will first describe the relatively little we know about thermoception and sensory signal transmission in both vertebrate and invertebrate models, then discuss our current understanding of the central control mechanisms for thermoregulation in the brain.

1.3 Temperature Coding Mechanisms Across Phylum

1.3.1 Temperature Detection in Invertebrate Model Organisms

Temperature detection is observed in both vertebrates and invertebrates. Because ectotherms, such as invertebrates, cannot regulate their internal body temperature, it is essential for their survival to detect external environmental temperatures to remove themselves from deadly situations. The nematode *Caenorhabditis elegans (C. elegans)* and the fruit fly *(Drosophila Melanogaster)* are able to detect external environmental temperature cues. *C. elegans* are able to sense the temperature environment on which a particular food source is located then navigate

towards the previous cultivation temperature when placed on a temperature gradient in the absences of food (Hedgecock and Russell 1975). Concurrently, *C. elegans* deprived of food at a particular temperature environment are able to navigate away from the aversive temperature zone in subsequent trials (Mohri et al., 2005). *C. elegens* also exhibit a nocifensive-like aversive withdrawal response to temperatures near 33 °C, a stereotypical thermal avoidance behavior that has been utilized to study noxious heat thermoception (Wittenburg and Baumeister 1999). *Drosophila* are another useful thermoception model as they exhibit a selective temperature preference for 24 °C when placed on a temperature gradient (McKemy 2007; Sayeed and Benzer 1996) and a stereotypical nocifensive-like withdrawal response to noxious heat (Tracey et al 2003; Kernan et al., 1994). The use of simplistic model organisms such as *Drosophila* and *C. elegenas* enables easy genetic manipulation of neuronal circuits, and has lead to the identification of several temperature-responsive sensory neurons (Liu et al., 2012; Saro et al., 2020).

1.3.2 Coding of Absolute Temperatures and Temperature Changes

How temperature is encoded in the nervous system is an age-old question that has adapted and changed throughout time. In the 1800s, Weber proposed a theory that thermosensory neurons encode temperature change rather than absolute temperature information in humans. Evidence to the contrary exists, such as the aftersensation of cold experienced by the skin even once a cold object has been removed. In 1950, Hensel and Zotterman recorded from cold receptors in the skin of cats and showed not only burst firing response to cooling (temperature change encoding neurons), but also

stable activity responses to sustained cold stimuli (absolute cold encoding neurons) demonstrating the existence of both temperature change and absolute temperature encoding neurons. Since then, numerous studies have worked towards characterizing temperature-responsive peripheral sensory neurons. Electrophysiological recordings performed in mice, cats, and primates combined with human psychophysical studies have been used to classify peripheral sensory neuron types that encode distinct temperature information. The identification of Transient Receptor Potential Channels (TRP channels) (see TRP Channels section below) and subsequent temperature sensitive thermoTRP channels, was a major breakthrough in understanding how external temperatures are detected and transmitted by peripheral thermosensory neurons. Despite recent advances in genetic, molecular, and viral techniques used to dissect neural circuits for temperature transmission, the coding of temperature in the central nervous system is complex and much remains unknown. The use of a variety of model organisms has begun to allow for the precise genetic, molecular, and physiological dissection of thermosensory neural circuits.

Since the Hensel and Zotterman's landmark electrophysiological experiments, several studies have been performed in support of Hensel and Zotterman's view of temperature change and absolute temperature encoding neurons. In *Drosophila*, the modified apical or subapical bristle arising from the last antennal segment is called the arista and contains receptors that respond to absolute temperatures and rapid temperature changes. Each arista contains three thermosensory sensilla, each containing a cold activated and a hot activated antennal thermosensory receptor neuron (TRN) (Gallio et al., 2011). TRNs generally have a preferential temperature range that

they respond to with increasing activity across stimulus intensity. TRNs can be further classified into cell types based upon their differential response dynamics to temperature stimuli into either “fast-adapting” cells that exhibit a fast but brief response to the onset of temperature changes, and “slow non-adapting” TPNs which exhibit sustained activity (Alpert et al., 2020; Frank et al., 2015; Liu et al 2015; Gallio et al., 2011). Hot and cold temperature TRNs synapse onto second order thermosensory projection neurons (TPN) that converge in the posterior antennal lobe of the drosophila brain. There are two identified types of TPNs, fast-adapting TPN-Is (temperature change neurons) and initial bursting TPN-IIs which produce an initial calcium spike at cooling onset then rapidly decreases to a plateau (Alpert et al., 2020). TPN-IIs encode absolute temperature in the cold-range, and synapse onto DN1a Dorsal Neurons of the Drosophila Circadian Clock Network to shut down the activity of clock-regulated activity rhythms resulting in prolonged sleep in cold conditions. Absolute and temperature change encoding neurons have also been found in *C. elegans* (Hawk et al., 2018; Clark et al; 2006; Ippolito et al., 2021), along with neural circuits to control temperature-dependent navigation (Matsuyama et al 2020). Homologous temperature coding mechanisms to those found in *C elegans* and *Drosophila* may be present in mammals, as well as evolutionarily conserved mechanisms for cross-talk between distinct sensory systems.

Drosophila and *C. elegans* have proven invaluable in facilitating our understanding of basic temperature coding mechanisms, however they lack the ability to precisely differentiate thermosensory perception between noxious and innocuous temperatures. Innocuous temperatures such as cool and warmth can generate pleasant or aversive sensations dependent upon the context (i.e. a cool breeze on a warm

summer day is pleasant whereas a cool breeze on a rainy afternoon is aversive). Noxious temperatures (above 45 °C or below 15 °C) elicit strong aversive sensations similar to those evoked by other noxious stimuli (such as sharp mechanical pain or chemical compounds such as capsaicin). While invertebrates such as *Drosophila* and *C. elegans* display robust thermotaxic avoidance behaviors to temperatures above or below their preferred temperature range, their ability to differentiate between innocuous and noxious stimuli has not been shown. Mammals exhibit distinct behavioral readouts to innocuous warmth and innocuous cool compared to noxious cold and noxious heat, therefore vertebrate studies are ideal for understanding how innocuous and noxious sensations are encoded.

1.3.3 The Mammalian Peripheral Nervous System

In mammals, pseudo-unipolar peripheral sensory neurons contain a single axon divided into two branches. One branch innervates peripheral tissues including the skin, mucosa, and internal organs (Vriens et al. 2014), while the second branch synapses onto second-order neurons of the spinal cord. The cell bodies of peripheral sensory neurons are housed in the dorsal root ganglia or trigeminal ganglia and innervate the body and face respectively. Peripheral sensory neurons can be classified based on the presence of myelin, diameter size, firing pattern, conduction velocity, threshold for activation, molecular markers, and the stimuli that they respond to. Classically, nociceptive peripheral sensory neurons have been categorized into two main types, medium diameter myelinated Aδ fibers (fast pain) and small diameter unmyelinated C fibers (slow pain). Medium diameter myelinated Aβ fibers respond to innocuous

mechanical stimulation and large diameter Aα mechanosensitive fibers which innervate the muscles to transmit proprioceptive information have also been classified. Aδ nociceptors can be further classified as either low- or high- threshold mechanoreceptors depending upon the threshold of stimulus intensity necessary to produce a response. Heterogeneous unmyelinated C fibers contain subpopulations for different sensations such as polymodal heat- and mechano- sensitive neurons or heat-sensitive mechano-insensitive neurons which may play a role in the development of mechanical allodynia. Furthermore, unmyelinated C-fibers are not always nociceptors, with some subpopulations only responding to cooling or innocuous touch but not chemical or heat stimulation (Olausson et al., 2008; Basbaum et al., 2009).

Various electrophysiological studies have identified of distinct populations of thermo-sensitive peripheral sensory neurons. At a thermoneutral skin temperature (33 °C), cool temperature-sensitive neurons display a spontaneous firing rate that increases upon presentation of a cool stimulus and reduced activity to warm temperatures (Campero et al., 2009; Hensel 1976; McKemy 2013; Vriens et al., 2014). Warm temperature-sensitive neurons similarly display an increased firing rate as temperature increases and reduced activity at cool temperatures (Zimmermann et al., 2009; Hensel and Iggo 1971; Campero et al., 2009; LaMotte and Campbell 1978). Polymodal noxious cold and noxious heat nociceptors are activated at temperature extremes (<15 °C and >45 °C respectively), and respond to noxious temperatures, severe mechanical stimulation, and chemical irritants such as capsaicin (McKemy 2007; Nagy and Rang 1999; Treede et al., 1995). Various fiber type for these temperature-sensitive neurons have been suggested, however their precise molecular identities are not well

understood (Dodt 1952). Additional molecular markers or thermo-sensory channels (see TRP channels below) may be useful for further defining these populations (Takashima et al., 2007; Dhaka et al., 2008).

1.3.4 Thermo-sensitive Neurons in the Dorsal Spinal Cord

The spinal cord receives input from the peripheral nervous system and acts as the first site of somatosensory information integration. Aδ and C nociceptive thermosensory fibers synapse onto neurons in laminae I, II, and V of the dorsal horn of the spinal cord (Basbaum et al. 2009). A large number excitatory (glutamatergic) or inhibitory (glycinergic or γ-aminobutric acid referred to as GABA -ergic) interneurons are located in the dorsal horn of the spinal cord (Todd 2010). Interneurons regulate transmission of somatosensory information to either motor neurons of the ventral horn to produce protective reflexive withdrawal movements (Vriens et al. 2014) or to projection neurons. Projection neurons located in lamina I and V of the dorsal horn of the spinal cord project through the spinoparabrachial (also referred to as the spinoreticulothalamic tract) and spinothalamic tract to different areas of the brain for further processing (Basbaum et al. 2009; Vriens et al., 2014). While lamina I projection neurons have been shown to receive monosynaptic connections from the DRG (Grudt and Perl, 2002) and from interneurons in lamina I and II (Luz et al., 2010), the coding mechanisms (inputs or temperature classification) has not characterized, and the role and molecular identity of local dorsal spinal interneurons in integrating temperature information to projection neurons remains unknown.

In 1970, Christensen and Perl first described cool-sensitive neurons in the superficial lamina of the dorsal horn. Although several electrophysiological studies have investigated the representation of temperature information in the spinal cord, considerable heterogeneity in responses to thermal and mechanical stimulation were observed and much remains unknown about the spinal coding mechanisms for thermoception (Andew and Craig 2001; Bester et al., 2000; Burton 1975; Craig et al 2001; Ran et al 2016). Recent calcium imaging experiments have begun to unravel the coding mechanisms of thermal sensations in the spinal cord. In the DRG and dorsal horn, heat sensitive neurons encode absolute temperatures in a graded population response, whereas cool-sensitive neurons are activated by relative temperature changes (Wang et al 2018, Ran et al 2016). These studies demonstrate that at an individual level, certain cells may be able to encode warm-hot temperatures based on their activity level, however cool-cold temperatures transmission is dependent upon patterns of cells activated at a population level. To delineate cell-type specific clusters of sensory neurons, several recent single cell RNA-sequencing studies of dorsal horn spinal cord neurons have been performed (Haring et al., 2018; Sathyamurthy et al., 2018; Russ et al., 2020). One study by Haring et al., performed single cell RNA-sequencing to identify clusters then validated several excitatory and inhibitory neuronal populations activated after noxious heat and noxious cold exposure *in vivo*. However, the precise cellular and molecular identities, micro-circuits, and mechanism of integration of peripheral inputs for temperature sensing in the spinal cord, especially at innocuous temperatures, remains unknown. Additional studies are necessary for a more complete understanding of spinal thermo-circuitry.

1.3.5 Innocuous and Noxious Temperature Coding

The coding mechanism of innocuous versus noxious stimuli has been hotly debated over the past century. The law of specific nerve energies proposed by Johannes Peter Muller in 1835 and refined by studies from Roger Sperry in 1945, postulates that the pathway that carries sensory information, not the stimuli itself, defines the nature of perception (Norrsell et al., 1999; Sperry; 1945). This theory for the first time decoupled a stimulus from perception, stating that it is not the origin of the sensation, such as a smell or sound, but rather the different nervous structures that these stimuli excite that drives sensation. Scientists then debated whether the same neurons activated by innocuous stimuli also transmits nociceptive signals once the intensity of the stimulus passed a certain threshold, or if separate sensory systems exist to differentiate between innocuous and noxious stimuli (Dubner et al.1978; Moayedi and Davis 2013; Collins et al. 1960, Torebjork 1985). These ideas have morphed into theories called pattern coding and labeled-line respectively. In 1965 Melzack and Wall attempted to reconcile these viewpoints by proposing the gate control theory of pain. For this theory, both nociceptive (C and Aδ) and innocuous mechanical touch (Aβ) fibers exist, each of which synapse onto both inhibitory cells within the substantia gelatinosa and pain transmission cells in the dorsal horn of the spinal cord. When the predominant input onto the inhibitory neurons is from touch fibers, the inhibitory neurons “gate” or inhibit the pain transmission neurons. However, when noxious fibers are activated upon presentation of a noxious stimulus, the inhibitory neurons are silenced, thereby releasing the gate and allowing for pain transmission to the brain for the perception of pain (Melzack and Wall, 1965, 1978). Since then, many studies have supported the

gate control theory of pain (Duan et al 2014; Pan et al 2019; Braz et a., 2014; Mendell, 2014; Prescott et al., 2014; Zeihofer et al., 2012; Sandkuhler, 2009; Price et al., 2009; Torsney and MacDermott, 2006; Baba et al., 2003; Lu et al., 2013; Miraucourt et al., 2007), while may aid in our understanding of innocuous and noxious temperature coding.

In 1896 Torsten Thunberg first demonstrated the thermal grill illusion, in which a grill interlaced with warm and cool bars (40 °C and 20 °C respectively) is perceived as a burning heat when the hand is placed flat against the grill (exposed to both warmth and cool), but as either warmth or cool when the hand is pressed against only the warm or cool bars respectively (Bach et al., 2011). The sensation can be adjusted to produce sensations ranging from warm to hot, and when pain is experienced, from mild to moderate (Bouhassira et al., 2005; Craig and Bushnell, 1994; Leung et al., 2005), (with the difference between warm and cool temperatures primarily driving this perception (Burnett and Dallenback, 1928; Gritman and Dallenback 1929). An adaptation of the gate theory of pain would suggest that warm peripheral sensory neurons may block an inhibitory gating pathway normally activated by innocuous cool fibers, allowing for the transmission of warmth and noxious heat (Ma 2010). Alternative theories have been proposed (Fardo et al., 2020), demonstrating the importance of such psychophysical human studies throughout history in developing theories of somatosensory (specifically thermosensory) coding.

1.4 TRP Channels

Thermosensation begins at the interface between the environment and the skin. External temperatures are first detected in the skin by thermal sensors expressed in primary sensory neurons whose cell bodies are housed in the dorsal root ganglia (DRG). Neurons of the peripheral nervous system signal the dorsal horn of the spinal cord for somatosensory integration. Over the past decade, intensive studies have classified distinct populations of peripheral neurons that transmit distinct noxious and innocuous temperature information.

Several members of the transient receptor potential (TRP) ion channel family have been classified as thermal sensors in mammals based on their ability to respond to a variety of stimuli ranging from noxious heat to innocuous cool. These thermoTRP channels are from the TRPA(TRPA1), TRPV(TRPV1-TRPV4), TRPC (TRPC5), and TRPM (TRPM2-TRPM5 and TRPM8) subfamilies, and most are cation permeable, non-selective channels. ThermoTRP channels are unique due to their ability to open in response to temperature change. ThermoTRP channels have been most extensively studied in mice and Figures 1.3 and 1.4 demonstrate their activation ranges by temperature. In humans, thermoTRP channels are present in the brain, peripheral nervous system, skin, cardiovascular system, renal system, liver, pulmonary system, digestive system, and reproductive system, however their function is not well understood. Various disorders in humans have been linked to thermoTRP channels, therefore they present as a likely target for therapeutic intervention.

In mammals, TRPV1 and TRPM3 channels are activated at hot temperatures (above 40 °C) (Caterina et al., 1997; Vriens et al., 2011; Vandewauw et al., 2018;

Yarmolinsky et al., 2016; Liu et al 2003), while TRPM2 is activated at warm temperatures (above 27 °C)(Figure 1.3)(Tan and McNaughton 2016; Xu et al., 2002; Guler et al., 2002; Huang et al., 2011; Togashi et al., 2006; Song et al., 2016). Although not a TRP channel, STIM1 has also been identified as a warmth sensor in skin keratinocytes (Liu et al., 2019). TRPM8, and TRPA1 have been suggested as cold receptors (Figure 1.4). While the structural biology of thermoTRP channels has been well classified, their distinctive range of activation temperatures, especially cold temperatures, under physiological conditions vary greatly depending on the species. For example, TRPA1 was the first proposed cold sensory channel, but in vivo experiments in mammals revealed that TRPA1 is actually activated by temperature increase from an intermediate start point (i.e. 17 °C), and the TRPA1 temperature sensitivity changes across phylogeny. Furthermore, several additional thermoTRP channels have been identified *in vitro*, however they have been functionally invalidated *in vivo* in mammals (TRPV2, TRPV3, TRPV4, TRPM4, and TRPC5) (Xiao and Xu, 2021; Xu et al., 2002; Guler et al., 2002; Huang et al., 2011; Zimmermann et al., 2011; Yao et al., 2011; Park et al., 2011; Talavera et al., 2005).

1.4.1 TRP8 Transmits Innocuous Cool Temperature Information

TRPM8 is activated at cool temperatures (below 28 °C) and by the exogenous chemical agonists, menthol and icillin, which elicit a cooling sensation in humans. TRPM8 is expressed endogenously in a subpopulation of small-diameter neurons of the dorsal root ganglion and trigeminal ganglion (Dhaka et al., 2008; Takashima et al., 2010). Spinal responses to mild cooling were abolished after selective ablation of

TRPM8 expressing sensory neurons, confirming the role of TRPM8 in innocuous cool sensing. In the temperature preference test, TRPM8 knockout mice show robust responses to noxious cold but abolished responses to the innocuous cool range (15-25 °C), suggesting TRPM8 is responsible for innocuous, not noxious cold transmission (Bautista et al., 2007; Dhaka et al., 2007). Interestingly, a greater deficit in cold sensitivity is observed in $TRPM8^{+}$ neurons-ablated animals compared to TRPM8 knockout animals (Knowlton et al., 2013; Pogorzala et al., 2013), suggesting a TRPM8-independent cold sensor must exist in vertebrates. Recently, Gong et al. demonstrated that GLR-3, the mouse homolog of GluK2, mediates cold sensations in the DRG of mice. Therefore, TRPM8 transmits innocuous cool temperatures, while GluK2 mediates cold sensations in the peripheral nervous system.

1.5 Spinal Nociceptive and Thermo-sensitive Projection Neurons

1.5.1 Pain and Projection Neurons

The sensation of pain is comprised of two key components, the sensory discrimination component and the effective emotional component (Melzack and Casey 1968; Groh et al., 2018). The sensory discrimination component of pain encodes information pertaining to the stimulus itself, such as the intensity, duration, and location. The effective emotional component of pain is usually aversive and drives behavioral responses to avoid the noxious stimulus and form memories to prevent future painful situations (Figure 1.1) (Basbaum et al., 2009).

Projection neurons in laminae I and V of the dorsal horn of the spinal cord transmit somatosensory information to the brain via the spinothalamic tract (STT) and

spinoparabrachial tract (SPB) (Basbaum et al. 2009; Vriens et al., 2014; Basbaum and Jessell, 2000; Cechetto et al 1985; Nakamura and Morrison 2008). Relatively little in known of lamina V projection neurons, whereas lamina I projection neurons have been better described (Wercberger and Basbaum, 2019) The spinothalamic tract and the orofacial equivalent trigeminothalamic tract, transmit noxious somatosensory information from the dorsal horn or spinal trigeminal nucleus respectively, to specific nuclei of the thalamus then to cortical structures. The lateral thalamic nuclei, including the ventroposterior lateral thalamus (VPL), targets primarily somatosensory cortices, such as the primary somatosensory cortex (S1) for the sensory discrimination component of pain (Figure 1.1) (Groh et al., 2018; Basbaum et al. 2009).

The spinoparabrachial tract synapses onto neurons in the lateral parabrachial nucleus of the brainstem. Pain information is relayed by projection neurons in the medial thalamus and parabrachial nucleus to the amygdala, and subsequently to the insular cortex, hippocampus, medial prefontal cortex, anterior insular cortex, and anterior cingulate cortex for emotional aspects of pain including aversion and discomfort (Figure 1.1) (Abraira et al., 2013; Basbaum et al., 2009; Vogt 2005; Bushnel et al., 2013). Local brain network activation rather than a single brain area is necessary for pain (Apkarian et al., 2005). Similar to pain, the insula, prefontal cortex, amygdala, cingulate and cingulate gyrus are activated after innocuous thermal stimuli is presented to the skin (Davis et al., 1998; Kanosue et al., 2002).

1.5.2 Spinothalamic Projection Neurons

Lamina I spinothalamic project neurons in the dorsal horn of the spinal cord have been classified into three different types: nociceptive-specific (NS), innocuous cool (COOL) or warm (WARM) thermo-sensing, and polymodal nociceptive noxious heat, pinch, and noxious cold (HPC) neurons, with distinct physiological and morphological properties (Craig et al., in 2001). Although there are some discrepancies in the presence of innocuous warm-specific spinothalamic projection neurons, innocuous-cool-responsive spinothalamic projection neurons have been identified in both the cat and monkey (Dostrovsky and Craig 1996; Criag et al., 2001; Andrew and Craig 2001). Similar to pain, the spinothalamocortical tract transmits the thermosensory discrimination component of cutaneous temperatures (Craig et al.,1994; Craig 2002), however this pathway is not necessary for homeostatic, autonomic, or behavioral responses to changes in skin temperature (Nakamura and Morrison 2008; Nakamura and Morrison 2010; Yahiro et al., 2017). The target of spinothalamic projection neurons in the ventroposterior lateral thalamus are predicted to encode sensory discrimination properties of the noxious stimulus. Indeed, studies have shown that the majority of ventroposterior lateral neurons respond to heat or mechanical stimulation in a graded manner corresponding to the intensity of the stimulus, with lower firing rates at innocuous levels and higher firing rate activity at noxious stimulus intensities (Groh et al., 2018; Kenshalo et al., 1980; Bordi and Quartaroli, 2000; Martin et al., 1996; Abdul Aziz et al., 2005).

1.5.3 Spinoparabrachial Projection Neurons

Although projection neurons in the superficial lamina of the dorsal horn were originally classified through their projects to the thalamus, it has since been discovered that 85-95% of lamina I projection neurons project to the lateral parabrachial nucleus (Cameron et al., 2015; McMahon and Wall, 1983; Polgar et al., 2010; Spike et al., 2003; Todd, 2010), with 80-97% of lamina I spinothalamic projection neurons also synapsing in the parabrachial nucleus (Al-Khater and Todd, 2009; Hylden et al., 1989). Nociceptive-specific and polymodal noxious heat, pinch, noxious cold responsive lamina I spinoparabrachial projection neurons, similar to spinothalamic projection neurons, have been identified (Chisholm et al., 2021; Hachisuka et al., 2020). Interestingly, Chisholm identified a unique subgroup of innocuous cool-specific spinoparabrachial projection neurons active at stable cold temperatures, suggesting the presence of absolute temperature encoding spinoparabrachial projection neurons specific for innocuous cool sensations. Alternatively, in agreement with previous calcium imaging studies in the dorsal root ganglia and dorsal horn (Ran et al., 2016; Wang et al., 2018), heating-responsive neurons encoded relative temperature changes (Chisholm et al., 2021).

Why the lateral parabrachial nucleus? The lateral parabrachial nucleus has several subnuclei, each containing neurons implicated in different aspects of homeostasis such as thermoregulation, cardiovascular function as well as feeding, thirst, and salt appetite (Tan and Knight 2018; Davern, 2014). The lateral parabrachial nucleus has two anatomically distinct subnuclei that receive cool (external lateral subdivision of the lateral parabrachial nucleus) and warm (dorsal subdivision of the

lateral parabrachial nucleus) signals. Each subnuclei contains neurons that are activated by their respective cool (LPBel) or warm inputs (dLPB) (Geerling et al., 2016; Bratincsak and Palkovits, 2004; Madden and Morrison, 2019; Bratincsak and Palkovits 2004; Nakamura and Morrison 2010; Nakamura and Morrison, 2008) and are necessary for various aspects of thermoregulation (Kobayashi and Osaka 2003, Nakamura and Morrison 2010; Nakamura and Morrison, 2008). Inhibition of lateral parabrachial nuclei neurons suppresses metabolic, cardiac, autonomic, and thermogenic responses to skin cooling and alters temperature preference in behavior assays, whereas activation of lateral parabrachial neurons parallels physiological response to skin cooling-evoked including increases in sympathetic nerve activity to thermogenic brown adipose tissue (Kobayashi and Osaka, 2003; Nakamura and Morrison, 2008; Nakamura and Morrison 2010; Yahiro et al., 2017).

The lateral parabrachial nucleus projects to various brain structures including the preoptic area (POA) (Figure 1.2), paraventricular hypothalamic nucleus (PVH), bed nucleus of the stria terminalis (BST), and dorsomedial hypothalamus (DMH) (Saper and Loewy 1980; Fulwiler and Saper 1984; Krukoff et al., 1993; Bester et al., 1997). Terminals of temperature-responsive dorsal spinoparabrachial projection neurons are located within close proximity of lateral parabrachial neurons projecting to the POA (LPB-POA). The POA located in the rostral pole of the hypothalamus is the thermoregulatory command center of the brain and provides descending efferent feedback to evoke behavioral, hormonal, autonomic, and somatic responses to maintain homeostasis. Noxious cold (4 °C)-activated neurons in the external lateral and central lateral subnuclei of the parabrachial nucleus and not the dorsal lateral or medial

subnuclei of parabrachial nucleus, project to the POA. Warm (36 °C)-activated neurons in the dorsal subnuclei and not the external lateral, central lateral, or medial lateral subnuclei of the parabrachial nucleus, also project to the POA (Nakamura and Morrison 2008; Nakamura and Morison 2010). LPB-POA neurons increase their firing rate in response to skin cooling, which is rapidly reversed upon skin-rewarming. Therefore, the thermosensory spinal-LPB-POA afferent pathway, not the spinothalamic system, is necessary for appropriate behavioral and autonomic thermoregulatory responses.

1.6 Temperature Coding in the Brain

1.6.1 The Lateral Parabrachial Nucleus in Thermosensory Integration

Endotherms use a variety of involuntary autonomic (i.e. shivering, vasomotion in blood vessels, and sweating) and voluntary (i.e. fluid intake and shelter-seeking) behaviors to maintain homeostasis. Thermosensory neurons innervate both the skin and visceral internal organs to monitor the body's energy needs. The spinothalamic tract transmits the sensory component of thermosensory information whereas the spinoparabrachial tract innervates the lateral parabrachial nucleus for the behavioral and autonomic components of thermosensation and thermoregulation (Figure 1.2). Visceral afferent thermosensory information is sent to the lateral parabrachial nucleus through the nucleus of the solitary tract (Saper, 2002). The lateral parabrachial nucleus integrates both visceral and somatosensory information and plays a role in the autonomic, cardia, metabolic, somatic, hormonal, and behavioral components of thermoregulation (Nakamura and Morrison 2008). The POA is the central homeostatic regulatory control center of the brain and receives direct projections from the lateral

parabrachial nucleus (Figure 1.2) (Nakamura and Morrison 2008). The lateral parabrachial nucleus has axonal branches that spread to several brain regions besides POA including the paraventricular hypothalamic nucleus (PVH), bed nucleus of the stria terminalis (BST), and dorsomedial hypothalamus (DMH)(Saper and Loewy 1980; Fulwiler and Saper 1984; Krukoff et al., 1993; Bester et al., 1997), and may directly provide thermosensory information to these regions for efferent thermoregulatory signaling (Nakamura and Morrison 2007; Nakamura et al., 2002; Madden and Morrison 2003; Zaretskaia et al., 2003; Madden and Morrison 2004; Nakamura 2004; Nakamura et al., 2005; Nakamura et al., 2005), although further studies would be helpful in elucidating the importance of these additional projection pathways in thermoregulation.

1.6.2 The Thermoregulatory Role of the Preoptic Area of the Anterior Hypothalamus

In 1938 Magoun et al., first described temperature-sensitive neurons in the preoptic area of the anterior hypothalamus (POA). Next, several studies worked to characterize the proportion of neurons that are warm-sensitive (30%), cold-sensitive (10%) or are temperature-insensitive (60%) in the POA (Boulant and Dean, 1986). Since these early studies, the POA has been shown to be necessary for thermoregulation. The POA ensures a steady internal temperature throughout prolonged periods of extreme hot or cold circumstances, exercise, the circadian cycle, ingestion of hot or cold fluids, and pathogen-induced fever (Nakamura, 2011; Refinetti and Menaker, 1992). Additionally, the POA controls the central efferent pathway for thermogenesis in brown adipose tissue in response to innocuous cooling cutaneous

tissue to regulate body temperature (Figure 1.2) (Nakamura and Morrison 2007; Hori et al., 1988; Morrison 2004). Alternatively, tonically active inhibitory projections from the POA to the DMH and rostral medullary raphe have been shown and are important in suppressing efferent thermogenic pathways when they are not needed to maintain homeostasis (Nagashima et al., 2000; Nakamura and Morrison 2007; Nakamura et al., 2005).

In 1965, Hammel prosed the set-point model of thermoregulation in which a synaptic network comprised of four different hypothalamic neurons: warm-sensitive neurons, temperature-insensitive neurons, heat loss effector neurons, and cold-sensitive heat production effector neurons (Hammel, 1965). In this model, warm-sensitive hypothalamic neurons receive and integrate visceral and peripheral thermal temperature information, then activate heat loss effector neurons and inhibit cold-sensitive heat production effector neurons to maintain homeostasis through an efferent pathway.

Several studies have tested key components of the set-point theory. In 2019, Wang et al. identified genetic markers for warm-sensitive POA neurons *(Ptgds*) and a negative feedback circuit that regulates body temperature (Duan and Xu, 2019; Wang et al., 2019). *Ptgds*-expressing warm-sensitive neurons produce lipocalin-type PGD2 synthase (L-PGDS) that generate the prostalganding PGD_2 in fever-like conditions. *Ptgds*-expressing POA neurons directly innervate and activate neurons of the ventral medial POA (vMPOA) expressing the PGD_2 receptor, DP1, which co-localizes with BDNF and PACAP, a marker for ambient-temperature-elevation-responsive neurons that may act as the heat loss effector neurons Hammel predicted. Recently, the TRPM2

channel was found in the hypothalamus to monitor internal body temperature (Song et al., 2016), however molecular markers for cold-sensitive heat production effector neurons for the set-point model have yet to be described.

1.6.3 Overview of Thermoregulatory System

The core body temperature of an animal is maintained through a combination of feedback and feedforward mechanisms (Morrison and Nakamura, 2019; Werner, 2010; Romanovsky, 2004; Kanosue et al., 2010). The afferent thermosensory system begins when cold and warm thermosensory signals are detected in the skin, then continues as temperature information is transmitted through the dorsal horn to the lateral parabrachial nucleus then to the POA. The POA integrates hot and cold temperature information, taking into consideration the current core body temperature to signal the efferent thermoregulatory system to maintain homeostasis. The POA controls parallel sympathetic and somatic efferent pathways to modulated brown adipose tissue thermogenesis, shivering, cutaneous vasoconstriction and vasodilation, and thermoeffector efferent circuits to maintain homeostasis (Figures 1.1, 1.3, and 1.4) (Morrison and Nakamura; 2019).

Figures

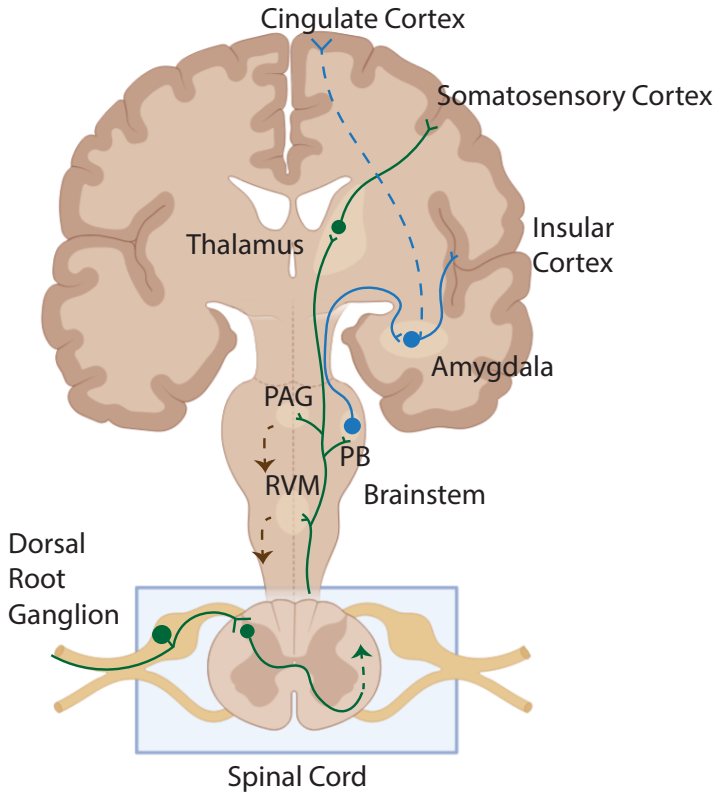

1.1 Overview of the Pain Pathway

Pseudo-unipolar primary afferent nociceptors detect noxious environmental stimuli and transmit noxious information to local interneurons and ascending projections neurons of the dorsal horn of the spinal cord. Projection neurons relay information through two major asending pathways to the brain, the spinothalamic and spinoparabrachial tracts. The spinothalamic pathway projections to neurons of the thalamus which provides information to the somatosensory cortex for the intensity discrimination components of the painful stimulus (such as the location and intensity). The spinoparabrachial pathway directly synapses onto neurons of the amygdala, and engages the cingulate and insular cortices through indirect connections, contributing to the affective component of the pain. Collateral ascending information is also transmitted to the rostral ventral medulla and midbrain periaqueductal grey and engaging the efferent system to regulate spinal cord output. Abbreviatsion: RVM: Rostral ventral medulla; PB: Parabrachial nucleus; PAG: Periaqueductal grey. Figure source data and legend adapted from: Basbaum et al., (2009) Cell. Schematic Image was created with BioRender.com

1.2 Ascending Neural Pathways that Transmit Warm and Cool Signals from the Periphery

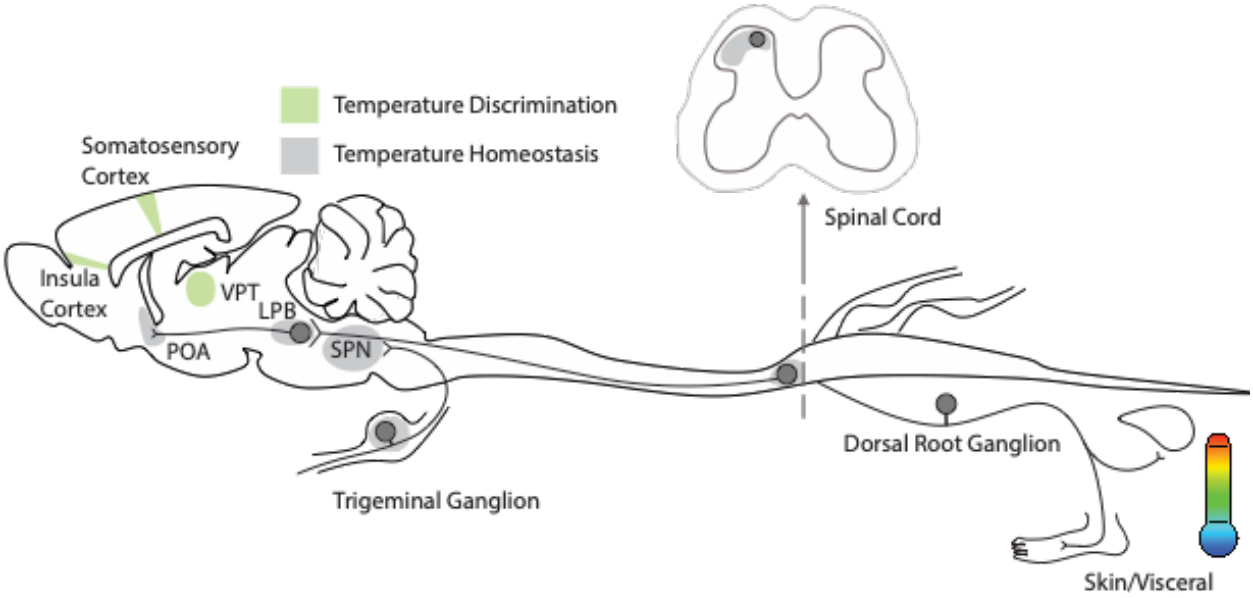

Primary sensory neurons of the dorsal root ganglion (or trigeminal ganglion) detect temperature information in the skin and/or visceral organs, then transmit this information to neurons of the dorsal horn of the spinal cord. Ascending projection neurons relay temperature information to the lateral parabrachial nucleus, which sends projection neurons that transmit temperature information to the preoptic area for further processing. Brain regions involved in homeostatic control are shown in gray while regions involved in temperature discrimination are shown in green. Abbreviations: VPT: Ventral posterior thalamus; LPB: Lateral parabrachial nucleus; SPN: Spinal Trigeminal Nuleus; Figure source data and legend: Tan and Knight (2018) Neuron Review.

1.3 Summary of molecular heat sensors in different model systems

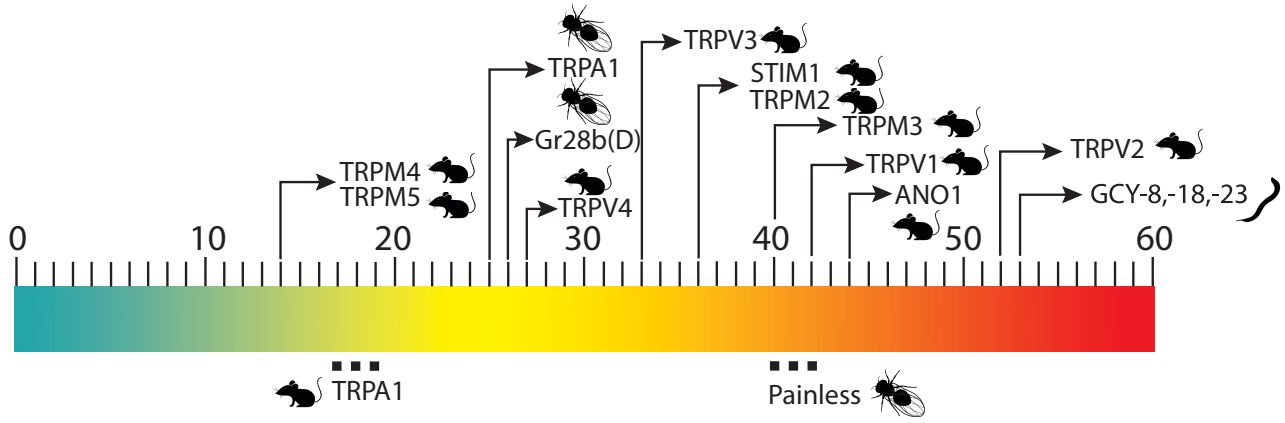

Molecular thermosensors involved in temperature sensation are observed in vertebrates and invertebrates. Innocuous warmth and noxious heat sensors have been identified, with some overlapping functions (such as TRMP4 and TRPM5 which are activated at the same threshold). Dashed lines represent a variable activation temperature. Figure source data adapted from: Xiao and Xu. 2020. Ann Rev Physiol.

1.4 Molecular Cold Sensors Throughout Model Systems

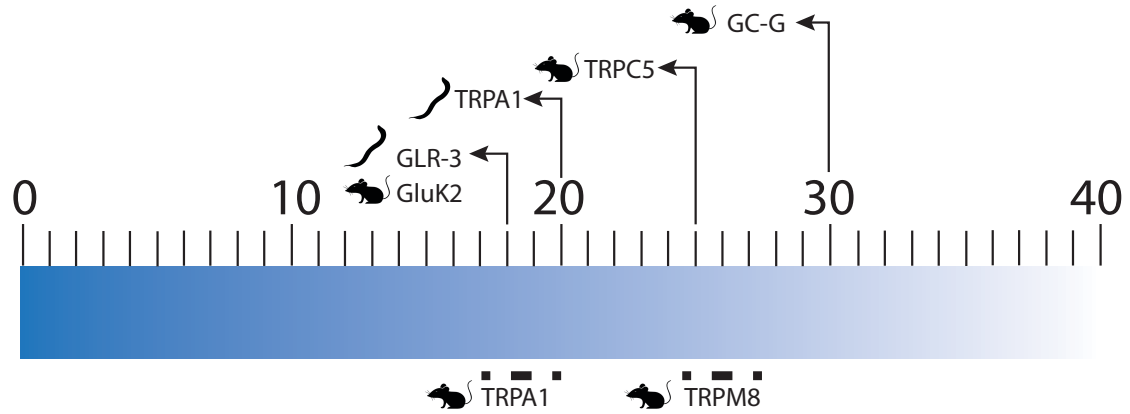

Summary of molecular cold sensors in different model systems. Dashed lines represent a variable activation temperature. Figure source data adapted from: Xiao and Xu. 2020. Ann Rev Physiol.

References

Abdul Aziz, A.A., Finn, D.P., Mason, R., Chapman, V. (2005). Comparison of responses of ventral posterolateral and posterior complex thalamic neurons in naïve rats and rats with hindpaw inflammation: mu-opiod receptor mediated inhibitions. Neuropharmacology. 48, 607-616.

Abraira, V. and Ginty, D. The sensory neurons of touch. Neuron. 79(4), 618-639.

Al-Khater, K.M. and Todd, A.J.(2009). Collateral projections of neurons in laminae I, III, and IV of rat spinal cord to thalamus, periaqueductal gray matter, and lateral parabrachial area. J Comp Neurol 515,629–46.

Alpert, M.H., Frank, D.D., Kaspi, E., Flourakis, M., Zaharieva, E.E., Allada, R., Para, A., Gallio, M. (2020). A Circuit Encoding Absolute Cold Temperature in *Drosophila*. Curr Biol. 30, 2275-2288.

Andrew, D. and Craig, A.D. (2001). Spinothalamic lamina I neurons selectively responsive to cutaneous warming in cats. J. Physiol. (Lond.) 537, 489–495.

Apkarian, A.V., Bushnell, M.C., Treede, R.D., Zubieta, J.K. (2005). Human brain mechanisms of pain perception and regulation in health and disease. Eur J Pain. 9, 463–484.

Baba, H., Ji, R.R., Kohno, T., Moore, K.A., Ataka, T., Wakai, A., Okamoto, M., and Woolf, C.J. (2003). Removal of GABAergic inhibition facilitates polysyn- aptic A fiber-mediated excitatory transmission to the superficial spinal dorsal horn. Mol. Cell. Neurosci. *24*, 818–830.

Bach, P., Becker, S., Kleinbohl, D., Holzl, R. (2011). The thermal grill illusion and what is painful about it. Neurosci Letters. 505(1), 31-35.

Basbaum, A.I. and Jessell, T. (2000).The Perception of Pain. In: Kandel ER, Schwartz J, Jessell T, editors. Principles of Neuroscience. New York: Appleton and Lange. 472–491.

Basbaum, A. I., Bautista, D. M., Scherrer, G. & Julius, D. (2009). Cellular and molecular mechanisms of pain. Cell 139, 267–284.

Bautista, D.M. et al. (2007). The menthol receptor TRPM8 is the principal detector of environmental cold. Nature 448, 204–208.

Bester, H., Besson, J-M. & Bernard, J-F. (1997). Organization of efferent projections from the parabrachial area to the hypothalamus: a *Phaseolus vulgaris*-leucoagglutinin study in the rat. J. Comp. Neurol. 383, 245–281.

Bester, H., Chapman, V., Besson, J.M. and Bernard, J.F. (2000).Physiological properties of the lamina I spinoparabrachial neurons in the rat. J. Neurophysiol. 83, 2239–2259.

Bordi, F.and Quartaroli, M. (2000). Modulation of nociceptive transmission by NMDA/glycine site receptor in the ventroposterolateral nucleus of the thalamus. Pain. 84, 213-224.

Bouhassira, D., Kern, D., Rouaud, J., Pelle-Lancien, E., Morain, F. (2005). Investigation of the paradoxical painful sensation (‘illusion of pain’) produced by a thermal grill. Pain. 114, 160-167.

Boulant, J.A. and Dean, J.B. (1986) Temperature receptors in the central nervous system. Annu Rev Physiol. 48, 639-654.

Bratincsak, A. and Palkovits, M. (2004). Activation of brain areas in rat following warm and cold ambient exposure. Neuroscience. 127, 385-397.

Braz, J., Solorzano, C., Wang, X., and Basbaum, A.I. (2014). Transmitting pain and itch messages: a contemporary view of the spinal cord circuits that generate gate control. Neuron 82, 522–536.

Burnett, N. C. and Dallenbach K.M. (1928). Heat Intensity. The American Journal of Psychology. 40(3), 484-494.

Burton, H. (1975). Responses of spinal cord neurons to systematic changes in hindlimb skin temperatures in cats and primates. J. Neurophysiol. 38, 1060–1079.

Bushnell, M. C., Ceko, M., Low, L.A. (2013). Cognitive and emotional control of pain and its disruption in chronic pain. Nat Rev Neurosci 14(7), 502-511.

Cameron D, Polgar E, Gutierrez-Mecinas M, Gomez-Lima M, Watanabe M, Todd AJ. (2015). The organization of spinoparabrachial neurons in the mouse. PAIN 156, 2061–71.

Campero, M., Baumann, T.K., Bostock, H, Ochoa, J.L. (2009). Human cutaneous C fibers activated by cooling, heating, and menthol. J Physiol. 587, 5633-5652.

Campero, M. and Bostock, H. (2010). Unmyelinated afferents in human skin and their responsiveness to low temperature. Neurosci. Lett. 470, 188–192.

Caterina, M.J., Schumacher M.A., Tom,inaga M., Rosen T.A., Levine J.D., Julius D. (1997). The capsaicin receptor: a heat-activated ion channel in the pain pathway. Nature 389, 816–24.

Cechetto, D.R., Standaert D.G., Saper C.B. (1985). Spinal and trigeminal dorsal horn projections to the parabrachial nucleus in the rat. J. Comp. Neurol. 153-160.

Chen, C.C., Rainville, P., Bushnell, M.C. (1996). Noxious and innocuous cold discrimination in humans: evidence for separate afferent channels. Pain. 68(1), 33-43.

Chery-Croze, S. (1983). Relationship between noxious cold stimuli and the magnitude of pain sensation in man. Pain. 15, 265-269.

Chery-Croze, S. and Duxlaux, R. (1980). Discrimination of painful stimuli in human beings: influence of stimulation area. J Neurophysiol. 44, 1-10

Chisholm, K.I., Lo Re, L., Polgár, E., Gutierrez-Mecinas, M., Todd, A. J., McMahon, S. B. (2021). Encoding of cutaneous stimuli by lamina I projection neurons. Pain. 162(9), 2405-2417.

Christensen, B.N. and Perl E.R. (1970). Spinal neurons specifically excited by noxious or thermal stimuli: marginal zone of the dorsal horn. J. Neurophysiol. 33, 293–307.

Clark, D.A., Biron, D., Sengupta, P., Samuel, A.D. (2006). The AFD sensory neurons encode multiple functions underlying thermotactic behavior in *Caenorhabditis elegans*. J Neurosci. 26(28), 7444–7451.

Collins, W. F., Nulsen, F.E., Randt, C.T. (1960). Relation of Peripheral Nerve Fiber Size and Sensation in Man. Arch Neurol 3(4), 381-385.

Craig, A.D. and Bushnell M.C. (1994). The thermal grill illusion: unmasking the burn of cold pain. Science 265, 252–255.

Craig, A.D., Bushnell, M.C., Zhang, E-T., and Blomqvist, A. (1994). A thalamic nucleus specific for pain and temperature sensation. Nature 372, 770–773.

Craig, A.D., Krout, K. and Andrew, D. (2001). Quantitative response characteristics of thermoreceptive and nociceptive lamina I spinothalamic neurons in the cat. J. Neurophysiol. 86, 1459–1480.

Craig, A.D. (2002). How do you feel? Interoception: the sense of the physiological condition of the body. *Nat. Rev. Neurosci.* 3, 655–666.

Craig, A.D., and Zhang, E.T. (2002). A Blomqvist Association of spinothalamic lamina I neurons and their ascending axons with calbindin-immunoreactivity in monkey and human Pain, 97, 105-115.

Croze, S. and Duclaux, R. (1978). Thermal pain in humans: influence of the rate of stimulation. Brain Res. 157, 418-421

Davern P.J., A role for the lateral parabrachial nucleus in cardiovascular function and fluid homeostasis. Front Phys. 5, 436.

Davis, K.D., Kwan, C.L., Crawley, A.P., Mikulis, D.J. (1998). Functional MRI study of thalamic and cortical activations evoked by cutaneous heat, cold, and tactile stimuli. J Neurophysiol. 80(3), 1533-1546.

Dhaka, A., Murray, A.N., Mathur, J., Earley T.J., Petrus, M.J., Patapoutian, A. (2007). TRPM8 is required for cold sensation in mice. Neuron 54, 371–378.

Dhaka, A., Earley, T.J., Watson, J. and Patapoutian, A. (2008). Visualizing cold spots: TRPM8-expressing sensory neurons and their projections. J. Neurosci. 28, 566–575.

Dodt, E. and Zotterman, Y. (1952). The discharge of specific cold fibres at high temperatures; the paradoxical cold. Acta Physiol Scand. 26(4), 358–365.

Dostrovsky, J.O. and Craig, A.D. (1996). Cooling-specific spinothalamic neurons in the monkey J Neurophysiol, 76, 3656-3665.

Duan B., Cheng L., Bourange S., Britz O., Padilla C., Garcia-Campmany L., Krashes M., Knowlton W., Velasques T., Ren X., et al (2014). Identification of spinal circuits transmitting and gating mechanical pain. Cell 159, 1417-1432.

Duan, B. and Xu, S.X.Z.. (2019). How to Break a Fever: A Feedback Circuit for Body Temperature Control. Neuron. 03, 179-181.

Dubner, R., Sessle, B.J., Storey, A.T.(1978). The Neural Basis of Oral and Facial Function. New York: Plenum.

Fardo, F., Beck, B., Allen, M., Brix Finnerup, N. (2020). Beyond labeled lines: A population coding accound of the thermal grill illusion. Neurosci Biobehav Rev. 108, 472-479.

Frank, D. D., Jouandet, G.C., Kearney, P.J., Macpherson L.J., Gallio M. (2015). Temperature representation in the Drosophila brain. Nature. 519(7543), 358-361.

Fulwiler, C.E. and Saper, C.B. (1984). Subnuclear organization of the efferent connections of the parabrachial nucleus in the rat. Brain Res. Rev. 7, 229–259.

Gallio, M., Ofstad, T.A., Macpherson, L.J., Wang J.W., Zuker C.S. (2011). The coding of temperature in the Drosophila brain. Cell. 144(4), 614-624.

Geerling, J.C., Kim, M., Mahoney, C.E., Abbot, S.B., Agostinelli, L.J., Garfield, A.S., Krashes, M.J., Lowell, B.B., Scammell, T.E. (2016). Genetic identity of thermosensory relay neurons in the lateral parabrachial nucleus. Am J Physiol Regul Integr Comp Physiol. 310, R41-R54.

Gong, J., Liu, J., Ronan, E.A., He, F., Cai, W., et al. (2019). A cold-sensing receptor encoded by a glutamate receptor gene. Cell 178, 1375–86.e11.

Green, B.G. (2009). Temperature perception on the hand during static versus dynamic contact with a surface. Attention, Perception, and Psychophysics. 71, 1185-1196.

Greenspan, J.D., Taylor, D.J., McGilis, S.L.B. (1993). Body site variation of cool perception thresholds, with observations of paradoxical heat. Somatosen. Mot. Res. 10, 467-474.

Gritman, W.B. and Dallenback, K.M. (1929). The formula for the intensive gradation of heat. Am J Psychol 41, 460-464.

Groh, A., Krieger, P., Mease, R.A., Henderson, L. (2018). Acute and Chronic Pain Processing in the Thalamocortical System of Humans and Animal Models. Neuroscience. 387, 58-71.

Grudt, T.J., and Perl, E.R. (2002). Correlations between neuronal morphology and electrophysiological features in the rodent superficial dorsal horn. J Physiol 540, 189-207.

Guler, A.D., Lee, H., Lida, T., Shimizu, I., Tominaga, M., Caterina, M. (2002). Heat-evoked activation of the ion channel, TRPV4. J. Neurosci. 22, 6408–14.

Hachisuka, J., Koerber, H.R., Ross, S.E. (2020). Selective-cold output through a distinct subset of lamina I spinoparabrachial neurons. PAIN 161, 185–94.

Hallin, R.G., Torebjork, E.H., Wiesenfeld, Z. (1981). Nociceptors and warm receptors innervated by C fibers in human skin. J Neurol, Neurosurg, Psych. 44, 313-319.

Hammel, H.T. (1965). Neurons and temperature regulation. Physiological controls and regulations 71-97.

Haring, M., Zeisel, A., Hochgerner, H., Rinwa, P., Jakobsson, J.E.T., Lonngerberg, P., La Manno, G., Sharma, N., Borgius, L., Kiehn, O., Lagerstrom, M.C., Linnarsson, S., Ernfors, P. (2018). Neuronal atlas of the dorsal horn defines its architecture and links sensory input to transcriptional cell types. Nat Neuro. 21, 869-880.

Hawk, J.D., Calvo, A.C., Liu, P., Almoril-Porras, A., Aljobeh,A.A., Torruella-Suarez, M.L., Ren, I., Cook, N., Greenwood, J., Luo, L., et al., (2018). Integration of plasticity

mechanisms within a single sensory neuron of C.elegans actuates a memory. Neuron. 97, 356-367 e 354.

Hedgecock, E.M. and Russell, E.L. (1975) Normal and mutant thermotaxis in the nematode Caenorhabditis elegans. Proc Natl Acad Sci Unit States Am. 72, 4061-4065.

Hensel, H. (1976). Functional and Structural Basis of Thermoreception. Somatosensory and Visceral Receptor Mechanisms, Proceedings of an International Symposium held in Leningrad, U.S.S.R. 105-118.

Hensel, H. and Iggo, A. (1971). Analysis of cutaneous warm and cold fibers in primates. Pflugers Arch. 329, 1–8.

Hensel, H. and Zotterman, Y. (1951). The effect of menthol on the thermoreceptors. Acta Physiol Scand. 24, 27–34.

Hori, T., Nakashima, T., Koga, H., Kiyohara, T. and Inoue, T. (1988). Convergence of thermal, osmotic and cardiovascular signals on preoptic and anterior hypothalamic neurons in the rat. Brain Res. Bull. 20, 879–885.

Huang, S.M., Li, X., Yu, Y., Wang, J., Caterina, M.J. (2011). TRPV3 and TRPV4 ion channels are not major contributors to mouse heat sensation. Mol. Pain 7, 37.

Hylden, J.L.K., Anton, F., Nahin, R.L. (1989). Spinal lamina I projection neurons in the rat: collateral innervation of parabrachial area and thalamus. Neuroscience. 28, 27–37.

Ippolito, D., Thapliyal, S., Glauser, D.A. (2021). Ca(2+)/CaM binding to CaMKI promotes IMA-3 importin binding and nuclear translocation in sensory neurons to control behavioral adaptation. Elife. 10.

Kanosue, K., Sadato, N., Okada, T., Yoda, T., Nakai, S., Yoshida, K., Hosono, T., Nagashima, K., Inoue, O., Kobayashi, K., Yonekura, Y. (2002). Brain activation during whole body cooling in humans studied with functional magnetic resonance imaging. Neurosci Lett. 329, 157–160.

Kanosue, K., Crawshaw, L.I., Nagashima, K., Yoda, T. (**2010).** Concepts to utilize in describing thermoregulation and neurophysiological evidence for how the system works. Eur. J. Appl. Physiol. 109, 5–11.

Kenshalo, D.R., Geisler, G.J., Leonard, R.B., Willis, W.D. (1980). Responses of neurons in the primate ventral posterior lateral nucleus to noxious stimuli. J Neurophysiol 43, 1594-1614.

Kernan, M., Cowan, D., Zuker, C. (1994). Genetic dissection of mechanosensory transduction: mechanoreception-defective mutations of *Drosophila*. Neuron. 12.(6), 1195–1206.

Knowlton, W.M., Palkar, R., Lippoldt, E.K., McCoy, D.D., Baluch, F., Chen, J., McKemy, D.D. (2013). A sensory-labeled line for cold: TRPM8-expressing sensory neurons define the cellular basis for cold, cold pain, and cooling-mediated analgesia. J. Neurosci. 33, 2837–48.

Kobayashi, A. and Osaka, T. (2003). Involvement of the parabrachial nucleus in thermogenesis induced by environmental cooling in the rat Pflugers Arch., 446, 760-765.

Krukoff, T.L., Harris, K.H. and Jhamandas, J.H. (1993). Efferent projections from the parabrachial nucleus demonstrated with the anterograde tracer *Phaseolus vulgaris* leucoagglutinin. Brain Res. Bull. 30, 163–172.

Kumazawat, Perler, Burgess, P.R, and Whitehorn, D. (1975). Ascending projections from marginal zone (lamina I) neurons of the spinal dorsal horn. J Comp Neurol. 162, 1–12.

Kunkle, E.C. (1949). Phasic pains induced by cold. J Appl Physiol 1, 811-824.

LaMotte, R. and Campbell, J. (1978). Comparison of Responses of Warm and Nociceptive C- Fiber afferents in Monkey With Human Judgments of Thermal Pain. Journal of Neurophysiology. 41(2), 509-528.

Leung, A.Y., Wallace, M.S., Schulteis, G., Yaksh T.L. (2005). Qualitative and quantitative characterization of the thermal grill. Pain, 116, 26-32

Liu, B., Hui, K., Qin, F. (2003). Thermodynamics of heat activation of single capsaicin ion channels VR1. Biophys. J. 85, 2988–3006

Liu, S., Schulze, E., Baumeister, R. (2012). Temperature- and touch-sensitive neurons couple CNG and TRPV channel activities to control heat avoidance in Caenorhabditis elegans. PLoS One. E32360.

Liu, W.W., Mazor, O., Wilson, R.I. (2015). Thermosensory processing in the Drosophila brain. Nature. 519, 353–57.

Liu, X., Wang, H., Jiang, Y., Zheng, Q., Petrus, M., Zhang, M., Zheng, S., Schmedt, C., Dong, X., Xiao, B. (2019). STIM1 thermosensitivity defines the optimal preference temperature for warm sensation in mice. Cell Res. 29, 95–109.

Lu, Y., Dong, H., Gao, Y., Gong, Y., Ren, Y., Gu, N., Zhou, S., Xia, N., Sun, Y.Y., Ji, R.R., and Xiong, L. (2013). A feed-forward spinal cord glycinergic neural circuit gates mechanical allodynia. J. Clin. Invest. *123*, 4050–4062.

Luz, L.L., Szucs, P., Pinho, R., and Safronov, B.V. (2010). Monosynaptic excitatory inputs to spinal lamina I anterolateral-tract-projecting neurons from neighbouring lamina I neurons. J Physiol 588, 4489-4505.

Ma, Q. (2010). Labeled lines meet and talk: population coding of somatic sensations. J. Clin. Invest. 120, 3773–3778.

Madden, C.J. and Morrison, S.F. (2003). Excitatory amino acid receptor activation in the raphe pallidus area mediates prostaglandin-evoked thermogenesis. Neuroscience 122, 5–15.

Madden, C.J. and Morrison, S.F. (2004). Excitatory amino acid receptors in the dorsomedial hypothalamus mediate prostaglandin-evoked thermogenesis in brown adipose tissue. Am. J. Physiol. Regul. Integr. Comp. Physiol. 286, R320–R325.

Madden, C.J., and Morrison, S.F. (2019). Central nervous system circuits that control body temperature. Neuroscience letters 696, 225-232.

Magoun, H.W., Harrison, F., Brobeck, J.R., Ranson, S.W. (1938). Activation of heat loss mechanisms by local heating of the brain. J Neurophysiol. 1,101-114.

Matsuyama, H.J. and Mori, I. (2020). Neural coding of thermal preferences in the nematode Caenorhabditis elegans. eNeuro. 7.

Martin, W.J., Hohmann, A.H., Walker, J.M. (1996). Suppression of noxious stimulus-evoked activity in the ventral posterolateral nucleus of the thalamus by a cannabinoid agonist: correlation between electrophysiological and antinociceptive effects. J Neurosci. 16, 6601-6611.

McKemy, D.D., Neuhausser, W.M., and Julius, D. (2002). Identification of a cold receptor reveals a general role for TRP channels in thermosensation. Nature 416, 52–58.

McKemy, D. D. (2007). Temperature sensing across species. Pflugers Arch. 454(5), 777-791.

McKemy, D. D. (2013). The molecular and cellular basis of cold sensation. ACS Chem Neurosci. 4(2), 238-247.

McMahon, S.B., and Wall, P.D. (1983). A system of rat spinal cord lamina 1 cells projecting through the contralateral dorsolateral funiculus. J Comp Neurol. 214, 217–23.

Melzack, R., and Wall, P.D. (1965). Pain mechanisms: a new theory. Science 150, 971–979.

Melzack, R., and Casey, K.L. (1968). Sensory, motivational, and central control determinants of pain: a new conceptual model. In: The Skin Senses, edited by Kenshalo D. Springfield, IL: C. C. Thomas. 423–439.

Mendell, L.M. (2014). Constructing and deconstructing the gate theory of pain. Pain 155, 210–216.

Menétrey, D., Pommery, J.,Thomasset, M., Baimbridge, K.G. (1992). Calbindin-D28K (CaBP28k)-like immunoreactivity in ascending projections Eur J Neurosci, 4, 70-76.

Moayedi, M. and Davis, K.D. (2013). Theories of pain: from specificity to gate control. J Neurophysiol. 109, 5-12.

Mohri, A., Kodama, E., Kimura, K.D., Koike, M., Mizuno, T., Mori, I. (2005). Genetic control of temperature preference in the nematode *Caenorhabditis elegans.* Genetics. 169(3), 1437-1450.

Morin, C., TenBokum, L., Bushnell, M.C. (1994). Temporal and qualitative differences in heat and cold pain. Soc Neurosci Abstr. 20, 127.

Morrison, S.F. (2004). Central pathways controlling brown adipose tissue thermogenesis. News Physiol. Sci. 19, 67–74.

Morrison, S.F. and Nakamura, K. (2019). Central Mechanisms for Thermoregulation. Ann Rev Physiol. 81, 285-308.

Mosso, J.A., and Kruger, L. (1973). Receptor categories represented in spinal trigeminal nucleus caudalis. J Neurophysiol. 36, 472– 488.

Nagashima, K., Nakai, S., Tanaka, M. and Kanosue, K. (2000). Neuronal circuitries involved in thermoregulation. Auton. Neurosci.. 85, 18–25.

Nagy, I., Rang, H.P. (1999). Similarities and differences be-tween the responses of rat sensory neurons to noxiousheat and capsaicin. J Neurosci 19,10647–10655.

Nakamura, K., Matsumura, K., Kaneko, T., Kobayashi, S., Katoh, H., Negishi, M. (2002). The rostral raphe pallidus nucleus mediates pyrogenic transmission from the preoptic area. J. Neurosci. 22, 4600–4610.

Nakamura, K. (2004). Fever-inducing sympathetic neural pathways. J. Therm. Biol. 29, 339–344.

Nakamura, K., Matsumura, K., Kobayashi, S., and Kaneko, T. (2005). Sympathetic premotor neurons mediating thermoregulatory functions. Neurosci. Res. 51, 1–8.

Nakamura, Y., Nakamura, K., Matsumura, K., Kobayashi, S., Kaneko, T., Morrison, S.F. (2005). Direct pyrogenic input from prostaglandin EP3 receptor–expressing preoptic neurons to the dorsomedial hypothalamus. Eur. J. Neurosci. 22, 3137–3146.

Nakamura, K. and Morrison, S.F. (2007). Central efferent pathways mediating skin cooling-evoked sympathetic thermogenesis in brown adipose tissue. Am. J. Physiol. Regul. Integr. Comp. Physiol. 292, R127–R136.

Nakamura K. and Morrison S.F. (2008). A thermosensory pathway that controls body temperature. Nat. Neurosci. 11, 62-71.

Nakamura, K. and Morrison S.F. (2010). A thermosensory pathway mediating heat-defense responses Proc. Natl. Acad. Sci. U. S. A., 107 (2010), pp. 8848-8853

Nakamura, K. and Morrison, S.F. (2011) Central efferent pathways for cold-defensive and febrile shivering. J Physiol. 589, 3641-3658.

Norrsell, U., Finger S. and Lajonchere, C. (1999) Cutaneous sensory spots and the "law of specific nerve energies": history and development of ideas. Brain Research Bulletin, 48(5), 457-465.

Olausson, H., Cole, J., Rylander, K., McGlone, F., Lamarre, Y., Wallin, B.G., Kramer, H., Wessberg, J., Elam, M., Bushnell, M.C., et al. (2008). Functional role of unmyelinated tactile afferents in human hairy skin: sympathetic response and perceptual localization. Exp. Brain Res. 184, 135–140.

Oyebola, B.O. and Odueso, V.T. (2017). LM35 Based Digital Room Temperature Meter: A Simple Demonstration. Equatorial J Comp Theoretical Sci. 2(1), 6-15.

Palkar, R., Lippoldt, E.K., McKemy, D.D. (2015). The molecular and cellular basis of thermosensation in mammals. Curr Opin Neurobiol. 34, 14-19.

Pan, H., Fatima, M., Li, A., Lee, H., Cai, W., Horwitz, L., Hor, C.C., Zaher, N., Cin, M., Slade, H.*, et al.* (2019). Identification of a Spinal Circuit for Mechanical and Persistent Spontaneous Itch. Neuron 103, 1135-1149 e1136.

Park, U., Vastani, N., Guan, Y., Raja, S.N., Koltzenburg, M., Caterina, M.J. (2011). TRP vanilloid 2 knock-out mice are susceptible to perinatal lethality but display normal thermal and mechanical nociception..J. Neurosci.. 31, 11425–36.

Peier, A.M., Moqrich, A., Hergarden, A.C., Reeve, A.J., Andersson, D.A., Story, G.M., Earley, T.J., Dragoni, I., McIntyre, P., Bevan, S., Patapoutian, A. (2002). A TRP channel that senses cold stimuli and menthol. Cell 108, 705–715.

Pogorzala, L.A., Mishra, S.K., Hoon, M.A. (2013). The cellular code for mammalian thermosensation. J. Neurosci. 33, 5533–41.

Polgár, E., Wright, L.L., Todd, A.J. (2010). A quantitative study of brainstem projections from lamina I neurons in the cervical and lumbar enlargement of the rat. Brain Res. 1308, 58–67.

Prescott, S.A., Ma, Q., and De Koninck, Y. (2014). Normal and abnormal coding of somatosensory stimuli causing pain. Nat. Neurosci. 17, 183–191.

Price, T.J., Cervero, F., Gold, M.S., Hammond, D.L., and Prescott, S.A. (2009). Chloride regulation in the pain pathway. Brain Res. Brain Res. Rev. 60, 149–170.

Ran, C., Hoon, M.A., Chen, X. (2016). The coding of cutaneous temperature in the spinal cord. Nat Neurosci 19,1201-1209.

Refinetti, R. and Menaker, M. (1992). The circadian rhythm of body temperature. Physiol Behav. 51(3), 613-637.

Romanovsky, A.A. (2004). Do fever and anapyrexia exist? Analysis of set point-based definitions. Am. J. Physiol. Regul. Integr. Comp. Physiol. 287, R992–95.
Russ, D.E., Patterson, Cross, R.B., Li, L., Koch, S.C., Matson, K.J.E., Levine, A.J. (2020). A Harmonized Atlas of Spinal Cord Cell Types and Their Compuational Classification. bioRxiv.

Sandku¨hler, J. (2009). Models and mechanisms of hyperalgesia and allodynia. Physiol. Rev. 89, 707–758.

Saper, C.B. and Loewy, A.D. (1980). Efferent connections of the parabrachial nucleus in the rat. Brain Res. 197, 291–317.

Saper, C.B. (2002). The central autonomic nervous system: conscious visceral perception and autonomic pattern generation. Annu. Rev. Neurosci. 25, 433–469.

Saro, G., Lia, A.S., Thapliyal, S., Marques, F., Busch, K.E., Glauser, D.A. (2020). Specific ion channels control sensory gain, sensitivity, and kinetics in a tonic thermonociceptor. Cell Rep. 30, 397-408 e 394.

Sathyamurthy, A., Johnson, K.R., Matson, K.J.E., Dobrott, C.I., Li, L., Ryba, A.R., Bergmen, T.B., Kelly, M.C., Kelley, M.W., Levine, A.J. (2018). Massively Parallel Single Nucleus Transcriptional Profiling Defines Spinal Cord Neurons and Their Activity during Behavior. Cell Reports. 22:2216-2225.

Sayeed, O. and Benzer, S. (1996). Behavioral genetics of thermosensation and hygrosensation in *Drosophila*. Proc Natl Acad Sci USA. 93(12), 6079–6084.

Song, K., Wang, H., Kamm, G.B., Pohle, J., de Castro Reis, F., Heppenstall, P., Wende, H., Siemens, J. (2016). The TRPM2 channel is a hypothalamic heat sensor that limits fever and can drive hypothermia. Science 353, 1393–98.

Sperry, R. W. (1945). Restoration of vision after crossing of optic nerves and after transplantation of eye. Journal of Neurophysiology*,* 8, 15-28.

Spike, R.C., Puskar, Z., Andrew, D., Todd, A.J. (2003). A quantitative and morphological study of projection neurons in lamina I of the rat lumbar spinal cord. Eur J Neurosci. 18, 2433–48.

Stevens, J.C. (1979). Variation of cold sensitivity over the body surface. Sensory Processes. 3, 317-326.

Takashima, Y., Daniels, R.L., Knowlton, W., Teng, J., Liman, E.R., McKemy, D.D. (2007). Diversity in the neural circuitry of cold sensing revealed by genetic axonal labeling of transient receptor potential melastatin 8 neurons. J. Neurosci*.* 27, 14147–14157.

Takashima, Y., Ma, L., McKemy, D.D. (2010). The development of peripheral cold neural circuits based on TRPM8 expression. Neuroscience 169, 828–42.

Talavera, K., Yasumatsu, K., Voets, T., Droogmans, G., Shigemura, N., Ninomiya, Y., Margolskee, R.F., Nilius, B. (2005). Heat activation of TRPM5 underlies thermal sensitivity of sweet taste. Nature. 438, 1022–25.

Tan, C-H. and McNaughton, P.A. (2016). The TRPM2 ion channel is required for sensitivity to warmth. Nature 536, 460–63.

Tan, C.L. and Knight, Z.A. (2018). Regulation of Body Temperature by the Nervous System. Neuron 98, 31-48.

Todd, A.J. (2010). Neuronal circuitry for pain processing in the dorsal horn. Nat Rev Neurosci. 11, 823–36.

Togashi, K., Hara, Y., Tominaga, T., Higashi, T., Konishi, Y., Mori, Y., Tominaga, M. (2006). TRPM2 activation by cyclic ADP-ribose at body temperature is involved in insulin secretion. EMBO J. 25, 1804–15.

Tominaga, M. and Caterina M.J. (2004). Thermosensation and pain. J Neurobiol. 61(1), 3-12. https://doi.org/10.1002/neu.20079.

Torebjork, E. (1985). Nociceptor Activation an Pain.pdf. Phil. Trans. R. Soc. Lond 308, 227-234.

Torsney, C., and MacDermott, A.B. (2006). Disinhibition opens the gate to pathological pain signaling in superficial neurokinin 1 receptor-expressing neurons in rat spinal cord. J. Neurosci. 26, 1833–1843.

Tracey, W. D., Wilson, R.I., Laurent G., Benzer, S. (2003). Painless, a Drosophila Gene Essential for Nociception. Cell 113(2), 261-273.

Treede, R.D., Meyer, R.A., Raja, S.N., Campbell, J.N. (1995). Evidence for two different heat transduction mechanisms in nociceptive primary afferents innervating monkey skin. J Physiol 483, 747–758.

Vandewauw, I., De Clercq, K., Mulier, M., Held, K., Pinto, S., Van Ranst, N., Segal, A., Voet, T., Vennekens, R., Zimmermann, K., Vriens, J., Voets, T. (2018). A TRP channel trio mediates acute noxious heat sensing. Nature 555, 662–66.

Vogt, B.A. (2005) Pain and emotion interactions in subregions of the cingulate gyrus. Nat Rev Neurosci. 6, 533.

Vriens, J., Owsianik, G., Hofmann, T., Philipp, S.E., Stab, J., Chen, X, Benoit, M., Xue, F., Hanssens, A., Kerselaers, S. et al., (2011). TRPM3 is a nociceptor channel involved in the detection of noxious heat. Neuron 70, 482–94.

Vriens, J., B. Nilius and T. Voets (2014). "Peripheral thermosensation in mammals." Nat Rev Neurosci 15(9): 573-589.

Wall, P.D. (1978). The gate control theory of pain mechanisms. A reexamination and restatement. Brain 101, 1–18.

Wang, F., Bélanger, E., Côté, S.L., Desrosiers, P., Prescott, S.A., Côté, D.C., De Koninck Y. (2018). Sensory afferents use different coding strategies for heat and cold Cell Rep. 23, 2001-2013.

Wang, T.A., Teo, C.F., Akerblom, M., Chen, C., Tynan-La Fontaine, M., Greiner, V.J., Diaz, A., McManus, M.T., Jan Y. N., Jan, L.Y. (2019). Thermoregulation via Temperature-Dependent PGD_2 Production in Mouse Preoptic Area. Neuron. 103(20, 309-322e7.

Weber, E.H., (1842). Handworterbuch der Physiologie: 1 (Friedrich Vieweg undSohn). Wercberger, R. and Basbaum, A.I. (2019). Spinal Cord Projection Neurons: A Superficial, and also Deep Analysis. Curr Opinion in Phys 11, 109-115.

Werner, J. (2010). System properties, feedback control and effector coordination of human temperature regulation. Eur. J. Appl. Physiol. 109, 13–25.

Wittenburg, N. and Baumeister, R. (1999). Thermal avoidance in *Caenorhabditis elegans:* an approach to the study of nociception. Proc Natl Acad Sci U S A, 96, 10477-10482.

Wolf, S. and Hardy, J.D. (1941). Studies on pain: observations on pain due to local cooling and on factors involved in the 'cold pressor' effect. J Clin Invest. 20, 521-533.

Xiao, R. and Xu, S.X.Z. (2021). Temperature Sensation: From Molecular Thermosensors to Neural Circuits and Coding Principles. Annu. Rev Physiol. 83, 205-230.

Xu, H., Ramsey, I.S., Kotecha, S.A., Moran, M.M., Chong, J.A., Lawson, D., Ge, P., Lilly, J., Silos-Santiago, I., Xie, Y., DiStefano, P.S., Curtis, R., Clapham, D.E. (2002). TRPV3 is a calcium-permeable temperature-sensitive cation channel. Nature 418, 181–86.

Yahiro, T., Kataoka, N., Nakamura, Y., Nakamura, K. (2017). The lateral parabrachial nucleus, but not the thalamus, mediates thermosensory pathways for behavioural thermoregulation. Sci. Rep. 7, 5031

Yarmolinsky, D.A., Peng, Y., Pogorzala, L.A., Rutlin, M., Hoon, M.A., Zuker, C.S. (2016). Coding and plasticity in the mammalian thermosensory system. Neuron 92, 1079–92

Yarnitsky, D. and Ochoa, J.K. (1990). Release of cold-induced burning pain by block of cold-specific afferent input. Brian. 113, 893-902.

Yao, J., Liu, B., Qin, F. (2011). Modular thermal sensors in temperature-gated transient receptor potential (TRP) channels. PNAS 108, 11109–14

Zaretskaia, M.V., Zaretsky, D.V. and DiMicco, J.A. (2003). Role of the dorsomedial hypothalamus in thermogenesis and tachycardia caused by microinjection of prostaglandin E2 into the preoptic area in anesthetized rats. Neurosci. Lett. 340, 1–4.

Zeilhofer, H.U., Wildner, H., and Yevenes, G.E. (2012). Fast synaptic inhibition in spinal sensory processing and pain control. Physiol. Rev. 92, 193–235.

Zimmermann, K. et al. Phenotyping sensory nerve endings *in vitro* in the mouse. Nature Protoc*.* 4, 174–196 (2009).

Zimmermann, K., Lennerz, J.K., Hein, A., Link, A.S., Kaczmarek, J.S., Turnquist, B.P., Clapham, D.E., Reeh, P.W. (2011). Transient receptor potential cation channel, subfamily C, member 5 (TRPC5) is a cold-transducer in the peripheral nervous system.PNAS 108,18114–19.

Chapter 2
Auditory Nociception Under Physiological and Pathological Conditions

In Chapter 1, I described our current understanding of a sensory system (temperature sensing) under physiological conditions. In this chapter, I will introduce a sensory system (auditory) in a disease state, and the interactions between the auditory and somatosensory systems that may help explain the pathogenesis of this auditory nociceptive disorder.

2.1 Overview of the Canonical Auditory System

The inner ear contains both the hearing organ (cochlea) and balance organs (vestibular system) which is mainly responsible for sound detection and balance respectively. The sensory epithelium of the cochlea, known as the Organ of Corti, is lined with a single row of inner hair cells and three rows of outer hair cells. These hair cells are the sensory cells of the auditory system. Each hair cell is topped with hair-like structures called stereocilia. Fluid in the cochlea known as perilymph moves in response to vibrations from the middle ear via the oval window, thus stimulating the hair cells. Movement of the stereocili of the inner hair cells converts motion due to auditory stimulation to electrical signals that are relayed through the auditory nerve fiber to the cochlear nucleus (Oghalai, 1997). A healthy cochlea can generate and amplify sounds to detect very faint sounds. Outer hair cells contain Prestin, a motor protein that can generate additional movement that couples back to the fluid-membrane wave, thus

amplifying the sound (Liberman et al., 2002). These specialized cochlear sensory hair cells cannot regenerate in mammals, therefore, after loud noise exposure, hearing cells can be damaged or lost resulting in hearing dysfunction (Fuchs and Glowatzki, 2015). Type I auditory nerve fibers are large diameter myelinated neurons that are excited by a single ribbon synapse of a single inner hair cell. This solitary transmission point allows for the transmission of key features of acoustic information including timing, intensity, and frequency composition to the central nervous system, thus providing the main pathway of auditory input to the brain (Heil and Peterson, 2015). Alternatively, unmyelinated type II auditory nerve fibers provide primary afferent innervation of outer hair cells of the cochlea and are insensitive to sound (Fuchs and Glowatzki, 2015). The majority of afferents (90-95%) are type I fibers, whereas there are much fewer type II. Type II cochlear afferent travels across the tunnel of Corti then extends hundreds of microns towards the cochlear base where each afferent gives off short branches to multiple outer hair cells (usually within one row). At least 6 outer hair cells must release vesicles to evoke an action potential, consistent with maximal acoustic stimulation. Additionally, type II afferents respond vigorously to ATP, which is released from hair cells after damage, and project centrally forming synapses in the cochlear nucleus (Fuchs and Glowatzki, 2015). In the somatosensory system, pain signals are transmitted through anatomically distinct subsets of small-diameter, unmyelinated afferent C-fibers similar to type II fibers. Pain receptors are absent in the cochlea; therefore, it is unclear how specific sounds can be perceived as painful, however type II fibers could act as cochlear nociceptors mediating the sensation of painfully loud

sounds. The role type II fibers in auditory sensitivity disorders such as hyperacusis, remains undefined.

The first site of neural integration is the cochlear nucleus followed by the Superior Olivary Complex located in the pons, then the Inferior Colluculus of the midbrain, and finally the auditory Thalamus and cortex. Additional projections directly from the cochlear nucleus to the Inferior Colluculus and auditory thalamus exist, contributing to the importance of cochlear nucleus integration along the canonical auditory pathway. In mammals, the cochlear nucleus can be further subdivided into the dorsal cochlear nucleus and ventral cochlear nucleus, both of which are innervated by the auditory nerve fibers. The granule cell domain of the cochlear nucleus receives somatosensory input from brainstem somatosensory nuclei (such as the spinal trigeminal nucleus) and is thought to play a role in regulation of self-generated sounds such as chewing (Zhou and Shore, 2004; Haenggeli et al., 2005; Zhou et al., 2007; Shore 2011). Anterograde tracing studies have indicated cochlear nucleus neurons can project directly to the thalamus (Anderson et al., 2006). Therefore, interaction between the somatosensory and auditory systems may prove a novel pathway to understand the precise neuronal circuitry of pain hyperacusis.

2.2 Convergence of the Auditory and Somatosensory Systems in a Disease State

Loud noise exposure and prolonged exposure to occupational noises can result in a number of auditory disorders including tinnitus, hyperacusis, noise-induced hearing loss, and hidden hearing loss. Hyperacusis is an auditory sensitivity disorder that can be classified into three different types, loudness hyperacusis, avoidance/discomfort

hyperacusis, and painful hyperacusis (Tyler et al., 2014). Loudness hyperacusis is characterized by the sensory discrimination component of loudness, similar to the sensory discrimination component of pain previously described (i.e. the location, duration, and intensity of the painful stimuli) (see Pain and Projection Neurons in Chapter 1). Alternatively, the avoidance, discomfort, and pain aspects are more similar to the affective emotional component of pain. Therefore, hyperacusis can be classified based on its sensory processing description through the pain pathway into two different types, loudness hyperacusis and affective hyperacusis. Under this definition, affective hyperacusis is an auditory sensitivity disorder in which conversational-level noises lead to discomfort, avoidance, or even pain.

Despite the debilitating nature of affective hyperacusis, little is known of the underlying mechanisms. Affective hyperacusis is particularly understudied due to two major challenges, the prevalence and characteristics of affective hyperacusis in the general population has not been well defined, and most studies of hyperacusis have inadvertently described loudness hyperacusis and not affective hyperacusis due to a lack of animal models for affective hyperacusis. Patients with any form of hyperacusis have a greatly impacted quality of life, including withdrawal from social interactions, and increased anxiety and stress (Valente et al., 2000; Blaesing and Kroener-Herwig, 2012). Clearly addressing these two limitations to affective hyperacusis research would greatly aid in the development of therapeutics for hyperacusis patients.

2.3 Hyperacusis in Humans

Few rigorous studies regarding the epidemiology of hyperacusis have been published making it difficult to accurately measure the population wide prevalence of hyperacusis. Reports of the prevalence of hyperacusis range from 2-15% of the population (Sammeth et al., 2000; Fabijanska et al., 1999), even at the most conservative estimate (2%), millions of Americans would be affected by hyperacusis. Furthermore, reports are generated from patients seeking medical attention for hyperacusis. These reports may be undercounting the true prevalence due to patients not seeking medical intervention for their loudness discomfort. Several questionnaires have been developed to assess the severity and presence of hyperacusis in patients. However, the reading level of these questionnaires is often higher than the American Medical association and US national institute of health recommendations for survey reading levels, calling into question the accuracy of these questionnaires (Margol-Gromada et al., 2020). Alternatively, physiological exams such as the loudness discomfort level (LDL) or uncomfortable loudness level (UCL) have also been used to assess the presence of hyperacusis (Anari et al., 1999; Goldstein and Shulman, 1996). The alternate binaural loudness balance tests instruct patients to match the loudness of a sound to the same or different loudness presented to the contralateral ear (Hood, 1977). A combination of several different methods may be useful in more accurately identifying and characterizing hyperacusis in patients.

Although hyperacusis can be the major complaint of patients, it is often co-morbid with auditory (tinnitus, hidden hearing loss, noise-induced hearing loss), neuro-developmental (autism, Williams syndrome, Meiners disease, superior canal

dehiscence, multiple sclerosis), chronic pain disorders due to somatosensory dysregulation (fibromyalgia, migraine, cutaneous allodynia, complex regional pain syndrome) and more (Schecklmann et a., 2014; Weber et al., 2002; Minor et al., 2001; Dang et al., 2014; Khalfa et al., 2004; Gomes et al., 2008; Geisser et al., 2008; Gothelf et al., 2006; Ashkenazi et al., 2010; Irimia et al., 2008; Abouzari et al., 2020). Additional symptoms may include concentration difficulties, tension, sleep disturbance, anxiety, depression, cognitive impairments, and sensitivity to light and/or color (global sensitization) (Andersson et al., 2002; Juris et al., 2013; Baguley et al., 2013; Malouff et al., 2011; Langguth et al., 2011; Loprinzi et al., 2013; Attanasio et al., 2013; Alster et al., 1993), many of which could impair accurate classification on a hyperacusis questionnaire (ie difficulties concentrating or cognitive impairments may affect the ability to accurately respond to the questionnaire). Loudness discomfort level matching and hyperacusis questionnaires can be employed to evaluate the presence of hyperacusis in humans, however these methods cannot be employed to test for hyperacusis in animals. By understanding the diverse etiology of hyperacusis patients, researchers can overcome this limitation by designing animal behavior models that directly test the avoidance, loudness, discomfort, and painful aspects of hyperacusis.

2.4 Current Animal Models of Hyperacusis

Advances in understanding pain hyperacusis have been hindered by the scarcity of animal behavioral models, and it is often difficult to accurately discriminate between types of hyperacusis (i.e., loudness, aversive, or painful) leading to misinterpretation of behavioral results especially as they relate to clinical data. For example, the Acoustic

Startle Response (ASR) has been used as a measure of hyperacusis in an animal model (Hickox and Liberman, 2014; Salloum, et al., 2014; Turner and Parrish, 2008), however, in humans, ASR was related to one metric of hyperacusis, but not to the self-reported symptoms of clinical patients. In animal models, acoustic startle is hypothesized to increase due to hyperacusis which may be true in loudness hyperacusis, but could produce freezing responses in rodents with pain hyperacusis thereby masking their responses. Similarly, in humans, acoustic startle is reflective of loudness discomfort levels rather than annoyance, fear, or avoidance of sounds (Knudson and Melcher, 2016). Operant conditioning and reaction time intensity-function responses have also been used to assess hyperacusis, however they more accurately represent loudness component rather than affective component of hyperacusis (Radwizon et al., 2020; Mohrle et al., 2019).

Interestingly, patients with hyperacusis report significantly more noise-related avoidance in daily life, which correlated significantly with distress (Blaesing and Kroener-Herwig, 2012). Perhaps a better model for studying painful hyperacusis would rely on the animal's choice to actively avoid a perceived harmful stimulus, which would be more representative of clinical phenomenon. A recent study in Sprague-Dawley rats demonstrated using a light/dark sound avoidance paradigm that at specific frequency sounds can trigger aversive behaviors after noise trauma (Manohar et al., 2017), however the two chambers were separated by a hallway and time spent in the hallway was considered towards one of the chambers, possibly altering the interpretation of results. By understanding the clinical manifestations of hyperacusis, more precise behavioral models for hyperacusis are being developed. Therefore, the clinical

understanding of hyperacusis must improve as well. As patients with hyperacusis often present with normal audiograms, alternative measures including questionnaires are necessary for diagnosing pain hyperacusis. A recent questionnaire was developed to differentiate between loudness, avoidance, and painful hyperacusis and can be paired with qualitative data collected from professional audiologists along with tinnitus information (Greenberg and Carlos, 2018). Using a multi-pronged approach to diagnosis, detailed assays of hyperacusis in both humans and animals are being created.

References

Abouzari, M., Tan, D., Sarna, B., et al., (2020). Efficacy of Multi-Modal Migraine Prophylaxis Therapy on Hyperacusis Patients. Ann Otol Phinol Laryngol. 129 (5), 421-427.

Alster, J., Shemesh, Z., Ornan, M., Attias, J. (1993) Sleep disturbance associated with chronic tinnitus. Biol Psychiatry. 34(1–2), 84–90.

Anari, M., Axelsson, A., Eliasson, A., Magnusson, L. (1999) Hypersensitivity to sound—questionnaire data, audiometry and classification. Scand Audiol 28(4),219–230.

Andersson, G., Lindvall, N., Hursti, T., Carlbring, P. (2002) Hypersensitivity to sound (hyperacusis): a prevalence study conducted via the internet and post. Int J Audiol 41(8), 545–554.

Ashkenazi, A., Yang, I., Mushtaq, A., Oshinsky, M.L. (2010) Is phonophobia associated with cutaneous allodynia in migraine? J Neurol Neurosurg Psychiatry. 81(11),1256–1260.

Attanasio, G., Russo, F.Y., Roukos, R., Covelli, E., Cartocci, G., Saponara, M. (2013). Sleep architecture variation in chronic tinnitus patients. Ear Hear. 34(4), 503–507.

Blaesing, L., Kroener-Herwig, B. (2012). Self-reported and behavioral sound avoidance in tinnitus and hyperacusis subjects, and association with anxiety ratings. Int. J. Audiol. 51, 611-617.

Baguley, D., McFerran, D., Hall, D. (2013) Tinnitus. Lancet. 382(9904), 1600–1607.

Dang, P.T., Kennedy, T.A., Gubbels, S.P. (2014). Simultaneous, unilateral plugging of superior and posterior semicircular canal dehiscences to treat debilitating hyperacusis. J Laryngol Otol. 128(2), 174–178.

Fabijanska, A., Rogowski, M., Bartnik, G., Skarzyński, H. (1999). Epidemiology of tinnitus and hyperacusis in Poland. Proc 6th Int Tinnitus Semin. 569–72.

Fuchs, P.A. and Glowatzki, E. (2015) Synaptic Studies form the functional diversity of cochlear afferents. Hear Res. 330, 18-25.

Geisser, M.E., Glass, J.M., Rajcevska, L.D., Clauw, D.J., Williams, D.A., Kileny, P.R. et al., (2008). A psychophysical study of auditory and pressure sensitivity in patients with fibromyalgia and healthy controls. J Pain. 9(5), 417–422.

Goldstein, B., Shulman, A. (1996). Tinnitus—hyperacusis and the loudness discomfort level test—a preliminary report. Int Tinnitus J. 2, 83–89.

Gomes, E., Pedroso, F.S., Wagner, M.B. (2008). Auditory hypersensitivity in the autistic spectrum disorder. Pro Fono. 20(4), 279–284.

Gothelf, D., Farber, N., Raveh, E., Apter, A., Attias, J. (2006) Hyperacusis in Williams syndrome: characteristics and associated neuroaudiologic abnormalities. Neurology. 66(3), 390–395.

Greenberg, B., Carlos, M. (2018). Psychometric Properties and Factor Structure of a New Scale to Measure Hyperacusis: Introducing the Inventory of Hyepracusis Symptoms. Ear and Hearing. 39(5),1025 – 1034.

Haenggeli, C.A., Pongstaporn, T., Doucet, J.R., Ryugo, D.K. (2005). Projections from the spinal trigeminal nucleus to the cochlear nucleus in the rat. J Comp Neurol. 484, 191–205.

Heil, P. and Peterson, A.J.(2015). Basic response properties of auditory nerve fibers: a review. Cell Tiss Res. 361, 129-158.

Hickox, A.E. and Liberman, C.M. (2014). Is noise-induced cochlear neuropathy key to the generation of hyperacusis or tinnitus? J. Neurophysiology. 111(3), 552-564.

Hood, J.D. (1977) Loudness balance procedures for the measurement of recruitment. Audiology. 16(3), 215–228.

Irimia, P., Cittadini, E., Paemeleire, K., Cohen, A.S., Goadsby, P.J. (2008). Unilateral photophobia or phonophobia in migraine compared with trigeminal autonomic cephalalgias. Cephalalgia. 28(6), 626–630.

Juris, L., Andersson, G., Larsen, H.C., Ekselius, L. (2013). Psychiatric comorbidity and personality traits in patients with hyperacusis. Int J Audiol. 52(4), 230–235.

Khalfa, S., Bruneau, N., Roge, B., Georgieff, N., Veuillet, E., Adrien, J.L. et al., (2004). Increased perception of loudness in autism. Hear Res 198(1–2), 87–92.

Knudson, I.M., Melcher, J.R. (2016). Elevated acoustic startle responses in humans: relationship to reduced loudness discomfort level, but not self-report of hyperacusis. J. Assoc. Res. Otolaryngol. 17, 223e235.

Langguth, B., Landgrebe, M., Kleinjung, T., Sand, G.P., Hajak, G. (2011) Tinnitus and depression. World J Biol Psychiatry. 12(7), 489–500.

Liberman, C. M., Gao, J., He, D.Z., Wu, X., Jia, S., Zuo, J. (2002). Prestin is required for electromotility of the outer hair cell and for the cochlear amplifier. Nature. 419, 300-304.

Loprinzi, P.D., Maskalick, S., Brown, K., Gilham, B. (2013). Association between depression and tinnitus in a nationally representative sample of US older adults. Aging Ment Health. 17(6), 714–717.

Malouff, J.M., Schutte, N.S., Zucker, L.A. (2011) Tinnitus-related distress: a review of recent findings. Curr Psychiatry. Rep 13(1), 31–36.

Manohar, S., Spoth, J., Radziqon, K., Auerbach, B., Salvi, R. (2017). Noise-induced hearing loss induces loudness intolerance in a rat active sound avoidance paradigm (ASAP). Hearing Research. 353,197-203.

Margol-Gromada, M., Sereda, M., Baguley, D.M. (2020). Readability assessment of self-report hyperacusis questionnaires. Int J Audiol. 59(7), 506-512.

Minor, L.B., Cremer, P.D., Carey, J.P., Della Santina, C.C., Streubel, S.O., Weg, N. (2001) Symptoms and signs in superior canal dehiscence syndrome. Ann N Y Acad Sci. 942, 259–273.

Mohrle, D., Hofmeier, B., Amend, M., Wolpert, S., Ni, K., Bing, D., Klose, U., Pichler, B., Knipper, M., Ruttiger, L. (2019). Enhanced Central Neural Gain Compensates Acoustic Trauma-induced Cochlear Impairment, but Unlikely Correlates with Tinnitus and Hyperacusis. Neurosci. 407, 146-169.

Oghalai, J.S. (1997). Hearing and Hair Cells. Hear Hair Cells. Nat Inst Health.

Radziwon, K.E., Manohar, S., Auerbach, B., Liu, X., Guang-Di, C., Salvi, R. (2020). Preclinical Animal Behavioral Models of Hyperacusis and Loudness Recruitment. New Therapies to Prevent or Cure Auditory Disorders. 135-157.

Salloum, R., Yurosko, C., Santiago, L., Sandridge, A., Kaltenbach, A. (2014). Induction of enhanced acoustic startle response by noise exposure: dependence on exposure conditions and testing parameters and possible relevance to hyperacusis. PloS One. 9: e111747.

Sammeth, C.A., Preves, D.A., Brandy, W.T. (2000). Hyperacusis: case studies and evaluation of electronic loudness suppression devices as a treatment approach. Scand Audiol. 29(1), 28-36.

Schecklmann, M., Landgrebe, M., Langguth, B., (2014). Phenotypic characteristics of hyperacusis in tinnitus. PloS One. 9(1), e86944.

Shore, S.E. (2011). Plasticity of somatosensory inputs to the cochlear nucleus—implications for tinnitus. Hear Res. 281(1-2), 38-46.

Turner, J. and Parrish, J. (2008). Gap detection methods for assessing salicylate-induced tinnitus and hyperacusis in rats. Am. J. Audiol. 17, S185-S192.

Tyler, R.S., Pienkowski, M., Roncancio, E.R., Jun, H.J., Brozoski, T., Dauman, N., Dauman, N., Andersson, G., Keiner, A.J., Cacace, A.T., Martin, N., Moore, B.C. (2014). A review of hyperacusis and future directions: part I. Definitions and manifestations**.** Am J Audiol.. 23, 402-419.

Valente, M., Goebel, J., Duddy, D., Sinks, B., Peterin, J. (2000). Evaluation and treatment of severe hyperacusis*.* J Am Acad Audiol. 11, 295-299.

Weber, H., Pfadenhauer, K., Stohr, M., Rosler, A. (2002) Central hyperacusis with phonophobia in multiple sclerosis. Mult Scler. 8(6): 505–509.

Zhou, J., Nannapaneni, N., Shore, S. (2007). Vesicular glutamate transporters 1 and 2 are differentially associated with auditory nerve and spinal trigeminal inputs to the cochlear nucleus. J Comp Neurol. 500, 777–787.

Zhou, J., Shore, S. (2004). Projections from the trigeminal nuclear complex to the cochlear nuclei: a retrograde and anterograde tracing study in the guinea pig. J Neurosci Res. 78, 901–907.

Chapter 3

A Spinal Circuit That Transmits Innocuous Cool Sensations [1]

Abstract

Temperature information is precisely processed in the nervous system. Following identification of thermoTRP channels, much progress has been made in identifying molecular thermosensors in the periphery that process temperature information. However, although thermosensitive neurons in the dorsal horn have been identified, the precise cellular and molecular identities, micro-circuits, and mechanism of integration of peripheral inputs for temperature sensing in the spinal cord, especially at innocuous temperatures, remains unknown. Here we have identified an essential node in the neural circuitry for innocuous cool sensations. We found that a population of excitatory interneurons co-expressing Calbindin1 and Lbx1 ($Calb1^{Lbx1}$) in the dorsal horn of the spinal cord is activated by innocuous cool temperatures. Genetic ablation or silencing of spinal $Calb1^{Lbx1}$ neurons causes loss of innocuous cool but not noxious cold sensations.

---

[1] Lorraine R Horwitz[1,2,7], Hankyu Lee[1,7], Chia Chun Hor[1], Fred Y Shen[2,3], Wei Cai[4], Chen Li[5], Emily Ling-Lin Pai[3], Tin Long Rex Fung[1], Ilma Rovcanin[1], Kevin P Pipe[5,6], X.Z. Shawn Xu[4], Dawen Cai[3], Bo Duan[1]*

1. Department of Molecular, Cellular, and Developmental Biology, University of Michigan, Ann Arbor, MI 48109, USA.
2. Neuroscience Graduate Program, University of Michigan, Ann Arbor, MI, 48019, USA
3. Department of Cellular Developmental Biology, University of Michigan, Ann Arbor, MI 48109, USA.
4. Life Sciences Institute, University of Michigan, Ann Arbor, MI 48109, USA; Department of Molecular and Integrative Physiology, University of Michigan, MI 48109, USA.
5. Department of Mechanical Engineering, University of Michigan, Ann Arbor, MI 48109, USA.
6. Department of Electrical Engineering and Computer Science, University of Michigan, Ann Arbor, MI 48109, USA.
7. These authors contributed equally.

Further Brainbow labelling with expansion microscopy and electrophysiology showed that a small cluster of spinal Calb1^{Lbx1} interneurons in lamina I and the outer layer of lamina II represents the cooling-transmission neurons. These neurons receive monosynaptic connections from TRPM8^{+} primary sensory neurons and amplify the activity of cool-sensitive spinoparabrachial projection neurons. Our findings reveal a microcircuit in the dorsal spinal cord that specifically transmits innocuous cool sensations.

Introduction

External temperatures are first detected in the skin and then transmitted via primary sensory neurons in the dorsal root ganglia (DRG) to the dorsal horn of the spinal cord for somatosensory integration (Montell and Caterina, 2007; Palkar et al., 2015; Patapoutian et al., 2003; Xiao and Xu, 2021). Thermal sensors for temperatures ranging from noxious heat/innocuous warm to innocuous cool/noxious cold allow the body to maintain homeostasis and protect against injury. Several members of the transient receptor potential (TRP) ion channel family have been classified as thermal sensors in mammals based on their ability to respond to a variety of stimuli ranging from noxious heat (TRPV1, TRPA1 and TRPM3) (Caterina et al., 2000; Caterina et al., 1997; Vandewauw et al., 2018) to innocuous cool (TRPM8) (Bautista et al., 2007; Colburn et al., 2007; Dhaka et al., 2007; McKemy et al., 2002; Milenkovic et al., 2014; Peier et al., 2002). TRPM8 is a ligand-gated, nonselective cation channel that is activated by cool temperatures (22-27 °C) and by exogenous chemical agonists menthol and icilin (McKemy et al., 2002; Peier et al., 2002). TRPM8 channels are expressed in a subset of primary sensory neurons in the DRG (McKemy et al., 2002; Peier et al., 2002). Mice

lacking *Trpm8* have severe deficits in the perception of innocuous cooling, but not noxious cold, suggesting the selective function of TRPM8 channels in the DRG for transmitting cool temperatures (Bautista et al., 2007; Colburn et al., 2007; Dhaka et al., 2007). TRPM8^{+} peripheral afferents project predominantly to laminae I and II outer layer (II_o) of the spinal cord (Dhaka et al., 2008). However, the precise identity of the neural circuitry in the spinal cord that transmits cool information remains unknown.

The dorsal horn of the spinal cord is an integral component of the central nervous system for sensory processing. It consists of a complex network of local interneurons and projection neurons (Todd, 2010). *In vivo* single unit recordings and *in vivo* two-photon Ca2^{+} imaging studies have shown that a large population of interneurons and projection neurons in the superficial dorsal horn are thermosensitive (Andrew and Craig, 2001; Bester et al., 2000; Burton, 1975; Chisholm et al., 2021; Christensen and Perl, 1970; Craig and Kniffki, 1985; Craig et al., 2001; Ran et al., 2016). However, the lack of genetic tools and unique promoters to functionally manipulate specific neuronal subtypes makes it challenging to determine the cellular identities of thermosensitive neurons and circuits in the spinal cord.

In this study, using intersectional genetic manipulations (Duan et al., 2014; Pan et al., 2019), we have identified a population of excitatory interneurons co-expressing Calbindin1 (Calbindin-D28K, Calb1) and Lbx1 (hereafter referred to as Calb1^{Lbx1}) in the dorsal horn that is essential to transmit innocuous cool but not noxious cold temperature information. Specifically, we found that a small cluster of Calb1^{Lbx1} interneurons in lamina I and II_o, which does not express the neuropeptide somatostatin (SOM^{-}), is required to transmit innocuous cool sensations. Alternatively, the subset of Calb1^{Lbx1}

interneurons expressing SOM (SOM^+) is required to transmit acute punctate mechanical pain. Finally, we showed that cool-sensitive $TRPM8^+$ sensory neurons monosynapticially innervate $Calb1^{Lbx1}$ interneurons in the superficial dorsal horn and that activation of $Calb1^{Lbx1}$ interneurons amplifies the activity of cool-sensitive spinoparabrachial projection neurons (hereafter referred as SPB neurons). Taken together, these results delineate a spinal circuit that selectively transmits innocuous cool information to the brain.

Results

Characterization of $Calb1^{Lbx1}$ interneurons in the dorsal horn of the spinal cord

The calcium-binding protein Calb1 is expressed across the central nervous system including the DRG, trigeminal ganglion, amygdala, cerebellum, hippocampus, and brainstem (Sequier et al., 1990; Zhang et al., 1990). In the dorsal horn of the spinal cord, Calb1 is present in laminae I-IV (Zhang et al., 1990), suggesting Calb1 may act as a heterogenous marker for multiple sensations. Crossing *Calb1*^{Cre} and *Lbx1*^{Flpo} with a *Cre*- and *Flpo*-dependent Tomato reporter stain *Rosa26*$^{CAG\text{-}ds\text{-}tdTomato}$ (Ai65) (hereafter referred to as *Calb1*^{Lbx1};Ai65), enabled the selective expression of Tomato protein in $Calb1^{Lbx1}$ neurons in the dorsal spinal cord. Immunohistochemical double staining showed that 44.0% (961/2183) of $Tomato^+$ neurons exhibited detectable Calb1 protein expression, and 85.3% (961/1126) of $Calb1^{Lbx1}$ neurons co-expressed Tomato (Figure 3.1A).

To better characterize the cellular identity of $Calb1^{Lbx1}$ neurons in the dorsal horn, sections of the lumbar spinal cord of *Calb1*^{Lbx1};Ai65 mice were immunostained with a panel of specific antibodies against markers of lamina layers. As shown in Figure 3.1B,

we found a small portion of Tomato^{+} neurons were located in the lamina I (10.5%, 38/363) and very few Calb1^{Lbx1} neurons colocalized with Neurokinin 1 receptor (NK1R, a marker of a large population of ascending projection neurons in lamina I) (1.5%, 6/392, Figure 3.1B and S3.1). We also observed that Calb1^{Lbx1} neurons were intermingled with both calcitonin gene-related peptide (CGRP) terminals in laminae I-II$_o$ (15.9%, 325/2039) and isolectin B4 (IB4) terminals in the dorsal part of lamina II inner layer ($_d$II$_i$) (23.4%, 742/3171) (Figure 3.1B). The largest populations of Calb1^{Lbx1} neurons were located in the ventral part of lamina II$_i$ ($_v$II$_i$) to the dorsal part of lamina III ($_d$III) (31.2%,1015/3253), which is marked by the expression of protein kinase Cγ (PKCγ), and the ventral to the PKCγ zone in lamina III-IV (33.0%, 941/2855) (Figure 3.1B). To further identify types of Calb1^{Lbx1} neurons, *in situ* hybridization and immunohistochemistry approaches were used. Figure 3.1B shows that the vast majority of Calb1^{Lbx1} neurons express vesicular glutamate transporter 2 (VGLUT2) mRNA (91.8%, 1692/1844), while only a small population of Calb1^{Lbx1} neurons express markers of inhibitory interneuron such as glutamic acid decarboxylase isoform 67 (GAD67)/glycine transporter 2 (GlyT2) mRNAs (9.0%, 180/2005) or paired box gene 2 (Pax2) protein (4.9%, 283/5793). These results indicate that Calb1^{Lbx1} neurons mainly represent a heterogeneous population of excitatory interneurons in laminae I-IV of the spinal cord.

Innocuous cool temperatures activate Calb1^{Lbx1} neurons in the superficial dorsal horn

It is well established that acetone evaporation mimics cool temperatures, but not noxious cold temperatures in the range of 15-20 °C (Bautista et al., 2007). Here, we explored whether Calb1^{Lbx1} neurons are cool-sensitive. To do this, acetone was topically administered to the right hindpaw of *Calb1^{Lbx1}*;Ai65 mice and the expression of the nuclear immediate early gene c-Fos in the lumbar spinal cord was assessed. We found that acetone treatment induced c-Fos protein expression in Tomato-expressing Calb1^{Lbx1} neurons in the ipsilateral spinal cord compared to naïve control mice (Figure 3.1C and 3.1D), and about half (49.6%, 69/139) of the Fos^{+} neurons were Tomato^{+} (Figure 3.1C and 3.1E). Interestingly, most Fos^{+};Tomato^{+} neurons were located in lamina I-II, suggesting that innocuous cool temperatures activate Calb1^{Lbx1} neurons in the superficial dorsal horn.

Ablation of Calb1^{Lbx1} neurons results in innocuous cool sensing deficits

To further assess the function of Calb1^{Lbx1} neurons in transmitting innocuous cool sensations, we genetically ablated Calb1^{Lbx1} neurons in the dorsal spinal cord using an intersectional genetic strategy (Figure S3.2A), and then performed a battery of somatosensory behavioral paradigms. The ablation of Calb1^{Lbx1} neurons was performed by injecting *Calb1^{Lbx1};Tau$^{ds\text{-}DTR}$* mice (which also carried a *Cre*-dependent Tomato reporter allele) with DTX (hereafter referred to as Calb1^{Abl} mice), resulting in a 91% reduction of Tomato^{+} neurons in the dorsal spinal cord (Figure 3.2A). It is worth mentioning that Calb1^{Cre} neurons in the brain, including somatosensation-related brain

regions (the parabrachial nucleus and somatosensory cortex), were not ablated in Calb1^{Abl} mice (Figure S3.2B).

To test locomotion in Calb1^{Abl} mice, we performed the rotarod assay and found that locomotor coordination remained intact in the ablated group (Figure S3.3A). Next, we assessed deficits in thermal temperature sensing in Calb1^{Abl} mice. As a first test, we asked whether acetone evaporation-induced cooling sensations were intact in Calb1^{Abl} mice. Following delivery of acetone to the plantar region of the hindpaw, we observed nocifensive responses that could be scored on a scale of 0 (no response or touch only without flinch) to 4 (noxious responses such as guarding, vocalizations, and escape behaviors). Compared to control littermates, Calb1^{Abl} mice showed nearly abolished responses to the innocuous cool stimuli (Figure 3.2B).

Next, we asked whether Calb1^{Abl} mice also exhibit deficits in their ability to discriminate between warm and cool using the two-temperature preference assay. Mice were given the choice between two temperature plates: a reference plate set to 30 °C and a test plate set to a fixed temperature from 10 °C to 50 °C. The percentage of time spent on the 30 °C surface was measured over a 5-minute period. When placed on equivalent temperatures (30 °C), both control and Calb1^{Abl} mice spent an equal amount of time on each plate (Figure 3.2C). When the test plate was set to 20 °C, control mice showed a clear preference for the reference plate at 30 °C. By contrast, Calb1^{Abl} mice did not display a preference, spending nearly equal amounts of time on each side. Nonetheless, Calb1^{Abl} mice displayed a normal preference for 30 °C at noxious cold (10 °C), noxious heat (50 °C), and warm (40 °C) temperatures. Next, we compared the

response of Calb1^{Abl} mice to 20 °C versus 10 °C, and found that Calb1^{Abl} mice did not show a deficit in this temperature-sensing test (Figure 3.2C).

To assess the thermal detection range of Calb1^{Abl} mice, the temperature gradient assay was performed. Mice were allowed to freely move across a surface temperature gradient of 5 °C to 50 °C. As shown in Figure 3.2D, Calb1^{Abl} mice spent significantly more time in the 17.5-20 °C temperature range and significantly less time in the 27.5-30 °C temperature range compared to controls, confirming innocuous cool sensing deficits. Neither control nor Calb1^{Abl} mice spent time in the temperature ranges of noxious cold (5-15 °C) and noxious heat (40-50 °C). Consistently, when mice were exposed to a cold plate (0 °C), a hot plate (46, 50, or 54 °C), or received dry ice application to the hindpaw, there was no significant difference in nocifensive responses to noxious cold or noxious heat stimuli between Calb1^{Abl} and control mice (Figure 3.2E, 3.2F, and S3.3H). Furthermore, rectal temperature was not significantly different between control (37.0 ± 0.2 °C) and Calb1^{Abl} mice (36.9 ± 0.3 °C). Overall, temperature-sensing deficits were observed in Calb1^{Abl} mice exclusively at innocuous cool temperatures, suggesting Calb1^{Lbx1} neurons in the dorsal spinal cord play an essential role in innocuous cool sensing but not noxious cold.

Additional somatosensory assays were used to measure mechanosensitivity in control and Calb1^{Abl} mice. We found that ablation of Calb1^{Lbx1} neurons led to a dramatic increase in the threshold for acute punctate mechanical pain (Figure 3.2G and S3.3F). However, there was no significant difference in sharp mechanical pain as measured by the pinch and pinprick assays (Figure S3.3D and S3.3E). We also observed that Calb1^{Abl} mice displayed a decreased nocifensive response to the gentle touch of a

paintbrush lightly brushed across the glabrous skin of the hindpaw (Figure S3B), but no difference in nocifensive responses to an innocuous sticky presentation to the glabrous skin of the hindpaw (Figure S3.3C).

Silencing Calb1^{Lbx1} neurons results in innocuous cool deficits

To ensure that the observed behavioral results could not be attributed to potential secondary effects due to spinal circuits reorganization after neuronal ablation, we used intersectional strategies to transiently silence spinal Calb1^{Lbx1} neurons by crossing *Calb1^{Cre}, Lbx1^{Flpo}* with a *Cre*- and *Flpo*-dependent hM4Di designer receptors exclusively activated by a designer drug (DREADD) strain *Rosa26$^{CAG\text{-}ds\text{-}hM4Di}$* (hereafter referred to as Calb1^{Silenced}) (Figure S3.4A). Clozapine N-oxide (CNO) was used to activate hM4Di thereby silencing spinal Calb1^{Lbx1} neurons, resulting in greatly attenuated responses to innocuous cool stimuli (Figure 3.3A-3.3C), whereas noxious cold sensations were unaffected (Figure 3.3D and 3.3E). Specifically, acute silencing of Calb1^{Lbx1} neurons resulted in a significant deficit in acetone-induced nocifensive responses (Figure 3.3A), compared to both baseline (before CNO treatment) and CNO-treated controls. In the two-temperature preference assay, Calb1^{Silenced} mice displayed a significant deficit in time spent in the 20 °C chamber, with no differences recorded at any other temperature (Figure 3.3B). Additionally, Calb1^{Silenced} mice spent significantly less time at the 27.5-30 °C temperature range, with the majority of time spent at cooler temperatures (Figure 3.3C). While Calb1^{Silenced} mice displayed innocuous cool sensing behavior deficits, their ability to detect noxious cold stimuli was not affected in response to a 0 °C cold plate (Figure 3.3D), or dry ice application to the hindpaw (Figure 3.3E). Calb1^{Sileneced} mice

also exhibited a significant increase in von Frey threshold (Figure 3.3F) and gentle touch deficits to light brushing (Figure S3.4C), while locomotion, innocuous touch, sharp mechanical pain, and thermal heat sensations remained intact (Figure S3.4B and S3.4D-S3.4H). Rectal temperature was not significantly different between control (37.3 ± 0.2 °C) and Calb1^{Silenced} (35.7 ± 1.2 °C) mice after CNO injection. Taken together, our results suggest that Calb1^{Lbx1} neurons represent a functionally diverse population in the dorsal spinal cord and are required to transmit innocuous cooling, acute punctate mechanical pain, and touch sensations.

A subpopulation of Calb1^{Lbx1} neurons is responsible for innocuous cool sensing

To identify Calb1^{Lbx1} subpopulations responsible for innocuous cool sensing or acute punctate mechanical pain, we examined the overlap with a known marker of spinal excitatory interneurons, somatostatin (SOM) (Figure 3.4A). *In situ* hybridization experiments revealed that Calb1^{Lbx1} neurons highly overlapped with SOM (44%, 949/2157) in lamina II. Using the same intersectional genetic strategy, we ablated SOM^{Lbx1} neurons in the dorsal spinal cord and examined behavioral responses to thermal stimuli (Figure 3.4B-4D). We found that there was no significant difference between SOM^{Abl} and control mice in either the acetone evaporation assay (Figure 3.4B), the two-temperature preference assay (Figure 3.4C), or the temperature gradient assay (Figure 3.4D). Furthermore, noxious cold sensing remained intact (Figure 3.4C, 3.4D, and S3.5B). Consistently, few SOM^{+} neurons were activated after a cool stimulus was presented (Figure S3.5A). All together, these results suggest that SOM^{+} neurons are dispensable for cool sensing. Of note, SOM^{Lbx1} neurons are shown to be

responsible for acute punctate mechanical pain (Duan et al., 2014), therefore the mechanical pain deficits exhibited in Calb1^{Abl} mice (Figure 3.2G), which are similar to the deficits in SOM^{Abl} mice (Figure 3.4E), could be attributed to Calb1^{Lbx1};SOM^{+} neurons. These results suggests that Calb1^{Lbx1};SOM^{-} neurons may form a subpopulation that transmits innocuous cool sensations, whereas Calb1^{Lbx1};SOM^{+} neurons may be required for sensing acute punctate mechanical pain (Figure 3.4F).

Calb1^{+} neurons in the superficial dorsal horn receive inputs from TRPM8^{+} primary sensory neurons

Previous studies have shown that the TRPM8 channel, a non-selective cation channel, is sensitive to innocuous cool stimuli (McKemy et al., 2002; Peier et al., 2002). We asked whether TRPM8^{+} neurons in the DRG are the primary sensory neurons that provide inputs to Calb1^{Lbx1} neurons in the spinal cord. For this, we injected the TRPM8 agonist icilin into the hindpaw and recorded cool-induced (wet-dog shaking) behavioral responses. Compared to control littermates, Calb1^{Abl} mice showed nearly abolished wet-dog shaking responses (Figure 3.5A), but no change in acute nocifensive behaviors due to the intraplantar injection (Figure S3.6A). To further investigate the connection between TRPM8^{+} sensory neurons and Calb1^{+} neurons in the dorsal horn at a synaptic level, we crossed *Calb1^{Cre}* and *TRPM8^{GFP}* mice, then retro-orbitally injected *Calb1^{Cre}*; *TRPM8^{GFP}* mice with a *Cre*-dependent AAV-PHP.eB Brainbow virus that can stochastically express either teal fluorescent protein (TFP) or mCherry (mCh) fluorophores. This allowed us to sparsely label Calb1^{+} neurons in the spinal cord (hereafter referred to as Calb1^{Brainbow}) without infecting the DRG (Figure S6B).

Expansion microscopy was then utilized to obtain the nano-scale resolution necessary for synaptic identification without the use of super-resolution light microscopy (Figure 3.5B and 3.5C). Colocalization of pre- and post-synaptic markers, Bassoon and Homer, respectively, with Calb1^{Brainbow} and TRPM8^{GFP} were used to identify monosynaptic connections between TRPM8^{+} cooling inputs and Calb1^{+} spinal neurons (Figure 3.5C). Quadruple-positive synaptic interactions were identified predominantly in the TRPM8-innervation zone located in lamina I-II$_o$ (Figure 3.5D and 3.5E), with unique multi-synaptic clusters identified (Figure S3.6C), suggesting that TRPM8^{+} cooling fibers synapse onto Calb1^{+} neurons in the superficial dorsal horn of the spinal cord. The monosynaptic connections from TRPM8^{+} sensory neurons to Calb1^{+} neurons were further confirmed by a pseudotyped rabies virus-based retrograde tracing combined with RNAscope staining in *Calb1^{Cre};Lbx1^{Flpo};Rosa26$^{ds\text{-}HTB}$* mice (Figure S3.6D-S3.6F).

Cooling-sensitive neurons in lamina I were previously described as pyramid cells, while polymodal heat-pinch-cold neurons were described as multipolar cells (Han et al., 1998). The sparse labeling of Calb1^{+} neurons in the dorsal horn allowed us to identify the morphology of Calb1^{Brainbow} neurons that received TRPM8^{+} inputs (Figure 3.5D-3.5F). We found that TRPM8-innervating Calb1^{Brainbow} neurons exhibit diverse morphologies, with somas located in the TRPM8-innervation zone (lamina I-II$_o$) (Figure 3.5F). While the majority of dendrites were located in lamina I-II$_o$ (green neurons in Figure 3.5F), several examples of neurons with at least one dendritic branch outside of lamina I-II$_o$ were identified (magenta neurons in Figure 3.5F), suggesting those neurons may also receive inputs from deeper layers of the dorsal horn.

Two distinct Calb1^{Lbx1} subpopulations in the superficial dorsal horn

To further characterize the Calb1^{Lbx1} spinal subpopulations and their sensory inputs, we performed whole-cell patch clamp recordings from Tomato^{+} spinal neurons across laminae I-II in naïve *Calb1^{Lbx1}*;Ai65 mice (Figure 3.6A and 3.6C), and then performed RT-PCR analysis to determine the type of neurons from which recordings were performed (Calb1^{Lbx1};SOM^{+} or Calb1^{Lbx1};SOM^{-}; Figure S3.8A and S3.8B). As a starting point, we characterized the firing pattern of recorded neurons and found that the firing pattern was similar between both populations, with the majority displaying an initial bursting pattern (Figure 3.6B and 3.6D). Next, we used high-frequency stimulation to characterize the monosynaptic/polysynaptic inputs to Calb1^{Lbx1} neurons. Evoked excitatory postsynaptic currents (eEPSCs) and action potentials (APs) were recorded under normal condition or under disinhibition conditions with the presence of strychnine and bicuculline (Str & Bic) to block glycine receptors and $GABA_A$ receptors, respectively. We found that 80.0% (28/35) of Calb1^{Lbx1};SOM^{-} neurons in lamina I-II$_o$ received C fiber inputs under normal condition, 68.6% (24/35) of Calb1^{Lbx1};SOM^{-} neurons received monosynaptic C fiber inputs, and 54.3% (19/35) of Calb1^{Lbx1};SOM^{-} neurons generated APs (Figure 3.6E and S3.7H). Under disinhibition condition, 75.0% (24/32) of Calb1^{Lbx1};SOM^{-} neurons received monosynaptic C fiber and 71.9% (23/32) of Calb1^{Lbx1};SOM^{-} neurons generated APs (Figure 3.6E and S3.7H). By contrast, none of Calb1^{Lbx1};SOM^{-} neurons in lamina I-II$_o$ received Aβ fiber inputs and very few receive Aβfiber inputs, even under disinhibition condition (Figure 3.6E, S3.7F and S3.7G).

Most TRPM8^{+} primary sensory neurons are unmyelinated C nociceptors and could mediate the C-fiber evoked APs. Application of icilin to acutely disassociated

TRPM8^{GFP} DRG neurons evoked Ca^{2+} influx in a dose dependent manner, with all neurons responding beginning at 1 μM, thereby mimicking cool-temperature induced activation of TRPM8^{GFP} DRG neurons (Figure S3.7A-S3.7C). To examine whether TRPM8^{+} C fibers activate Calb1^{Lbx1};SOM^{-} neurons in lamina I-II$_o$, a specialized two-chamber recording apparatus was used to isolate the intact and attached DRG in a separate chamber from the spinal cord (Figure S3.7D). Application of icilin (1 μM) to the DRG chamber but not the spinal cord chamber elicits large EPSCs (Icilin-EPSCs or I-EPSCs) and AP responses (Icilin-APs or I-APs) in neurons located in lamina I-II$_o$ (Figure S3.7E). We then recorded from Calb1^{Lbx1};SOM^{-} neurons in lamina I-II$_o$ using icilin application to the DRG chamber. We found that 37.1% (13/35) of Calb1^{Lbx1};SOM^{-} neurons in lamina I-II$_o$ generated icilin-evoked EPSCs (Figure 3.6F and 3.6H), all of which were blocked by co-application of TRPM8 antagonist, AMTB, to the DRG chamber (Figure 3.6I and 3.6J), suggesting that the Calb1^{Lbx1};SOM^{-} subpopulation receives C fiber inputs from TRPM8^{+} primary sensory neurons. Interestingly, 8 out of 13 icilin-responding neurons generated APs (Figure 3.6H), and all exhibited initial bursting firing pattern (Figure 3.6H) and received monosynaptic C fiber-inputs (Figure S3.8A). These results indicate the presence of a unique subpopulation of Calb1^{Lbx1};SOM^{-} neurons in lamina I-II$_o$ is cooling-sensitive.

Next, we examined the sensory inputs to Calb1^{Lbx1};SOM^{+} neurons in lamina I-II. We found that few recorded Calb1^{Lbx1} neurons in lamina I were SOM^{+} and the majority of Calb1^{Lbx1};SOM^{+} neurons were located in lamina II$_i$ (Figure 3.6C). In total, 30 Calb1^{Lbx1};SOM^{+} neurons in lamina II were recorded under normal conditions, 40.0% (12/30) of Calb1^{Lbx1};SOM^{+} neurons received C fiber inputs and 23.3% (7/30) of

Calb1^{Lbx1};SOM^{+} neurons generated AP outputs (Figure 3.6E, S3.7K and S3.8B). Under disinhibition condition, 51.8% (14/27) of Calb1^{Lbx1};SOM^{+} neurons received C fiber inputs and 29.6% (8/27) of Calb1^{Lbx1};SOM^{+} neurons generated AP outputs (Figure 3.6E, S3.7K and S3.8B). In addition, we found that about half of Calb1^{Lbx1};SOM^{+} neurons in lamina II received Aβ fiber and (or) Aδ inputs (Figure 3.6E, S3.7I, S3.7J and S3.8B). Interestingly, we found that none of Calb1^{Lbx1};SOM^{+} neurons in lamina II generated icilin-EPSCs or icilin-APs (Figure 3.6G, 3.6H and S3.8B), suggesting that Calb1^{Lbx1};SOM^{+} neurons do not receive inputs from TRPM8^{+} primary sensory neurons. Given the loss of acute punctate mechanical pain in SOM^{Abl} and Calb1^{Abl} mice, C fiber sensory neurons that form synaptic connections with Calb1^{Lbx1};SOM^{+} neurons in lamina II likely represent mechanical nociceptors.

Calb1^{Lbx1} interneurons amplify the activity of cooling-sensitive SPB neurons

In lamina I, ~95% of spinal projection neurons target the lateral parabrachial nucleus (Todd, 2010). To determine whether Calb1^{Lbx1} spinal neurons that transmit cool sensations are interneurons or projection neurons, we first bilaterally injected fluorophore-conjugated cholera toxin subunit-B (CTB) into the lateral parabrachial nucleus followed by acetone administration onto the hindpaw to induce c-Fos expression in the ipsilateral spinal cord (Figure 3.7A and 3.7B). Although double-positive neurons (CTB^{+} and Fos^{+}) representing cool-sensitive SPB neurons were detected, none of the cooling-sensitive SPB neurons were Tomato^{+} in *Calb1^{Lbx1}*;Ai65 mice (Figure 3.7C), confirming that Calb1^{Lbx1} neurons are local interneurons and not cooling-sensitive SPB neurons.

To examine the function of Calb1^{Lbx1} neurons in the cooling-transmission pathway, we recorded from CTB-labeled SPB neurons in control and Calb1^{Abl} naïve mice using the two-chamber recording system (Figure 3.7D). Icilin application to the DRG chamber was used to identify cooling-sensitive SPB neurons. We found that the vast majority of SPB neurons exhibit an initial bursting pattern in both groups (Figure 3.7D and 3.7E). Next, we examined the sensory inputs to recorded SPB neurons. In control mice, all recorded SPB neurons in lamina II$_o$ received C fiber inputs and 84.0% (21/25) of SPB neurons generated APs (Figure 3.7D and 3.7F). In Calb1^{Abl} mice, 86.4% (19/22) of recorded SPB neurons received C fiber inputs and 63.6% (14/22) of recorded SPB neurons generated APs (Figure 3.7E and 3.7F). Compared to control animals, ~26% (1-63.6/86.4) of SPB neurons were not activated by C fiber inputs after ablating Calb1^{Lbx1} neurons. We also detected a small portion of SPB neurons that received polysynaptic Aβ inputs and mono/polysynaptic Aδ inputs in control mice (Figure 3.7F). However, Aβ/Aδ evoked APs were abolished in Calb1^{Abl} mice, suggesting a small population of Calb1^{Lbx1} neurons may link Aβ/Aδ inputs with SPB neurons. Next, we recorded icilin (1 μM)-evoked EPSCs and APs in cooling-sensitive SPB neurons. We found that icilin-evoked EPSCs and APs in 52.0% (13/25) and 24.0% (6/25) of SPB neurons in control mice, respectively (Figure 3.7D and 3.7F). By contrast, a small portion of icilin-evoked EPSCs (36.4%, 8/22) and no icilin-evoked APs (0%, 0/22) were recorded in SPB neurons of Calb1^{Abl} mice (Figure 3.7E and 3.7F), consistent with the reduction of C fiber-evoked EPSCs and APs in Calb1^{Abl} mice. Interestingly, cooling-sensitive SPB neurons display a right-shifted icilin-EPSCs dose response curve in Calb1^{Abl} mice compared to controls (Figure 3.7G) with significance reductions in icilin-

EPSCs (Figure 3.7H) and icilin-APs (Figure 3.7I) at different concentrations of icilin. These results suggest that Calb1^{Lbx1} spinal interneurons are essential for the activation of cooling-sensitive SPB neurons, opening up the possibility that Calb1^{Lbx1} interneurons may act as a cool-signal amplifier to prioritize cool temperature information for projection neuron integration in the spinal cord (Figure 3.7J).

Discussion

In the present study, we demonstrated the presence of a subpopulation of Calb1^{Lbx1} excitatory interneurons in the superficial spinal cord that is essential for innocuous cool temperature transmission, but not noxious cold. Particularly, we identified at least two functionally distinct subpopulations of Calb1^{Lbx1} neurons in lamina I-II of the dorsal horn of the spinal cord: 1) a Calb1^{Lbx1};SOM^{-} subpopulation of excitatory interneurons in lamina I-II$_o$ that transmits cool sensations, and 2) a Calb1^{Lbx1};SOM^{+} subpopulation of excitatory interneurons in lamina II that transmits acute punctate mechanical pain. In lamina I-II$_o$, most Calb1^{Lbx1} neurons are SOM^{-} and receive C-fiber inputs. Cooling-activated Calb1^{+} neurons cover ~50% Calb1^{Lbx1};SOM^{-} neurons in lamina I-II$_o$ (Figure 3.6E). Lamina I-II$_o$ Calb1^{Lbx1};SOM^{-} neurons are innervated by TRPM8^{+} C-cooling neurons and amplify cooling signals to projection neurons in lamina I. However, we do not exclude the possibility that the TRPM8-innervated Calb1^{+} neurons may be polymodal.

In lamina II, most neurons receive C and Aδ inputs directly and some neurons also receive polysynaptic inputs from Aβ fibers (Braz et al., 2014; Todd, 2010). MrgprD^{+} polymodal nociceptors innervate multiple types of interneurons in lamina II (Wang and Zylka, 2009). Interestingly, ablation of MrgprD^{+} nociceptors or SOM^{+} interneurons in the

dorsal horn of the spinal cord attenuated acute punctate mechanical pain (Cavanaugh et al., 2009; Duan et al., 2014). Thus MrgprD$^+$ nociceptors may connect with Calb1$^+$;SOM$^+$ interneurons for transmitting acute punctate mechanical pain. Previous single-cell RNA sequence results showed that Calb1 partially overlaps with CCK and neurotensin (NTs) in lamina III (Haring et al., 2018; Russ et al., 2021). Ablation of CCK$^+$ neurons impaired brush-induced paw withdrawal responses and activation of NTs$^+$ neurons in lamina III facilitated brush-induced paw withdrawal responses (Gatto et al., 2021). Our results suggest that Calb1$^+$;CCK$^+$;NTs$^+$ interneurons in lamina III may be required for transmitting innocuous paw withdrawal responses.

Previous *in vivo* single unit recording studies showed that an innocuous cool stimulus can activate two groups of spinal neurons: (1) “COOL” neurons responding selectively to innocuous cool, and (2) CMH neurons responding to innocuous cool, noxious mechanical (pinch) and heat stimuli (Craig et al., 2001). Consistently, *in vivo* imaging results in lamina I SPB neurons confirmed that there are two populations of cooling-sensitive neurons: cooling-specific projection neurons (14%) and polymodal projection neurons that response to cool, cold, pinch and heat (76%) (Chisholm et al., 2021). Under this paradigm it is possible that distinct spinal populations for cold/cool sensing exist, in particular, a population specific for innocuous cool sensation and a population of polymodal (combination of cold/cool, mechanical pain, and/or heat pain) neurons for burning sensation. Lamina I projection neurons receive monosynaptic connections from the DRG (Grudt and Perl, 2002) and interneurons in lamina I and II (Luz et al., 2010). Our present study reveals a feed-forward microcircuit that transmits innocuous cool sensations in the superficial dorsal horn. In this circuit, a small cluster of

Calb1^{Lbx1};SOM^{-} neurons (~23%, 8/35, Figure 3.6H) in lamina I-II$_o$, exhibits an initiate bursting firing pattern and receives monosynaptic inputs from TRPM8^{+} cooling-sensitive primary sensory neurons. Activation of TRPM8^{+} neurons is able to evoke AP firing in Calb1^{Lbx1};SOM^{-} neurons, and pharmacological silencing of Calb1^{Lbx1} neurons largely attenuated the activity of cooling-sensitive SPB neurons. There results suggest that the Calb1^{Lbx1};SOM^{-} subpopulation of neurons presents a potent source of excitatory signaling that could amplify cooling afferent outputs to cooling-sensitive SPB neurons. Further studies characterizing the synaptic connections from Calb1^{Lbx1};SOM^{-} neurons to cooling-sensitive SPB neurons will advance our understanding of the role in cool transmission.

Taken together, our present study has identified a small cluster of Calb1^{Lbx1} excitatory interneurons in the superficial dorsal spinal cord that acts as a critical node in a circuit linking cooling-sensitive TRPM8^{+} primary sensory neurons and SPB neurons for innocuous cooling transmission from the skin to the brain.

Methods

STAR★Methods

KEY RESOURCES TABLE

Reagent or Compound	Source	Identifier
Antibodies		
Rabbit anti-NK1R	MilliporeSigma	Cat#S8305; RRID: AB_261562
Rabbit anti-α-CGRP	Peninsula Lab	Cat# T-4032; RRID: AB_2307330
Alexa Fluor 647-conjugated Isolectin GS-IB4	ThermoFisher	Cat#I32450; RRID: SCR_014365
Rabbit anti-PKCγ	Santa Cruz	Cat# sc-211; RRID: AB_632234
Rabbit anti-Pax2	ThermoFisher	Cat# 71-6000; RRID: AB_2336046
Rabbit anti c-Fos	Abcam	Cat# ab190289, RRID:AB_2737414
Goat anti-Rabbit IgG (H+L) Alexa Fluor plus 647	ThermoFisher	Cat# A32733; RRID: AB_2633282
Goat anti-Mouse IgG (H+L) Alexa Fluor plus 488	ThermoFisher	Cat# A32723; RRID: AB_2633275
Goat anti-Rabbit IgG (H+L) Alexa Fluor plus 488	ThermoFisher	Cat# A32731; RRID: AB_2633280
Mouse anti-Calb1	EnCor Biotech	Cat# MCA-5A9 RRID:AB_2572239
Chicken anti-Homer	Synaptic Systems	Cat# 160 006 RRID:AB_2631222
Guinea Pig anti-Bassoon	Synaptic Systems	Cat# 141 004 RRID:AB_2290619
Rabbit anti-mCherry	Cai Lab custom made	NA
Rabbit anti-TFP	Cai Lab custom made	NA
Sheep anti-GFP	Biorad	Cat# 4745-1051
Donkey anti-Sheep IgG (H+L) Alexa Fluor plus 488	Jackson Immunoresearch	Cat# 713-546-147 **RRID:** AB_2340746
Donkey anti-rabbit IgG (H+L) Alexa Fluor plus Cy3	Jackson Immunoresearch	Cat# 711-166-152 **RRID:** AB_2313568
Donkey anti guinea pig IgG (H+L) Alexa Fluor plus 594	Jackson Immunoresearch	Cat# 706-585-148 **RRID:** AB_2340474
Donkey anti chicken IgG (H+L) Alexa Fluor plus 647	Jackson Immunoresearch	Cat# 703-606-155 **RRID:** AB_2340380
Bacterial and Viral Strains		
EnvA-pseudotyped G-deleted-mCherry rabies virus	Generated by Cai lab	Addgene #32636
pAAVPHPeB-EF-mChT(Bb1.0)	Generated by Cai lab	NA
Cholera Toxin Subunit B (Recombinant), Alexa Fluor 488 Conjugate	ThermoFisher	Cat# C34775
Cholera Toxin Subunit B (Recombinant), Alexa Fluor 647 Conjugate	ThermoFisher	Cat# C34778
Chemicals, Peptides and Recombinant Proteins		
Diphtheria toxin	Millipore Sigma	Cat# D0564
Clozapine N-oxide (CNO)	Millipore Sigma	Cat# C0832
Icilin	Millipore Sigma	Cat# I9532

AMTB hydrochloride	Tocris	Cat# 3989
Acetone	Millipore Sigma	Cat# 650501
Strychnine	Millipore Sigma	Cat# S0532
Bicuculline	Millipore Sigma	Cat# B7561
Experimental Models: Organisms / Strains		
Mouse: B6;129S-*Calb1*$^{tm2.1(cre)Hze}$/J	Jackson Laboratory	Cat# 028532
Mouse: **SOM-IRES-Cre**	Jackson Laboratory	Cat # 013044
Mouse: *B6;129S-Lbx1 < tm1(flpo)Gou > (Lbx1-Flpo)*	Generated by Goulding Lab	Duan et al., 2014
Mouse: *Rosa26*$^{CAG\text{-}LSL\text{-}FSF\text{-}HTB}$	Generated by Goulding Lab	Bourane et al., 2015
Mouse: B6.129-Tau <tm1(LSL.FSF.DTR)Gou>(Tau-loxP-STOP-loxP-FRT-STOP-FRT-DTR)	Generated by Goulding Lab	Duan et al., 2014
Mouse: *B6;129S6-Gt(ROSA)26Sortm9(CAG-mCherry,- CHRM4*)Dym/J (Rosa26*$^{CAG\text{-}FSF\text{-}LSL\text{-}hM4Di}$*)*	Jackson Laboratory	Cat# 029040
Mouse: *B6;129S-Gt(ROSA)26Sortm2.1Ksvo/J*	Jackson Laboratory	Cat# 024846
TRPM8^{GFP}	Generated by Patapoutian Lab	Dhaka et al., 2007
Mouse: Ai14	Jackson Laboratory	007914
Mouse: Ai65	Jackson Laboratory	021875
Oligonucleotides		
GAPDH see table 1	Primer-BLAST	N/A
SOM (Sst) see table 1	Primer-BLAST	N/A
Algorithms and Software		
Adobe Creative Cloud (Illustrator / Photoshop / Premiere Pro)	Adobe	https://www.adobe.com/
ImageJ	NIH	https://imagej.nih.gov/ij/
Prism 6, 9	GraphPad Software	RRID: SCR_002798
MATLAB R2020, 2021	MathWorks	https://www.mathworks.com/products/matlab.html
MetaFluor	Molecular Devices	RRID: SCR_014294
pClamp 10.0	Molecular Devices	RRID: SCR_011323

Experimental Model and Subject Details

All animal experiments were performed in accordance with protocols approved by the Institutional Animal Care and Use Committee at University of Michigan following NIH guidelines. Both male and female mice were used for all experiments. Mice were group housed at room temperature with *ad libitum* access to standard lab mouse pellet food and water on a 12 hours light/12 hours dark cycle. The mouse lines used in the present study were: *Calb1*^{Cre} (#028532, JAX), *SOM*^{Cre} (#013044, JAX), *Rosa26*$^{LSL\text{-}tdTomato}$ (Ai14, #007914, JAX), Ai65 (#021875, JAX), *Lbx1*^{Flpo} (Duan et al., 2014), *Rosa26* $^{CAG\text{-}ds\text{-}hM4Di}$ (#029040, JAX), *Rosa26* $^{CAG\text{-}ds\text{-}ReaChR}$ (#024846, JAX), *Rosa26* $^{CAG\text{-}LSL\text{-}FSF\text{-}HTB}$ (*Rosa26*$^{ds\text{-}HTB}$) (Bourane et al., 2015) and *Tau*$^{LSL\text{-}FSF\text{-}DTR}$ (*Tau*$^{ds\text{-}DTR}$) (Duan et al., 2014). *SOM*^{Cre} mice were crossed with Ai14 reporter mice (*SOM*^{Cre};Ai14) to label the SOM^{Cre}-derived neurons. *Calb1*^{Cre} mice were crossed with *Lbx1*^{Flpo} and *Rosa26*$^{CAG\text{-}ds\text{-}tdTomato}$ (Ai65) reporter mice to label the *Calb1*^{cre} and *Lbx1*^{Flpo}-derived (Calb1^{Lbx1}) neurons. We ablated DTR-expressing neurons as previously described (Duan et al., 2014). 6-10 weeks old mice were intraperitoneally injected with diphtheria toxin (DTX, 50 mg/kg; MilliporeSigma, St. Louis, MO) at day 1, day 4, and day 7. In most strains, we performed behavioral or histochemical experiments 4 weeks after DT injection. *Rosa26* $^{CAG\text{-}ds\text{-}hM4Di}$ mice were crossed with *Calb1*^{Cre} mice and *Lbx1*^{Flpo} mice, clozapine N-oxide (CNO, 5 mg/kg, MilliporeSigma, St. Louis, MO) was injected to acutely silence Calb1^{+} neurons. Behavioral tests were performed 40 minutes after CNO injection. Rectal temperature was assessed after all behavioral experiments were completed. *Calb1*^{Cre} mice were crossed with *TRPM8*^{GFP} mice and injected with AAV-PHP.eB-mCherry-TFP

virus at 6-10 weeks old; 3 to 4 weeks later the mice were perfused for histology experiments.

Method Details

***In Situ* Hybridization and Immunohistochemistry**

In situ hybridization (ISH) procedures were performed to detect mRNA expression as described previously (Pan et al., 2019). Prior to performing ISH, Tomato fluorescent signals were first captured under a fluorescent microscope (Leica DMi8, Germany) for double staining analysis. After ISH, bright field images were converted into pseudo-fluorescent signals and merged onto the Tomato before images in Photoshop (Adobe Photoshop CS6). 3-5 mice per genotype were used for quantitative analysis. Only cells containing nuclei and showing levels of expression or staining clearly above background were scored. To detect protein expression, immunohistochemistry was performed using rabbit anti-NK1R (1:1000, #S8305 MilliporeSigma, St. Louis, MO), rabbit anti-α-CGRP (1:500, #T-4032, Peninsula Lab, San Carlos, CA), Alexa fluor 647-conjugated isolectin GS (IB4) (10 μg/mL, #I32450, ThermoFisher Scientific, Waltham, MA), rabbit anti-PKCγ (1:500, # sc-211, Santa Cruz Biotechnology, Dallas, TX), rabbit anti-Pax2 (1:100, #71-6000,ThermoFisher, Waltham, MA), mouse anti-Calb1 (1:500,# MCA-5A9, EnCor Biotech Gainesville, FL), or rabbit anti-c-Fos (1:500, #ab190289, Abcam, Cambridge, United Kingdom) which were diluted in 0.2% of Triton X-100 and 10% normal goat serum in PBS (blocking buffer) and photographed under a fluorescent microscope.

RNAscope

To detect *TRPM8* mRNA colocalization with rabies virus-induced mCherry expression in presynaptic neurons, RNAscope was utilized. As described previously (Gong et al., 2019), paraformaldehyde(PFA)-fixed mouse DRG segments from L1 to L6 were frozen in optimal cutting temperature (OCT) freezing medium then cryosectioned (12-16 μm thickness) onto glass slides and stored at -20 °C. Prior to performing RNAscope, a fluorescent microscope (Leica DMi8, Germany) captured Tomato fluorescent signals. RNAscope was performed using a TRPM8-probe (1:2000, #420451-C3, ACD Bio, Newark, CA) with TSA 647 fluorophore (#K1052-100-300, Apex Bio, Houston, TX) according to manufacturer's instructions. After RNAscope, Photoshop (Adobe Photoshop CS6) was used to merge fluorescent signals onto the Tomato before images.

Behavioral Tests

Mice of either sex were used, and for all behavior tests the experimenter was blinded to the genotype of the animals and littermate mice (B6J/129 mixed genetic background) were used as controls. After three to five 'habituation' sessions (20 minutes per day) in the behavior testing apparatus, acute somatosensory measures were recorded on five consecutive days in the given order: rotarod, light brushing, von Frey and Hargreaves (day 1); hot plate and cold plate (day 2), acetone and sticky tape (day 3); pinprick and pinch (day 4), dry ice (day 5). A cutoff of 60 seconds (46 °C), 30 seconds (50 °C), 20 seconds (54 °C), and 15 seconds (pinch) was applied to prevent injury to the animal (Duan et al., 2014; Pan et al., 2019). Temperature gradient assay was performed over

at least two days to allow for complete habituation before the testing began. Similarly, the two-temperature preference assay was performed over three to five days to prevent the development of a place preference (not a temperature preference).

Two-Temperature Preference Assay

To test preference when given the choice between two temperatures (two-temperature preference), mice were placed onto two adjacent temperature plates (BIO-CHP Cold Hot Plate Test, Bioseb, Pinellas Park, FL) for five minutes and the time spent on each plate was recorded (BIO-T2CT, Bioseb, Pinellas Park, FL). If mice exhibited a place preference (less than 30% time spent on each plate), when both temperature plates were set to the same temperature (30 °C), they were excluded from further testing. To avoid the development of a place preference due to a negative association of the chamber to a noxious temperature, mice were tested over three days in the following order: 30 °C vs 30 °C and 30 °C vs 20 °C (day 1), 30 °C vs 10 °C (day 2), 30 °C vs 50 °C (day 3).

Gradient Temperature Assay

The gradient temperature device is a rectangular plate machined out of copper 101, with the top surface deburred to allow for a uniform and smooth finish. Thermoelectric coolers (TECs) with heatsinks are installed at several places underneath the assay. The TECs are feedback-controlled and can operate in either cooling or heating mode, allowing for customized temperature profiles along the length of the plate. Mice were acclimatized in the arena for at least 30 minutes or until the mouse was habituated,

followed by a 30-minute video recording period to track the mouse's movement within the arena. Only one mouse was tested at a time. The gradient temperature arena measures 140 cm in length, 10 cm in width and has opaque plexiglass walls with a height of 40 cm. The copper floor of the arena was maintained at a gradient temperature of 5-50 °C. The arena is virtually divided into 18 zones with distinct temperatures. Time spent within each zone was analysed using MATLAB.

Acetone Evaporation Assay

Animals were placed in an elevated chamber with mesh floor. During 'habituating' periods, acetone was exposed to the environment to control for olfactory stimulation during the testing period. Using a syringe mounted with a plastic tubing, a single drop of acetone was applied to the glabrous skin of the hindpaw of the animal once every 30 seconds, alternating between paws for a total of two applications per paw (4 total). The assay was digitally recorded and analyzed later by a blinded experimenter. To identify cool-induced nocifensive responses but not touch, the following scoring system was utilized: hind paw flinch was scored as a 1, as single lick was scored as a 2, multiple licks was scored as a 3, guarding, vocalization, and/or escape behaviors were scored as a 4. An average was then calculated across all four trials and used to represent a final score.

Dry Ice Assay

Animals were placed in an elevated chamber with mesh flooring for all 'habituation' and testing periods. Following three 'habituation' sessions (20 minutes per day) in the

behavior testing apparatus, a compacted pellet of dry ice was applied to the hindpaw of the animal once every 30 seconds, alternating between paws for a total of two applications per paw (4 total). The assay was digitally recorded and later analyzed by a blinded experimenter. To identify noxious cold nocifensive responses, a score was given one a scale of 0 to 2, where hindpaw flinch was scored as a 1, and one or more licks was scored as a 2. An average was then calculated across all four trials and used to represent a final score.

Rectal Temperature Measurement

Briefly, the thumb and index fingers were used to gently grasp the nape of the neck, restraining the mouse for the duration of the testing period (1-2 minutes at most). A rectal thermometer (Right Temp Jr. Kent Scientific Corporation, Torrington, CT) was placed approximately 1.5 cm into the rectum, then held in place until a steady temperature could be recorded. For Calb1^{Silenced} experiments, the mouse was first weighed to determine the correct dosage of CNO (5 mg/kg), then the baseline rectal temperature was recorded, immediately followed by intraperitoneal injection of CNO, and then the final temperature was recorded 40 minutes later.

C-Fos Induction

Following three 'habituation' sessions (20 minutes per day) in the behavior testing apparatus, a single acetone drop was applied to the hindpaw of *Calb1^{Lbx1}*;Ai65 or *SOM^{Cre}*;Ai14 mice once every 30 seconds over a 30-minute timespan. 1.5 hours later, mice were euthanized by isoflurane and perfused with 4% PFA in PBS. The lumbar

spinal cord was then dissected, post-fixed for 2 hours at room temperature, cryoprotected for ≥ 24 hrs in sucrose solution (20% sucrose in PBS) at 4 °C, embedded in OCT, then sliced into 12-16 μm transverse sections on a cryostat (Leica Microsystems) for further c-Fos immunostaining (see *In Situ* Hybridization and Immunohistochemistry section above). For counting, the "peak c-Fos zone" was first identified, then a slice before and after was used for further quantification (ipsilateral and contralateral hemi-sections n = 9 each from 3 mice per experimental condition).

Icilin Assay

As previously described (Dhaka et al., 2007), animals were habituated in a clear plexiglass experimental chamber for 20 minutes each day for two days prior to testing. On testing day, the mice were habituated for 20 minutes in the experimental chamber then 10 μl of 2.4 mg/ml icilin dissolved in 80% DMSO/20% PBS was injected into the right hindpaw. The mouse was then placed back into the behavior chamber and behavioral responses (hindpaw licking, flinching, and wet-dog shaking) were video-recorded for 60 minutes post-injection.

Brainbow Virus Tracing

Schematic Image was created with BioRender.com (Figure 3.5B). Brainbow 3.0 AAV-PHP.eB was obtained from University of Michigan vector core. To systemically label dorsal spinal cord neurons, 50 μl of mCherry-TFP (1E12 gc total) was injected into the retro-orbital sinus of 3 mice. A new, clean needle will be inserted, bevel down, at an angle of approximately 45° through the inferior fornix conjunctival membrane (6 o'clock

position into the eye socket). The needle was positioned behind the globe of the eye in the retro-bulbar sinus. After virus injection, the needle was gently removed to avoid injury to the eye. Six weeks after injection, adult mice were perfused with 1x PBS followed by 4% PFA. The spinal cords were dissected out and post-fixed in the 4% PFA overnight then used for expansion microscopy.

Expansion Microscopy (ExM) and Immunohistochemistry

Fixed spinal cord ExM specimens were generated following the MiriEx expansion protocol (Shen et al., 2020). Briefly, adult mice were perfused with 1x PBS followed by 4% PFA. Spinal cords were dissected out, post-fixed in the 4% PFA overnight, then embedded in 2% low-melting agarose (Lanza, #50115) and vibratome (VT1200S, Leica, Germany) sectioned at 100μm. Representative sections were treated in 1.0 mM acrylic acid N-hydroxysuccinimide ester (AAx, Sigma, A8060) at 4 °C overnight, followed by 1x TBS washes for 3-4 hours (1 hour per wash). Subsequently the specimens were incubated in the MiriEx monomer solution (containing 5.3% Sodium Acrylate, 4% Acrylamide, 0.1% Bis acrylamide, 0.5% VA-44, and Triton X-100) at 4 °C overnight. The next morning, a 0.20mm iSpace (Sunjin Lab, IS312) was sealed onto a glass slide to create a gel chamber. The chamber was first half-filled with fresh 1x MiriEx monomer solution, next the tissues were gently laid flat in the chamber, then sealed with a glass cover slip and placed in a humidified container at 37 °C to allow gel polymerization for 2.5 hours. After polymerization, a clean razor blade was used to carefully trim away excess gel and scrape the gelled tissue off into a 2 ml centrifuge tube filled with denaturing buffer (200 mM SDS in 1x TBST) to allow protein denaturation at 70 °C

overnight. The denatured tissues were washed with 0.1% PBST at least 4-5 times (1 hour per wash) at 50 °C. The washed tissue were then moved into new 1.5 ml centrifuge tubes for primary antibody staining (usually diluted 1:100 – 1:500) with: chicken anti-Homer (160006, Synaptic Systems, Goettngen, Germany), guinea pig anti-Bassoon (#141004, Synaptic Systems, Goettngen, Germany), rabbit anti-mCherry (generated by Cai lab, University of Michigan, Ann Arbor, MI, USA), rabbit anti-TFP (generated by Cai lab, University of Michigan, Ann Arbor, MI, USA), sheep anti-GFP (#4745-1051, Bio-Rad Laboratories, Hercules, CA, USA), then secondary antibody staining (1:1000) donkey anti-sheep Alexa fluor plus 488 (#713-546-147, Jackson Immunoresearch, West Grove, PA, USA), donkey anti-rabbit Alexa fluor Cy3 (#711-166-152, Jackson Immunoresearch, West Grove, PA, USA), donkey anti-guinea pig Alexa fluor 594 (#706-585-148, Jackson Immunoresearch, West Grove, PA, USA), donkey anti-chicken Alexa fluor 647 (#703-606-155, Jackson Immunoresearch, West Grove, PA, USA), followed by confocal imaging. A test round was performed to determine the number of staining rounds needed. If the morphology of the neurons could be completely defined by a single Brainbow fluorophore, then a single round of imaging was performed (synapse markers, Brainbow, and GFP). If the dendritic arbors partially overlapped, then two rounds of staining were performed (1: synaptic markers, GFP; 2: Brainbow markers, GFP; GFP channel was used for registration). For multi-round immunostaining and imaging, primary and secondary antibodies were stripped as previously described (Shen et al. 2020).

Confocal Microscopy and Image Processing

The samples were gradually expanded 3-4 fold through multiple washes in 0.01x PBS. The expanded tissues were mounted in Poly-L-Lysine coated 6mm dishes (Corning, #356517). Confocal images were acquired with Zeiss LSM780 using a 20x 1.0 NA water immersion objective (421452-9800-000). The 32-channel GaAsP array detector was used to allow multi-track detection of four fluorophores with proper channel collection. All images were corrected for chromatic aberration using 0.5 mm TretraSpek fluorescent bead calibration images and the Detection of Molecules (DoM) ImageJ/Fiji plug in. Histogram matching was done to normalize intensity between z-slices in image stacks using the nTracer Align-Master ImageJ/Fiji plugin. nTracer, an ImageJ/Fiji plugin, was used to trace somas, dendrites, and axons of Brainbow labeled neurons (manual and tutorial videos can be found at **https://www.cai-lab.org/ntracer-tutorial**).

Image Registration and Alignment Between Rounds

For experiments in which multiple rounds of immunostaining, imaging, and stripping were performed, image registration and alignment were implemented as previously described (Shen et al., 2020). Briefly, each round's fiducial marker channel (GFP) was loaded into ImageJ/Fiji Big Warp plugin for rough, initial alignment. Elastix was then used to register the fiducial marker channels using B-splines. The resulting transformation was applied to each individual channel to create a merged image hyperstack. To register and align images from different rounds that are different expansion sizes, the lower resolution fiduciary channel was upsampled using bilinear interpolation to match the voxel size of the higher resolution fiduciary channel.

Rabies Virus Tracing

As described previously (Pan et al., 2019), adult *Calb1::Cre;Lbx1*^{Flpo}*, Rosa26*$^{ds\text{-}HTB}$ mice (n = 3) were anesthetized by isoflurane and a laminectomy was performed at the lumbar spinal cord (L3-L4). A fine needle was used to remove the dura matter and expose the spinal cord, then a fine glass capillary held by a nanoliter injector (WPI, Sarasota, FL) with stereotaxic device (David Kopf Instruments, Tujunga, CA) was inserted into the right side of the dorsal spinal cords. Focal injections of EnvA-pseudotyped, G-deleted-mCherry rabies virus (300 nl; ~1E9 unit per ml, gift from Dr. Zhigang He at Boston Children's Hospital) were injected into the dorsal spinal cord to target Calb1^{+} neurons in laminae I-III (50-300 μm depth from the surface) under the control of a micro-controller (Micro4, Sarasota, FL). Mice were perfused 10 days later and processed for further RNAscope experiments.

Electrophysiology

Spinal Cord Slice Preparation

As described previously (Pan et al., 2019), the parasagittal spinal cord slices attached with the full length of the dorsal root and DRG were collected. Mice were deeply anesthetized with isoflurane, decapitated and the lumbar spinal cord was rapidly removed and placed in an ice-cold modified artificial cerebrospinal fluid (ACSF) containing (in mM): 80 NaCl, 2.5 KCl, 1.25, NaH_2PO_4, 0.5 $CaCl_2$, 3.5 $MgCl_2$, 25 $NaHCO_3$, 75 sucrose, 1.3 sodium ascorbate and 3.0 sodium pyruvate, with pH at 7.4 and osmolality at 310-320 mOsm, bubbled with 95% O_2 and 5% of CO_2. Spinal cord slices (350-480 μm) attached with dorsal roots and DRGs were cut sagittally by a

vibratome (VT1200S, Leica, Germany), as illustrated in Figure 3.7A. The slice was then incubated for about 1 hour at 33 °C in oxygenated (95% O_2 and 5% CO_2) cutting solution which contains (in mM): 125 NaCl, 2.5 KCl, 2 $CaCl_2$, 1 $MgCl_2$, 1.25 NaH_2PO_4, 26 $NaHCO_3$, 25 D-glucose, 1.3 sodium ascorbate and 3.0 sodium pyruvate, with pH at 7.2 and osmolality at 310-320 mOsm. Icilin (1 μM), strychnine (2 μM), bicuculline (10 μM) and AMTB (100 μM) were diluted with a normal bath solution. All chemicals were purchased from MilliporeSigma (St. Louis, MO).

Whole-cell Patch Clamp Recordings

After incubation, spinal cord slices were placed in a recording chamber and perfused with oxygenated recording solution at a rate of 5 ml/minute at room temperature. Whole-cell recording experiments were then performed on $Calb1^{Lbx1}$ dorsal horn neurons. Borosilicate glass pipettes (Sutter instrument, Novato, CA) with resistance of 3-6 MΩ were then filled with internal solution that contains (in mM): 130 potassium gluconate, 5 KCl, 4 Na_2ATP, 0.5 NaGTP, 20 HEPES, 0.5 EGTA, pH 7.3 with KOH, and measured osmolality at 310-320 mOsm. Data were acquired by pClamp 10.0 software (Molecular Devices, San Jose, CA) with MultiClamp 700B patch clamp amplifier and Digidata 1550B (Molecular Devices, San Jose, CA). Responses were low pass filtered online at 2 kHz and digitized at 5 kHz.

Dorsal Root Stimulation

Different responses of dorsal horn neurons to primary afferent inputs were recorded under different recording conditions. Firstly, evoked excitatory postsynaptic currents

(eEPSCs) were detected by holding membrane potential at -70 mV, which minimized evoked inhibitory postsynaptic currents (eIPSCs) (Yoshimura and Jessell, 1990). Whether a neuron receives Aβ, Aδ or C-fiber inputs directly (mono-eEPSC) or indirectly (poly-eEPSC) were determined under this recording condition. Monosynaptic inputs for Aβ, Aδ or C fibers were determined by high frequency stimulation at 20, 2 or 1 Hz, respectively (Pan et al., 2019; Torsney and MacDermott, 2006). Transduction velocity was also used to determine monosynaptic inputs: Aβ, 2.16-4.06 m/s; Aδ, 0.92-1.04 m/s; C, 0.18-0.62 m/s. Secondly, eIPSCs were recorded by holding membrane potential at 0mV when eEPSCs were minimized. Bicuculline (10 μM, MilliporeSigma, St. Louis, MO) and/or strychnine (2 μM, MilliporeSigma, St. Louis, MO) were used to disinhibit dorsal horn neurons. Thirdly, dorsal root stimulation-evoked IPSP, EPSP, or APs were detected by current clamp recording at the resting membrane potential. Action potential firing patterns were determined by current clamp recording at the resting membrane potential.

Characterization of Firing Pattern

The steady-state firing pattern was isolated from the initial transient phase, i.e. the firing pattern immediately after the beginning of the current phase. There were three main starting patterns characterized: The onset was indistinguishable from the rest of the spike response (tonic), neurons responded with a much greater frequency of spikes in the transient (initial burst) than in the steady state, and neuron firing started with a delay (delay). After an initial transient, neurons displayed a steady-state pattern. Again, there

were three main types: regularly spaced spikes (tonic), gradually increasing interspike interval (adapting), or regular alternating between short and long intervals (bursting).

Single Cell RT-PCR

PCR-amplified cDNA libraries for single cells were generated from individual spinal cord neuron cells (SuperScript™ IV Single Cell cDNA PreAmp, Cat: 11752048, Thermo, CA). The cDNA quality of each cell was confirmed by PCR for GAPDH and Somatostatin (SOM). Primers were designed with primer-BLAST of the GAPDH and SOM genes (Table 1). 1x reaction mix, 2 mM $MgCl_2$, 250 μM each deoxynucleotide for each reaction; (Thermo, CA), 0.25 μM forward primer, 0.25 μM reverse primer and 2.5U SuperScript™ One-Step RT-PCR (Thermo, CA) were combined with 1 μl template cDNA. PCRs for SOM and GAPDH were performed with 35 cycles of initial 10-minute denaturation (94 °C), 30-second denaturation (94 °C), 30-second annealing (55 °C), and 2-minute extension (72 °C). After 10-minute post-elongation (72 °C). Table 1 shows the annealing temperature range of 35-cycle (SOM, GAPDH), the annealing temperature range of 20-cycle. Amplified products were run on 1.5% agarose gels. Certain bands were observed in the control spinal cord neurons, but no bands were seen in the water (AM9935, Thermo, CA).

Table1. Primers for RT-PCR

GAPDH	Forward primer	TGAAGGTCGGTGTGAACGAATT
	Reverse primer	GCTTTCTCCATGGTGGTGAAGA

SOM	Forward primer	GCCCAACCAGACAGAGAATGA
	Reverse primer	TGGGTTCGAGTTGGCAGAC

Ca^{2+} Imaging

As previously described (Pan et al., 2019), acutely dissociated DRG neurons from 4 mice were first incubated in at 37 °C for 30 minutes in 4 mm Fura-2-acetoxymethyl ester and 0.2% Pluronic® F127 (Thermo Fisher Scientific, Waltham, MA), washed three times, then incubated for 20 minutes in standard extracellular solution (in mM): 10 HEPES [pH 7.4], 5 KCl, 140 NaCl, 2 $MgCl_2$, 2 $CaCl_2$, and 10 glucose. Calcium imaging was performed using a 20x water-immersion objective with high transmission efficiency of UV light (Olympus IX73, Japan). A Roper Cool-Snap CCD camera was used for image acquisition, and images were processed with MetaFluor software (Molecular Devices, San Jose, CA). Icilin (in μM): 0.1, 0.3, 1, 3, 5, and 10, and KCl (50 mM) were dissolved in standard extracellular solution. Temperature was maintained and verified using Heating and Cooling Application Fundamentals (Warner Instruments LLC, Hamden, CT).

Tracing SPB Neurons

Adult *Calb1$^{Lbx1;}$*Ai65 mice were anesthetized by isoflurane and a craniotomy was performed. To mark SPB neurons, we bilaterally injected cholera-toxin B (2%, #C34775, #C34778, ThermoFisher, Waltham, MA), a retrograde tracer, into the lateral parabrachial nucleus (lPB) in *Calb1$^{Lbx1;}$*Ai65 mice. A nanoliter injector (WPI, Sarasota, FL) coordinated with a stereotaxic device (David Kopf Instruments, Tujunga, CA) was

positioned at the coordinates and a dental drill (8149285, Meisingerusa, Centennial, CO) was used to expose the brain. Next, a fine glass capillary containing CTB, was inserted bilaterally into the lPB and a microcontroller (micro4, Sarasota, FL) was used to deliver 1-1.5 μl of CTB to each region. To label Calb1^{Lbx1}-Tomato cooling-sensitive SPB neurons, 6-10 days after surgery, 3 *Calb1^{Lbx1};*Ai65 mice were habituated to the behavior chamber for two days before acetone-induced c-Fos protocol (as previously described). For electrophysiological recordings of Calb1^{Lbx1}-Tomato SPB neurons, 5 control and 4 Calb1^{Abl} mice were injected in the lPB with CTB, then 7–14 days later the spinal cord and DRG were dissected out together and recorded.

Quantification and Statistical Analysis

Results are expressed as mean ± SEM. Statistical analysis was performed in Prism 6 or 9 (GraphPad). A threshold of $p < 0.05$ was accepted as statistically different and $p > 0.05$ considered non-significant. For ablation experiments, locomotion coordination, touch, acute pain assessment, and temperature (except two temperature preference and gradient temperature) data were subjected to Student's t tests. Temperature preference assay and gradient temperature data were subjected to two-way ANOVA with Sidak and Bonferroni post hoc analyses respectively. For silencing experiments, all behavior data were subjected to two-way ANOVA with Sidak post hoc analysis. C-Fos data were subjected to two-way ANOVA with Sidak post hoc analysis. For electrophysiological results, data were analyzed with two-way ANOVA with Tukey (AMTB application; percent Icilin Responding cells; percent icilin-induced APs in icilin responding cells) and Sidak (Current by icilin) post hoc analyses. No statistical methods

were used to predetermine sample sizes, but our sample sizes are similar to those reported in previous publications (Duan et al., 2014; Pan et al., 2019). Sex differences were analyzed (two-way ANOVA with Sidak post hoc analysis) and no statistical significance was determined (data not shown).

Figures

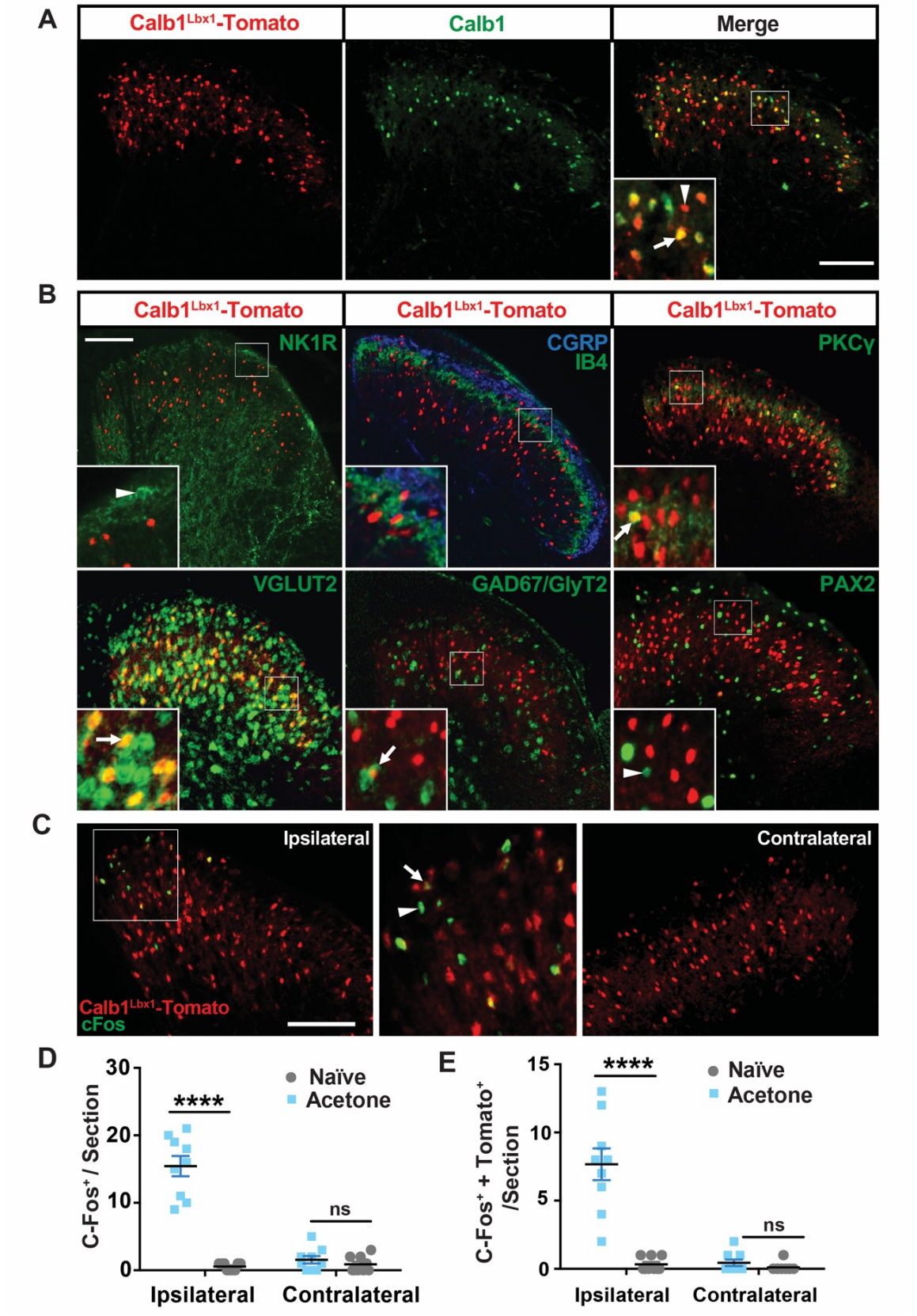
A
Calb1Lbx1-Tomato
Calb1
Merge
B
Calb1Lbx1-Tomato
NK1R
Calb1Lbx1-Tomato
CGRP
IB4
Calb1Lbx1-Tomato
PKCγ
VGLUT2
GAD67/GlyT2
PAX2
C
Ipsilateral
Contralateral
Calb1Lbx1-Tomato
cFos
D
C-Fos+ / Section
30
20
10
0
****
ns
Naïve
Acetone
Ipsilateral
Contralateral
E
C-Fos+ + Tomato+ /Section
15
10
5
0
****
ns
Naïve
Acetone
Ipsilateral
Contralateral

Figure 3.1 An Innocuous Cool Stimulus Activates Calb1^{Lbx1}-Tomato^{+} neurons in the Superficial Dorsal Horn of the Spinal Cord

(A) Images represent double staining of Calb1^{Lbx1}-Tomato (red) and Calb1 protein (green) in *Calb1^{Lbx1}*;Ai65 mice. Arrow denotes Calb1 protein and Tomato double-positive cell. Arrowhead indicates a Calb1^{Lbx1}-Tomato positive cell that does not colocalize with Calb1 protein. n = 17 sections. Scale bar, 100 μm.

(B) Double staining of Tomato with lamina markers (NK1R, CGRP, IB4, and PKCγ), excitatory neuronal marker VGLUT2, or inhibitory neuronal markers (GAD67 plus GlyT2 or Pax2) by immunohistochemistry or *in situ* hybridization in the dorsal horn of *Calb1^{Lbx1}*;Ai65 mice. Arrows denote double-positive cells for indicated mRNA and Tomato. Arrowhead indicates a protein^{+} cell that does not colocalize with Tomato. The percentage is calculated as double-positive neurons over total number of Calb1^{Lbx1}-Tomato^{+} neurons. Insets represent higher magnification of the boxed areas. n = 17-26 sections. Scale bar, 100 μm.

(C) Double staining of c-Fos and Tomato signals in acetone-treated *Calb1^{Lbx1}*;Ai65 mice. Inset (middle) represents higher magnification of the boxed area (left). Arrow indicates a double-positive cell for c-Fos protein and Tomato, and arrowhead shows a cell positive for c-Fos alone. Scale bar, 100 μm.

(D) Total number of c-Fos positive neurons per hemi-section in either the ipsilateral or the contralateral dorsal horn of naïve (grey) and acetone-treated (light blue) *Calb1^{Lbx1}*;Ai65 mice. n = 9 hemi-sections in each group; **** $p < 0.0001$ two-way ANOVA with Sidak post hoc analysis.

(E) Quantification of c-Fos colocalization between c-Fos^{+} and Calb1^{Lbx1}-Tomato^{+} neurons per hemi-section in either the ipsilateral or contralateral dorsal horn of naïve (grey) and acetone-treated (light blue) *Calb1^{Lbx1}*;Ai65 mice. n = 9 hemi-sections in each group; **** $p < 0.0001$; two-way ANOVA with Sidak post hoc analysis.

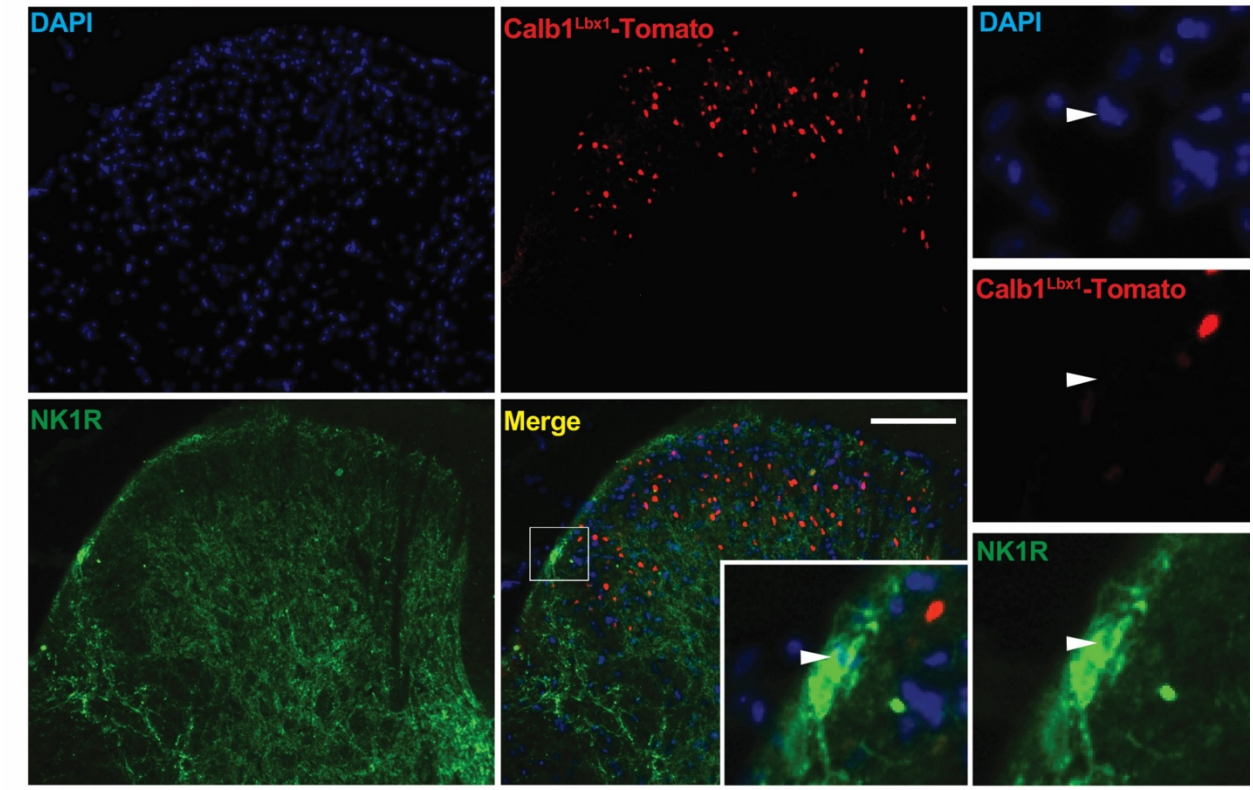

Figure 3.2 Classification of NK1R$^+$ Neuronal Quantification

Triple staining of Calb1^{Lbx1}-Tomato$^+$ signals (red) with NK1R immunostaining (green). Colocalization with DAPI (blue) was used to identify NK1R$^+$ projection neurons. Insets represent higher magnification of the boxed area. Arrowhead indicates NK1R and DAPI double-labeled cell, but not Tomato$^+$. n = 18 sections. Scale bar, 100 μm.

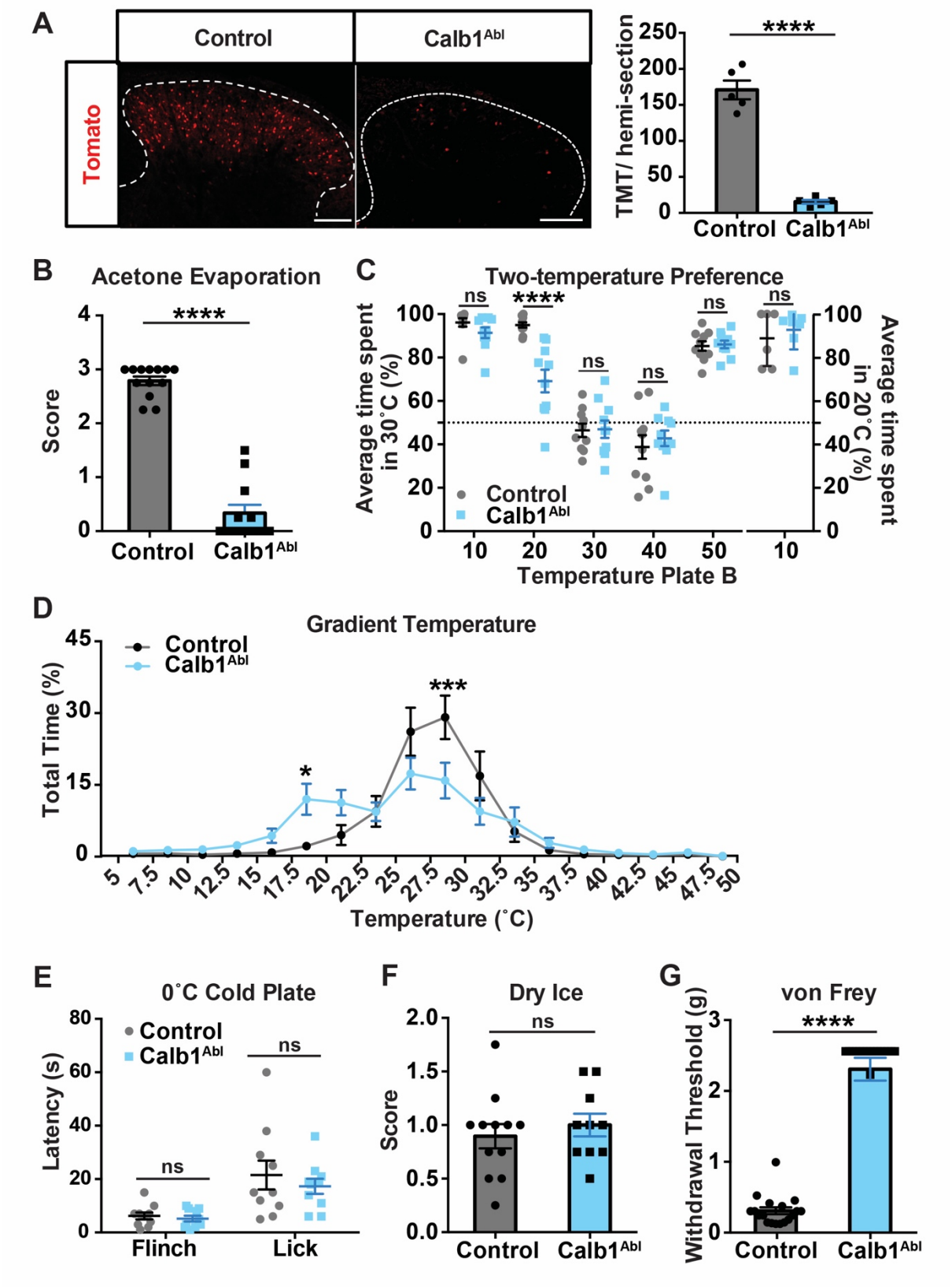
A
Control
Calb1Abl
Tomato
TMT/ hemi-section
****
Control
Calb1Abl
B
Acetone Evaporation
Score
****
Control
Calb1Abl
C
Two-temperature Preference
Average time spent in 30˚C (%)
Average time spent in 20˚C (%)
ns
****
Control
Calb1Abl
Temperature Plate B
D
Gradient Temperature
Total Time (%)
Control
Calb1Abl
*
***
Temperature (˚C)
E
0˚C Cold Plate
Latency (s)
Control
Calb1Abl
ns
Flinch
Lick
F
Dry Ice
Score
ns
Control
Calb1Abl
G
von Frey
Withdrawal Threshold (g)
****
Control
Calb1Abl

Figure 3.3 Loss of Innocuous Cool Sensations in Calb1^{Abl} Mice

(A) Ablation of Calb1^{Lbx1} neurons in the dorsal horn. Bar graph represents quantified data for Calb1^{Cre}-Tomato signals in control and ablated animals. n = 27-30 sections; **** $p < 0.0001$, Student's unpaired t test. Scale bar, 100 μm.

(B) The acetone evaporation assay in Calb1^{Abl} and control groups. Control: n = 17; Calb1^{Abl}: n = 14; **** $p < 0.0001$, Mann-Whitney test.

(C) Two-temperature preference between two temperature plates. Left panel: Reference plate is set at 30 °C, and test plate temperature is set at 10 °C, 20 °C, 30 °C, 40 °C, and 50 °C. Control: n = 10-11; Calb1^{Abl}: n = 10; ns, no significant difference; **** $p < 0.0001$ two-way ANOVA with Sidak post hoc analysis. Right panel: Reference plate is set at 20 °C, test plate temperature is set at 10 °C. Data points represent the average percentage of time spent on the reference plate across two trials over the total trial time. Control: n = 6; Calb1^{Abl}: n = 7; ns, no significant difference; Student's unpaired t test.

(D) Gradient temperature ranging from 5 °C to 50 °C is quantified as percentage of time spent in each temperature zone over the total trial time. Control: n = 13; Calb1^{Abl}: n = 18; * $p < 0.05$; *** $p < 0.001$; two-way ANOVA with Bonferroni post hoc analysis.

(E) Quantified forelimb withdrawal latency to 0 °C cold plate, including forelimb lick and flinch responses. n = 10 in each group; ns, no significant difference; Student's unpaired t test.

(F) Quantitative nocifensive response to dry ice application to the hindpaw. Score represents average response across four trials per mouse. Control: n = 12; Calb1^{Abl}: n = 10; ns, no significant difference; Student's unpaired t test.

(G) Acute punctate mechanical pain threshold as measured by up-down von Frey withdrawal threshold was significantly increased in Calb1^{Abl} mice compared to controls. Control: n = 18; Calb1^{Abl}: n = 13; **** $p < 0.0001$, Student's unpaired t test.

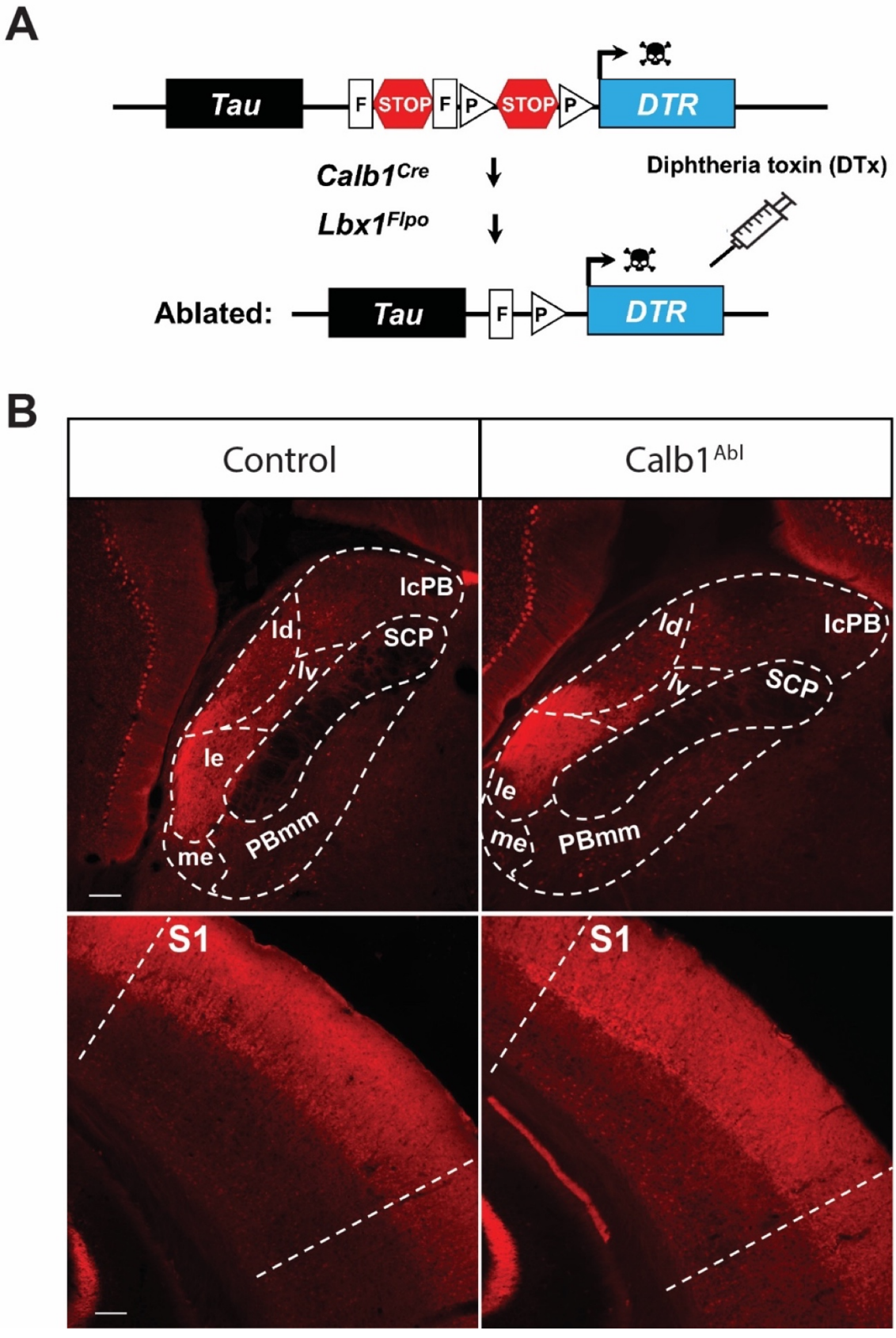
A
Tau
F
STOP
F
P
STOP
P
DTR
Calb1Cre
Lbx1Flpo
Diphtheria toxin (DTx)
Ablated:
Tau
F
P
DTR
B
Control
Calb1 Abl
lcPB
ld
SCP
lv
le
PBmm
me
S1

Figure 3.4 Ablation of Calb1^{Lbx1} Neurons in the Spinal Cord Does Not Affect the Expression of Calb1^{+} Neurons in the Brain

(A) Schematic demonstrating intersectional genetic ablation strategy to express diphtheria toxin receptor in Calb1^{Lbx1} neurons to selectively ablate the Calb1^{Lbx1} population in adulthood.

(B) Ablation of Calb1^{Lbx1} neurons does not affect the expression of Calb1^{Cre}-Tomato^{+} neurons in the parabrachial nucleus (top panels) or the somatosensory cortex region (S1) (bottom panels) in control and Calb1^{Abl} mice. Scale bar: 100 μm.

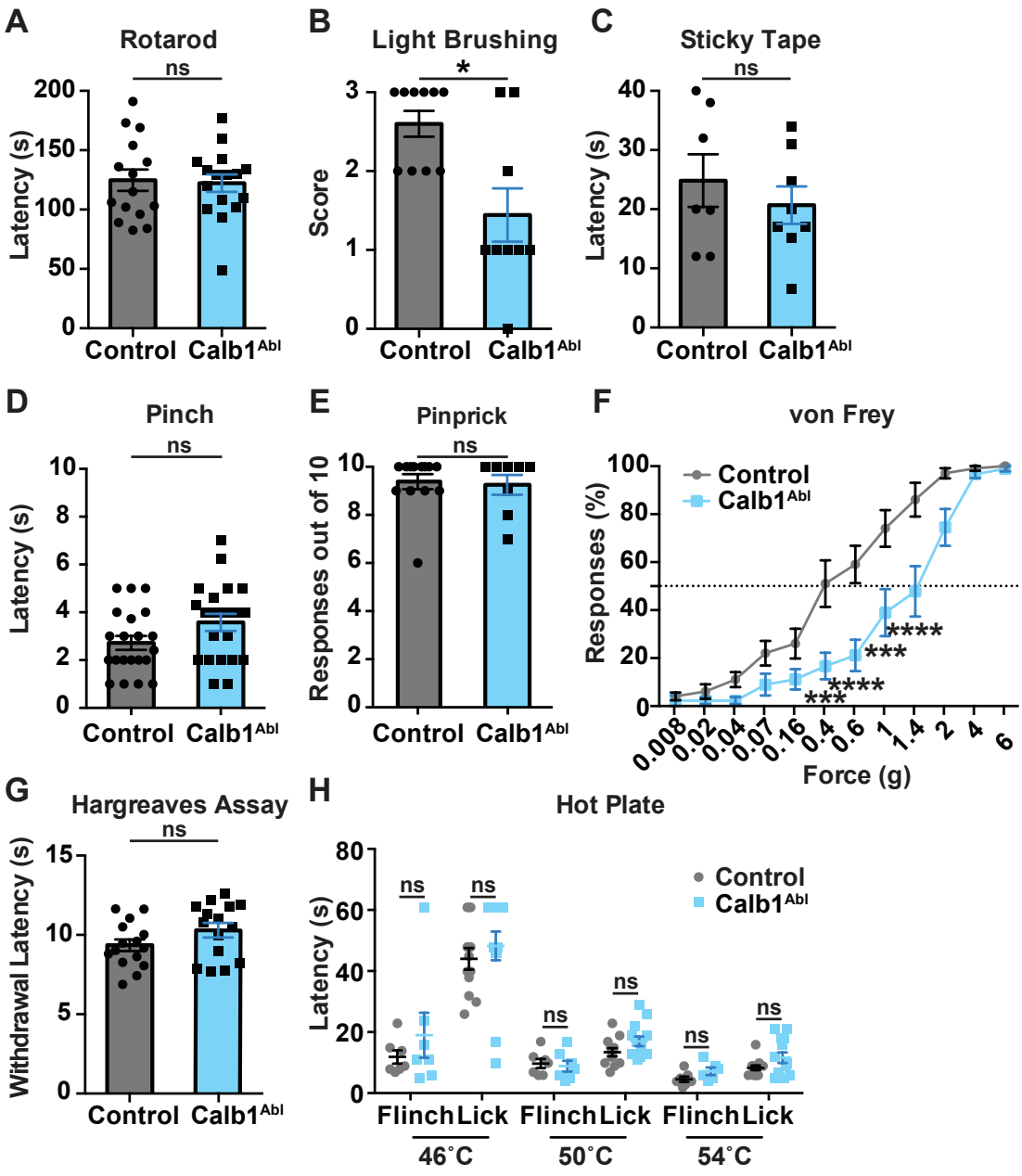
A
Rotarod
ns
Latency (s)
200
150
100
50
0
Control
Calb1Abl
B
Light Brushing
*
Score
3
2
1
0
Control
Calb1Abl
C
Sticky Tape
ns
Latency (s)
40
30
20
10
0
Control
Calb1Abl
D
Pinch
ns
Latency (s)
10
8
6
4
2
0
Control
Calb1Abl
E
Pinprick
ns
Responses out of 10
10
8
6
4
2
0
Control
Calb1Abl
F
von Frey
Control
Calb1Abl
Responses (%)
100
80
60
40
20
0
****
***
****
***
0.008
0.02
0.04
0.07
0.16
0.4
0.6
1
1.4
2
4
6
Force (g)
G
Hargreaves Assay
ns
Withdrawal Latency (s)
15
10
5
0
Control
Calb1Abl
H
Hot Plate
Control
Calb1Abl
Latency (s)
80
60
40
20
0
ns
ns
ns
ns
ns
ns
Flinch
Lick
Flinch
Lick
Flinch
Lick
46˚C
50˚C
54˚C

Figure 3.5 Behavioral Assessment of Locomotion, Touch, and Nociceptive Sensations in Calb1^{Abl} Mice

(A) Bar graph represents latency to fall in control and Calb1^{Abl} animals in the Rotarod assay. No significant difference in the Rotarod assay. Control: n = 15; Calb1^{Abl}: n = 16; ns, no significant difference; p = 0.8364, Student's unpaired t test.

(B) Light-brushing evoked a significantly higher score in control compared to Calb1^{Abl} mice (Control: n = 10; Calb1^{Abl}: n = 9; * $p < 0.05$; Mann-Whitney test).

(C) No significant difference in latency to respond to sticky tape administration in control and Calb1^{Abl} mice was observed. Control: n = 7; Calb1^{Abl}: n = 8; p = 0.04623; ns, no significance; Student's unpaired t test.

(D) Latency to respond to pinch was not significantly different between control and Calb1^{Abl} mice. n = 21 in each group; p = 0.0697; ns, no significance; Student's unpaired t test.

(E) Pinprick assay was not significantly different in control compared to Calb1^{Abl} mice. Control: n = 13; Calb1^{Abl}: n = 8; p = 0.7979; ns, no significance; Student's unpaired t test.

(F) Acute punctate mechanical pain as measured by von Frey response rate threshold across increasing force. Control: n = 10; Calb1^{Abl}: n = 9; *** $p < 0.001$, **** $p < 0.0001$, two-way ANOVA with Sidak post hoc analysis.

(G-H) Noxious heat thermosensation was measured through Hargreaves assay **(G)** and hot plate assay set to 46 °C, 50 °C, or 54 °C **(H)**. No significant difference in latency to flinch the front paw or lick the hindpaw between control and Calb1^{Abl} animals. n = 6-13 in each group; ns, no significance, two-way ANOVA with Sidak post hoc analysis.

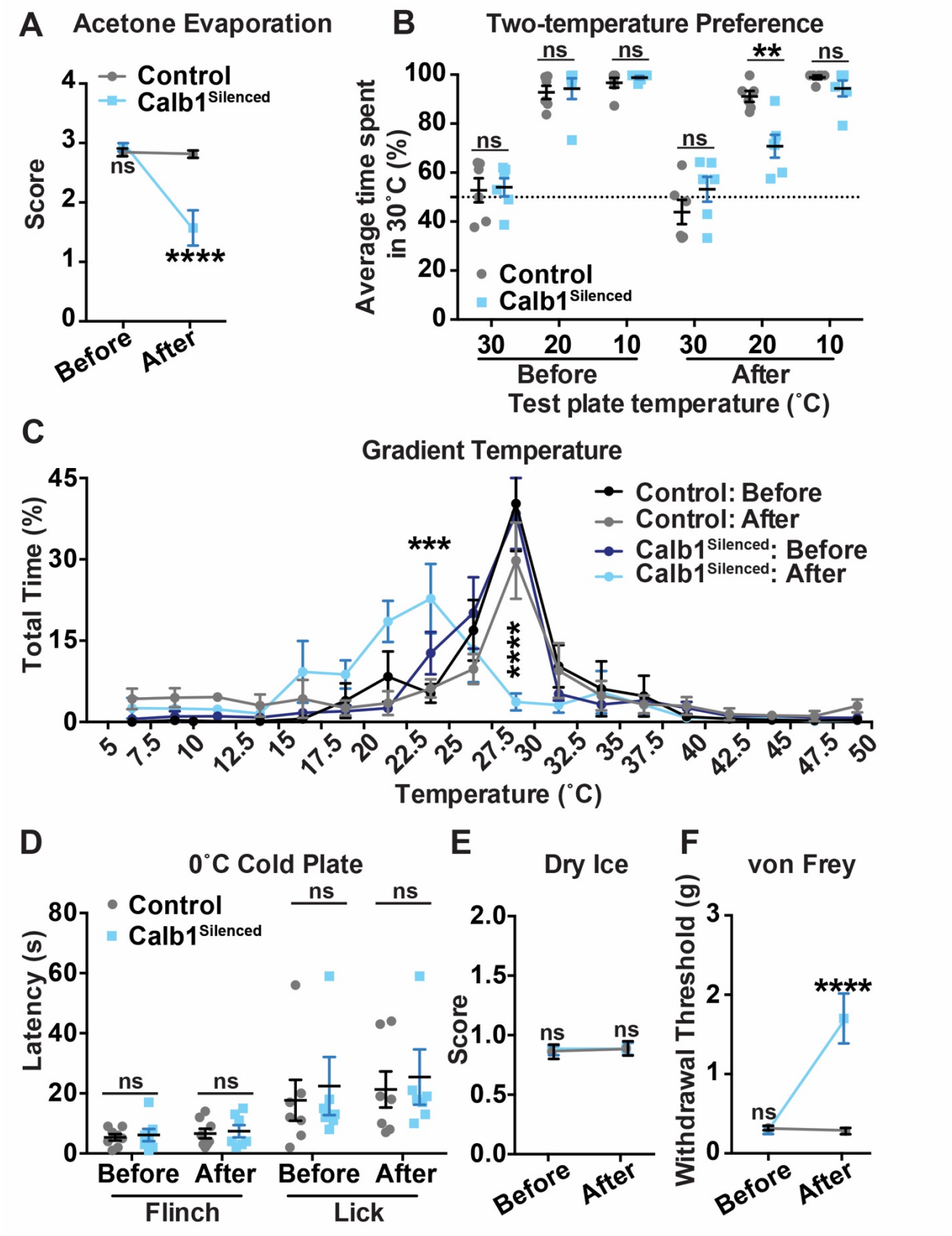
A
Acetone Evaporation
Control
Calb1Silenced
Score
ns
****
Before
After
B
Two-temperature Preference
Average time spent in 30˚C (%)
ns
**
Control
Calb1Silenced
30 20 10 30 20 10
Before
After
Test plate temperature (˚C)
C
Gradient Temperature
Total Time (%)
Control: Before
Control: After
Calb1Silenced: Before
Calb1Silenced: After
***
****
Temperature (˚C)
D
0˚C Cold Plate
Latency (s)
Flinch
Lick
E
Dry Ice
Score
F
von Frey
Withdrawal Threshold (g)

Figure 3.6 Silencing Spinal Calb1^{Lbx1} Neurons Leads to Deficits in Innocuous Cool Sensations

(A) The acetone evaporation assay before and 40 minutes after CNO injection in mice with hM4Di receptors in spinal Calb1^{Lbx1}-neuron silenced (Calb1^{Silenced}) and control groups. Control: n = 8; Calb1^{Silenced}: n = 7; **** $p < 0.0001$, two-way ANOVA with Sidak post hoc analysis.

(B) Two-temperature preference between two temperature plates before and 40 minutes after CNO injection in Calb1^{Silenced} and control groups. Reference plate is set at 30 °C, and test plate temperature is set at 30 °C, 20 °C and 10 °C. Data points represent the average percentage of time spent on the reference plate across two trials over the total trial time. n = 6 in each group; ** $p < 0.01$; two-way ANOVA with Sidak post hoc analysis.

(C) Gradient temperature ranging from 5 °C to 50 °C was quantified as percentage of time spent in each temperature zone before and 40 minutes after CNO injection in Calb1^{Silenced} and control groups. Control: n = 4; Calb1^{Silenced}: n = 7; *** $p < 0.001$; **** $p < 0.0001$; two-way ANOVA with Bonferroni post hoc analysis.

(D) Quantified forelimb flinch and lick withdrawal latency to 0 °C cold plate before and 40 minutes after CNO injection in Calb1^{Silenced} and control groups. Control: n = 8; Calb1^{Silenced}: n = 7; ns, no significant difference; two-way ANOVA with Sidak post hoc analysis.

(E) Nocifensive responses to hindpaw application of dry ice stimulus before and 40 minutes after CNO injection in Calb1^{Silenced} and control groups. Score represents

average response across four trials per mouse. Control: n = 9; Calb1^{Silenced}: n = 11; two-way ANOVA with Sidak post hoc analysis.

(F) Acute punctate mechanical pain measured using the up-down von Frey assay before and 40 minutes after CNO injection in Calb1^{Silenced} and control groups. Control: n = 8; Calb1^{Silenced}: n = 7; **** $p < 0.0001$; two-way ANOVA with Sidak post hoc analysis.

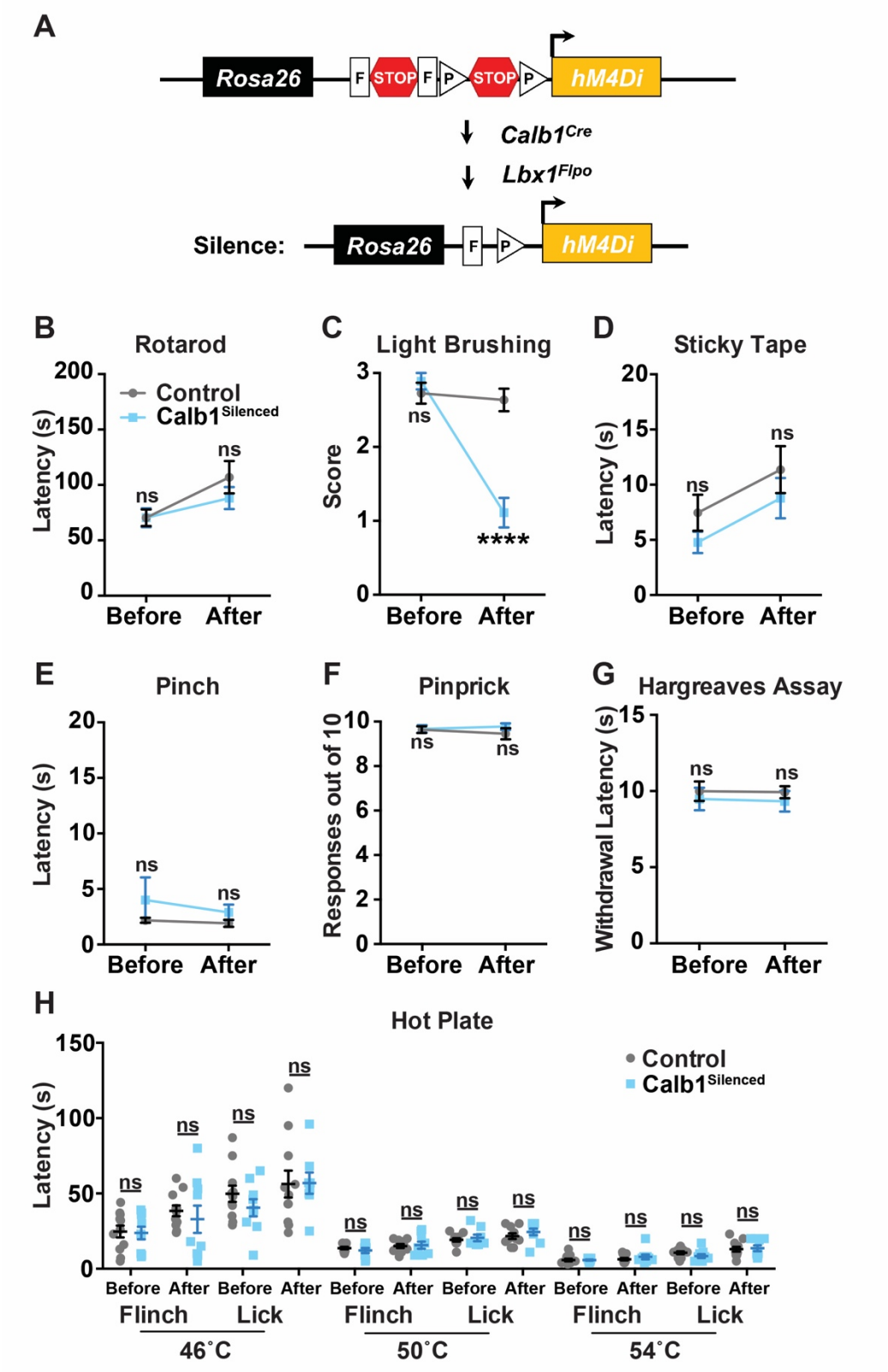
A
Rosa26
F
STOP
F
P
STOP
P
hM4Di
Calb1Cre
Lbx1Flpo
Silence:
Rosa26
F
P
hM4Di
B
Rotarod
Control
Calb1Silenced
Latency (s)
200
150
100
50
0
ns
ns
Before
After
C
Light Brushing
Score
3
2
1
0
ns
****
Before
After
D
Sticky Tape
Latency (s)
20
15
10
5
0
ns
ns
Before
After
E
Pinch
Latency (s)
20
15
10
5
0
ns
ns
Before
After
F
Pinprick
Responses out of 10
10
8
6
4
2
0
ns
ns
Before
After
G
Hargreaves Assay
Withdrawal Latency (s)
15
10
5
0
ns
ns
Before
After
H
Hot Plate
Control
Calb1Silenced
Latency (s)
150
100
50
0
Before
After
Before
After
Before
After
Before
After
Before
After
Before
After
Before
After
Before
After
Flinch
Lick
Flinch
Lick
Flinch
Lick
46˚C
50˚C
54˚C

Figure 3.7 Behavioral Assessment of Locomotion, Touch, and Nociceptive Sensations in Calb1^{Silenced} Mice

(A) Schematic showing the intersectional genetic strategy to temporally restrict the silencing of spinal Calb1^{Lbx1} neurons.

(B) Locomotor agility as measured by latency to fall in the rotarod assay was not significantly different between control and Calb1^{Silenced} mice, or between Calb1^{Silenced} mice before compared to 40 minutes after CNO administration. Control: n = 11; Calb1^{Silenced}: n = 9; ns, no significant differences, two-way ANOVA with Sidak post hoc analysis.

(C) Calb1^{Silenced} mice displayed a significant deficit in light brushing-evoked responses 40 minutes after CNO administration within group (Calb1^{Silenced} before CNO administration) and compared to control animals. Control: n = 11; Calb1^{Silenced}: n = 9; **** $p < 0.0001$, two-way ANOVA with Sidak post hoc analysis.

(D) Latency to respond to sticky tape administration was not significantly altered 40 minutes after CNO administration in Calb1^{Silenced} mice compared to baseline (before CNO administration) and control animals. Control: n = 11; Calb1^{Silenced}: n = 9; ns, no significant difference, two-way ANOVA with Sidak post hoc analysis.

(E) No significant difference in pinch response latency was observed in Calb1^{Silenced} mice compared to before CNO administration or controls animals. Control: n = 11; Calb1^{Silenced}: n = 9; ns, no significant difference, two-way ANOVA with Sidak post hoc analysis.

(F) Pinprick assay was not significantly different in Calb1^{Silenced} mice compared to littermate control or across time (before compared to 40 minutes after CNO

administration). Control: n = 11; Calb1^{Silenced}: n = 9; ns, no significant difference, two-way ANOVA with Sidak post hoc analysis.

(G-H) Noxious heat thermosensation was measured through Hargreaves assay **(G)** and hot plate assay at 46 °C, 50 °C, or 54 °C **(H)**. There was no significant difference in the latency to flinch the front paw of lick the hindpaw between Calb1^{Silenced} mice across time before compared to 40 minutes after CNO administration, or compared to littermate controls. Control: n = 11; Calb1^{Silenced}: n = 9; ns, no significant difference, two-way ANOVA with Sidak post hoc analysis.

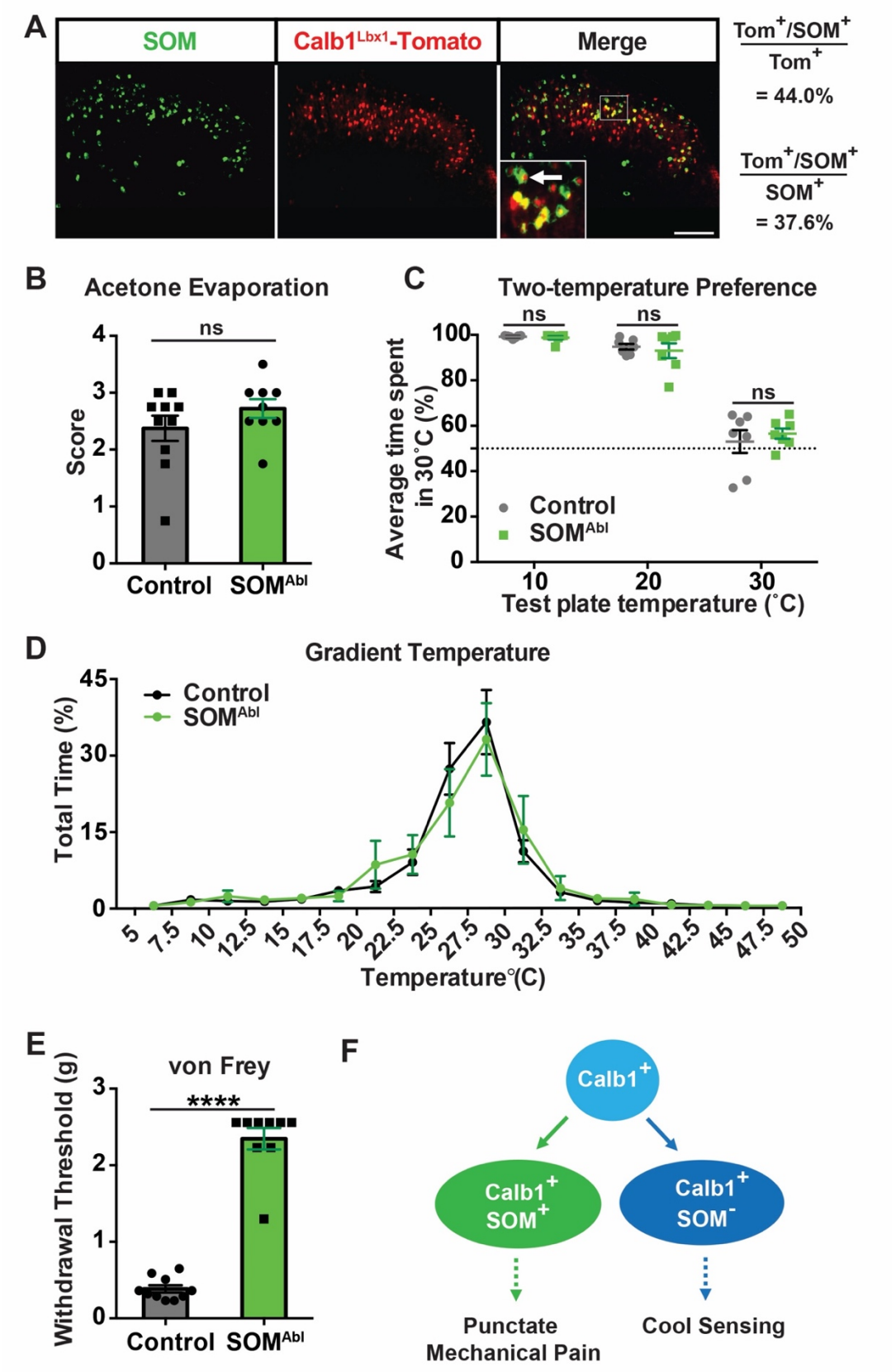
A
SOM
Calb1Lbx1-Tomato
Merge
Tom+/SOM+ / Tom+ = 44.0%
Tom+/SOM+ / SOM+ = 37.6%
B
Acetone Evaporation
ns
Score
Control
SOMAbl
C
Two-temperature Preference
ns
ns
ns
Average time spent in 30˚C (%)
Control
SOMAbl
Test plate temperature (˚C)
D
Gradient Temperature
Control
SOMAbl
Total Time (%)
Temperature°(C)
E
von Frey
****
Withdrawal Threshold (g)
Control
SOMAbl
F
Calb1+
Calb1+ SOM+
Calb1+ SOM-
Punctate Mechanical Pain
Cool Sensing

Figure 3.8 Ablation of SOM^{Lbx1} Neurons Leads to Deficits in Acute Punctate Mechanical Pain but Not Innocuous Cool Sensations

(A) Double staining of SOM mRNA (green) by *in situ* hybridization with Calb1^{Lbx1}-Tomato signals (red). The percentage is calculated as double-positive neurons over total number of Calb1^{Lbx1}-Tomato^{+} neurons (top) or double-positive neurons over total number of SOM^{+} neurons (bottom). Inset represents higher magnification of the boxed area. Arrow indicates double-positive cells for SOM and Tomato. n = 18 sections. Scale bar, 100 μm.

(B) The acetone evaporation assay in SOM^{Abl} and control groups. Control: n = 10; SOM^{Abl}: n = 9; ns, no significant difference; Mann-Whitney test.

(C) Two-temperature preference between two temperature plates. Reference plate is set at 30 °C, and test plate temperature is set at 30 °C, 20 °C and 10 °C. n = 7 in each group; ns, no significant difference; two-way ANOVA with Sidak post hoc analysis. Data points represent the average percentage of time spent on the reference plate across two trials over the total trial time.

(D) Gradient temperature ranging from 5 °C to 50 °C was quantified as time spent in each temperature zone. Control: n = 7; SOM^{Abl}: n = 5; ns, no significant differences; two-way ANOVA with Bonferroni post hoc analysis.

(E) Acute punctate mechanical pain measured using the up-down von Frey assay. Control: n = 10; SOM^{Abl}: n = 9; **** $p < 0.0001$; Student's unpaired t test.

(F) Schematic showing proposed Calb1^{Lbx1} subpopulations for cool sensations and acute punctate mechanical pain. Calb1^{+} neurons (light blue) represent the entire Calb1^{Lbx1} population, which can be further classified into at least two distinct subgroups:

Calb1^{Lbx1};SOM^{+} (green) for mechanical punctate pain and Calb1^{Lbx1};SOM^{-} (dark blue) for cool sensing.

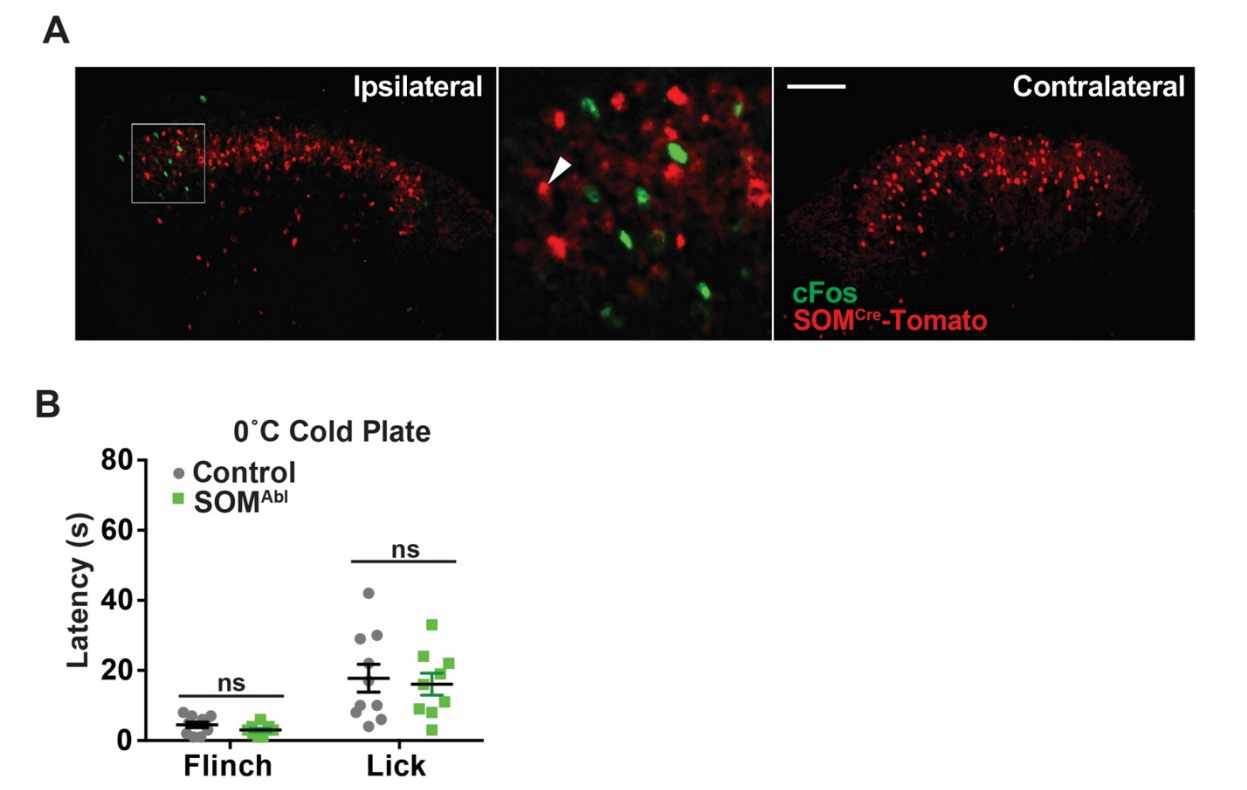

Figure 3.9 SOM^{Cre}-Tomato Neurons are Not Cooling-sensitive

(A) Double staining of c-Fos and Tomato^{+} signals in the ipsilateral (left) and contralateral (right) dorsal horn of acetone-treated *SOM^{Cre}*;Ai14 mice. Inset (middle) represents higher magnification of the boxed area. Arrowheads shows a cell positive for Tomato alone. Scale bar, 100 μm. Very little overlap was observed. n = 9 from each hemi-section.

(B) Quantified forelimb flinch and lick withdrawal latency to 0 °C cold plate. Control: n = 10; SOM^{Abl}: n = 9; ns, no significant difference; two-way ANOVA with Sidak post hoc analysis.

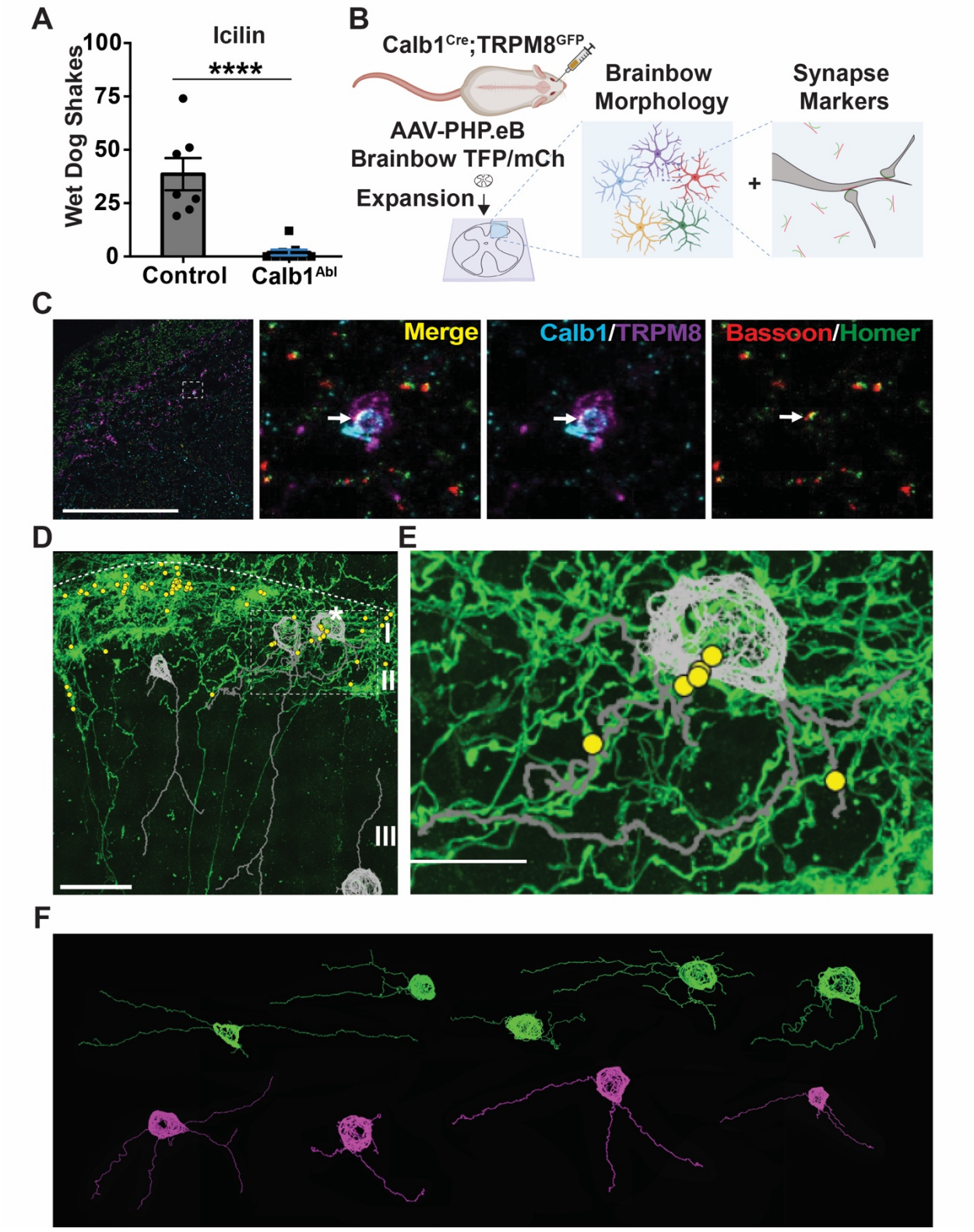
A
Icilin
****
Wet Dog Shakes
100
75
50
25
0
Control
Calb1Abl
B
Calb1Cre;TRPM8GFP
AAV-PHP.eB
Brainbow TFP/mCh
Expansion
Brainbow Morphology
Synapse Markers
+
C
Merge
Calb1/TRPM8
Bassoon/Homer
D
I
II
III
E
F

Figure 3.10 Calb1^{+} Neurons Receive Monosynaptic Inputs from Cool-sensitive TRPM8^{+} Primary Sensory Neurons in the Superficial Dorsal Horn of the Spinal Cord

(A) The number of wet-dog shakes in response to an agonist of TRPM8 channels, icilin, is abolished in Calb1^{Abl} mice compared to controls. Control: n = 7; Calb1^{Abl}: n = 9; **** p < 0.0001; Student unpaired t test.

(B) Schematic representing the experimental approach to virally label individual Calb1^{+} neurons in the spinal cord and TRPM8^{GFP} afferent neurons in the DRG using *Calb1^{Cre};TRPM8^{GFP}* mice. Spinal cord tissue is embedded in a gel and expanded to enable reconstruction of morphology of Calb1^{Brainbow} neurons and identify the location of synaptic pairs.

(C) Left: Overview of the dorsal horn of *Calb1^{Cre};TRPM8^{GFP}* mice following Brainbow labelling and immunostaining excitatory pre- and post-synaptic markers Bassoon and Homer, respectively. Right three panels: Higher magnification of insets depicting representative images of quadruple-positive interaction. Cyan: The dendritic branch of a Calb1^{Brainbow} neuron; purple: the axon terminal of a TRPM8^{+} sensory neuron; red: the presynaptic marker Bossoon; green: the postsynaptic marker Homer. Arrow shows a quadruple-positive synaptic connection. Scale bar, 30 μm estimated based on anticipated expansion factor.

(D) Representative image showing the location of identified quadruple-positive synaptic connections (yellow dots) and cell morphology of Calb1^{Brainbow} neurons (grey) across the superficial dorsal horn. Scale bar, 30 μm estimated based on anticipated expansion factor.

(E) Higher magnification of inset depicting representative image showing the morphology of a Calb1^{Brainbow} neuron that forms synaptic pairs with TRPM8^{+} afferents. Green: TRPM8^{GFP}; grey: Calb1^{Brainbow} neuron; yellow: identified synaptic pairs between TRPM8^{+} afferents and this Calb1^{+} neurons. Scale bar, 15 μm estimated based on anticipated expansion factor.

(F) Schematic summarizing the morphology of Calb1^{Brainbow} neurons that form synaptic connections with TRPM8^{+} primary sensory neurons. Green: Calb1^{Brainbow} neurons with local dendritic arborization in TRPM8-innervation zone; magenta: Calb1^{Brainbow} neurons that contain at least one dendritic arbor outside of the TRPM8-innervating zone. n = 6 sections.

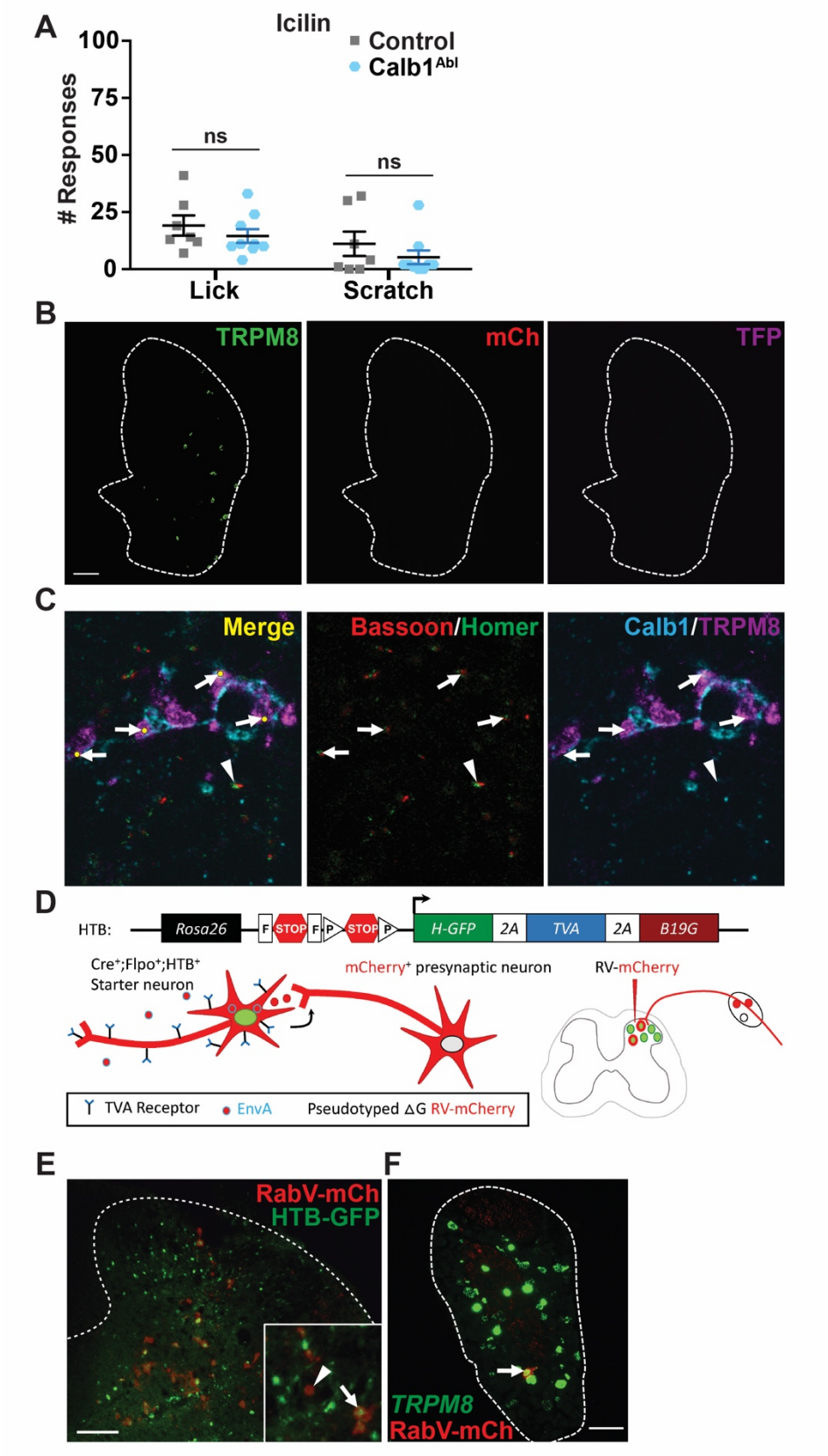
A
Icilin
Control
Calb1Abl
Responses
100
75
50
25
0
ns
ns
Lick
Scratch
B
TRPM8
mCh
TFP
C
Merge
Bassoon/Homer
Calb1/TRPM8
D
HTB:
Rosa26
F
STOP
F
P
STOP
P
H-GFP
2A
TVA
2A
B19G
Cre+;Flpo+;HTB+
Starter neuron
mCherry+ presynaptic neuron
RV-mCherry
TVA Receptor
EnvA
Pseudotyped ΔG RV-mCherry
E
RabV-mCh
HTB-GFP
F
TRPM8
RabV-mCh

Figure 3.11 Calb1^{Cre} Neurons in the Superficial Dorsal Horn Receive Monosynaptic Inputs from TRPM8^{+} Primary Sensory Neurons

(A) Quantification of nocifensive responses (lick or scratch) after icilin injection into the plantar region of the hindpaw in control and Calb1^{Abl} mice. control: n = 7; Calb1^{Abl}: n = 9; no significance, two-way ANOVA with Sidak post hoc analysis.

(B) Retro-orbital injection of *Cre*-dependent AAV-PHP.eB Brainbow in *Calb1^{Cre}; TRPM8^{GFP}* mice to selectively infect the central nervous system and not the periphery (DRG). TRPM8^{GFP}: Green; mCh: Brainbow expressing mCherry; TFP: Brainbow expressing Teal Fluorescent Protein.

(C) TRPM8^{+} presynaptic neurons formed multiple synaptic connections in close proximity with Calb1^{Brainbow} postsynaptic spinal neurons. Arrowhead indicates quadruple positive synaptic pairs (red: presynaptic marker Bassoon; green: postsynaptic marker Homer; purple: presynaptic neuron TRPM8^{+}; blue: postsynaptic neuron Calb1^{Brainbow}). Arrowhead indicates an orphan synaptic pair (colocalized pre- and post- synaptic markers only).

(D) Schematic adapted from Pan et al., demonstrating strategy for monosynaptic labeling of pre-synaptic neurons after selective infection of Calb1^{+} neurons (GFP^{+}) with pseudotyped EnvA-mCherry rabies virus (RV-mCherry^{+}) in the dorsal spinal cord in a HTB transgenic mouse line.

(E) Dorsal spinal cord after rabies virus infection of *Calb1^{Lbx1};* HTB animals (HTB-GFP: green). Arrow indicates an infected Calb1^{+} neuron (GFP^{+} and mCherry^{+}). Arrowhead indicates a presynaptic neuron of Calb1^{+} infected neurons (mCherry^{+} only). Scale bar: 100 μm.

(F) Representative image of the DRG showing infected presynaptic neurons (Rabies virus labeled mCherry$^+$ denoted as RabV-mCh) and RNAscope-labeled *TRPM8* mRNA (green) neurons. Arrow indicates rabies virus infected Rabies virus labeled mCherry$^+$ (denoted as RabV-mCh) colocalized with a TRPM8$^+$ (green) presynaptic peripheral sensory neurons. Scale bar: 100 μm.

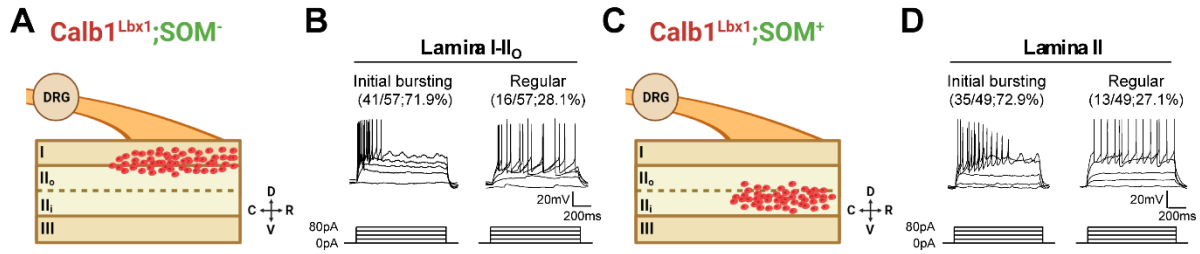

E

Region		Aβ- eEPSCs	Aβ- eIPSCs	Aβ - eAPs	Aδ- eEPSCs	Aδ- eIPSCs	Aδ- eAPs	C-eEPSCs	C-eIPSCs	C-eAPs
Lamina I-IIo (Calb1Lbx1;SOM-)	Normal	0/35 (0%)	0/35 (0%)	0/35 (0%)	2/35 (5.7%)	1/35 (2.9%)	0/35 (0%)	M; 24/35 (68.6%) P ; 4/35 (11.4%)	10/35 (28.6%)	19/35 (54.3%)
	Str & Bic	0/32 (0%)	0/32 (0%)	0/32 (0%)	2/32 (6.3%)	0/32 (0%)	0/32 (0%)	M; 24/32 (75%) P; 3/32 (9.3%)	0/32 (0%)	23/32 (71.9%)
Lamina II (Calb1Lbx1;SOM+)	Normal	M; 7/30 (23.3%) P; 2/30 (6.7%)	11/30 (36.7%)	7/30 (23.3%)	M; 6/30 (20%) P; 5/30 (16.7%)	10/30 (33.3%)	5/30 (16.7%)	M; 8/30 (26.7%) P; 4/30 (13.3%)	4/30 (13.3%)	7/30 (23.3%)
	Str & Bic	M; 9/27 (33.3%) P; 5/27 (18.5%)	0/27 (0%)	7/27 (25.9%)	M; 6/27 (22.2%) P; 6/27 (22.2%)	0/27 (0%)	7/27 (25.9%)	M; 9/27 (33.3%) P; 5/27 (18.5%)	0/27 (0%)	8/27 (29.6%)

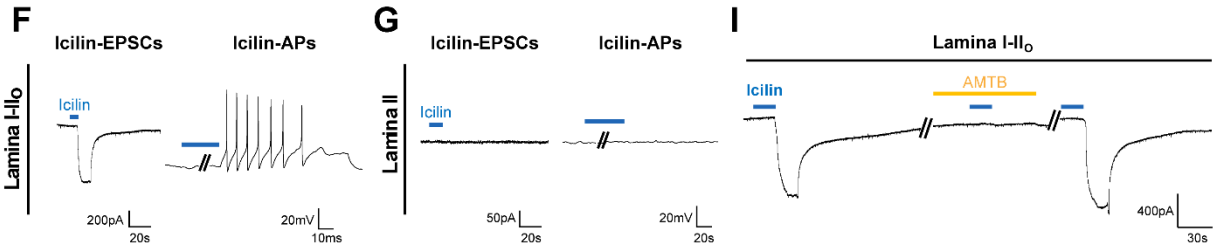

H

Region	Icilin-EPSCs	Icilin-APs	Firing pattern	
			Initial Bursting	Regular
Lamina I-IIo (Calb1Lbx1;SOM-)	13/35 (37.1%)	8/35 (22.9%)	8/8 (100%)	0/8 (0%)
Lamina II (Calb1Lbx1;SOM+)	0/30 (0%)	0/30 (0%)	N/A	N/A

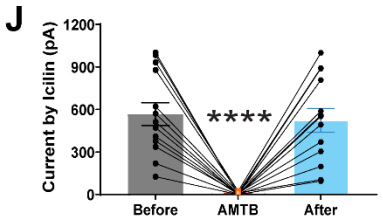

Figure 3.12 Firing Patterns and Sensory Inputs of Two Subpopulations of Calb1^{Lbx1} Neurons in the Superficial Dorsal Horn of the Spinal Cord

(A) Schematic demonstrating the location of Calb1^{Lbx1};SOM^{-} neurons in lamina I-II$_o$. Red dots: recorded Calb1^{Lbx1};SOM^{-} neurons. n = 57 from 10 naïve *Calb1^{Lbx1}*;Ai65 mice.

(B) Firing properties of Calb1^{Lbx1};SOM^{-} neurons in lamina I-II$_o$.

(C) Schematic demonstrating the location of Calb1^{Lbx1};SOM^{+} neurons in lamina II. Red dots: recorded Calb1^{Lbx1};SOM^{+} neurons. n = 47 from 10 naïve *Calb1^{Lbx1}*;Ai65 mice.

(D) Firing properties of Calb1^{Lbx1};SOM^{+} neurons in lamina II.

(E) Summary of Aβ-, Aδ- or C- evoked EPSCs, IPSCs, and APs in Calb1^{Lbx1};SOM^{-} neurons in lamina I-II$_o$ (top) and Calb1^{Lbx1};SOM^{+} neurons in lamina II (bottom) under normal conditions, and after strychnine and bicuculline application. Table represents a summary of sensory inputs in 35 Calb1^{Lbx1};SOM^{-} neurons in lamina I-II$_o$ under normal condition, and 32 Calb1^{Lbx1};SOM^{-} neurons in lamina I-II$_o$ upon strychnine and bicuculline application; 30 Calb1^{Lbx1};SOM^{+} neurons in lamina II under normal condition, and 27 Calb1^{Lbx1};SOM^{+} neurons in lamina II upon strychnine and bicuculline application. M, monosynaptic inputs. P, polysynaptic inputs.

(F) Representative traces of icilin-induced eEPSC (left) and icilin-induced eAPs (right) in Calb1^{Lbx1};SOM^{-} neurons in lamina I-II$_o$. Horizontal blue line indicates 1μM icilin application to the DRG chamber.

(G) Representative traces of icilin-induced eEPSC (left) and icilin-induced eAPs (right) in Calb1^{Lbx1};SOM^{+} neurons in lamina II. Horizontal blue line indicates 1μM icilin application to the DRG chamber.

(H) Summarized table of icilin-induced eEPSCs and icilin-induced eAPs at 1 μM concentration in Calb1^{Lbx1};SOM^{-} neurons in lamina I-II$_o$ (top) and Calb1^{Lbx1};SOM^{+} neurons in lamina II (bottom) from 10 naïve *Calb1^{Lbx1}*;Ai65 mice. Right panel: All icilin-responsive Calb1^{Lbx1};SOM^{-} neurons demonstrate an initial bursting firing pattern.

(I) Representative trace showing a Calb1^{Lbx1};SOM^{-} neuron recorded upon administration of icilin (before), during co-administration of icilin and AMTB (middle), and upon administration of icilin (after). Diagonal lines indicate passage of time between chemical administrations. Blue lines represent 1 μM icilin application. Yellow line represents 100 μM AMTB administration.

(J) Quantification of icilin-induced eEPSCs in Calb1^{Lbx1};SOM^{-} neurons. n = 13 from 10 naïve *Calb1^{Lbx1}*;Ai65 mice; **** p < 0.0001 two-way ANOVA with Tukey post hoc analysis.

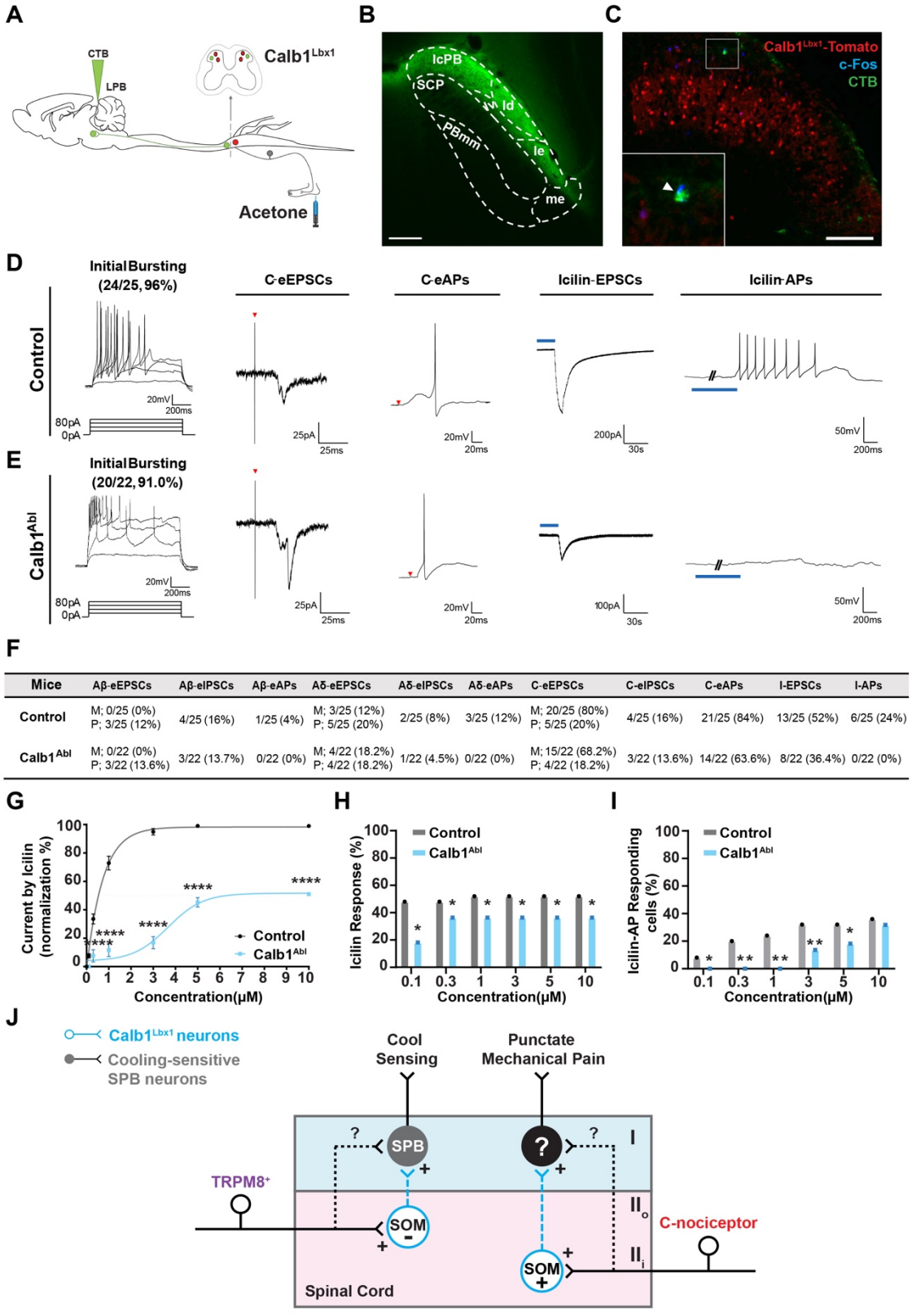

Mice	Aβ-eEPSCs	Aβ-eIPSCs	Aβ-eAPs	Aδ-eEPSCs	Aδ-eIPSCs	Aδ-eAPs	C-eEPSCs	C-eIPSCs	C-eAPs	I-EPSCs	I-APs
Control	M; 0/25 (0%) P; 3/25 (12%)	4/25 (16%)	1/25 (4%)	M; 3/25 (12%) P; 5/25 (20%)	2/25 (8%)	3/25 (12%)	M; 20/25 (80%) P; 5/25 (20%)	4/25 (16%)	21/25 (84%)	13/25 (52%)	6/25 (24%)
Calb1Abl	M; 0/22 (0%) P; 3/22 (13.6%)	3/22 (13.7%)	0/22 (0%)	M; 4/22 (18.2%) P; 4/22 (18.2%)	1/22 (4.5%)	0/22 (0%)	M; 15/22 (68.2%) P; 4/22 (18.2%)	3/22 (13.6%)	14/22 (63.6%)	8/22 (36.4%)	0/22 (0%)

Figure 3.13 Calb1^{Lbx1} Neurons Amplify the Activity of Cooling-sensitive SPB Neurons

(A) Schematic demonstrating bilateral injection of fluorescent fluorophore conjugated cholera toxin subunit B (CTB) into the lateral parabrachial nucleus to label SPB neurons (green) and acetone co-administration onto hindpaw to label cooling-sensitive neurons in *Calb1^{Lbx1}*;Ai65 mice (red).

(B) Representative image of the injection site in the lateral parabrachial nucleus. Scale bar, 100 μm.

(C) Out of 68 labeled SPB neurons, no triple-positive (red: Calb1^{Lbx1}-Tomato^{+}; green: CTB; blue: Fos^{+}) cool SPB neurons were identified (0%, 0/68) in the ipsilateral dorsal horn of the spinal cord following acetone treatment. Inset represents high magnification of the boxed area. Arrowhead indicates a c-Fos and CTB double-positive cooling-sensitive SPB neuron that is Tomato^{-}. n = 9 sections from 3 mice. Scale bar, 100 μm.

(D-E) Representative firing properties, C fiber inputs, and icilin-induced eEPSCs and eAPs in CTB^{+} SPB neurons in control **(D)** and Calb1^{Abl} **(E)** mice. The majority of CTB^{+} SPB neurons in control (96%, 24/25) and Calb1^{Abl} (91.0%, 20/22) animals display an initial bursting firing pattern upon current injection. Horizontal blue line: Icilin 1μM. Red triangle: presentation of stimulus.

(F) Summary of Aβ-, Aδ-, and C- evoked EPSC, IPSC, and APs, and icilin-induced eEPSCs and APs in CTB^{+} SPB neurons in control and Calb1^{Abl} mice. Control: 25 neurons from 5 mice; Calb1^{Abl}: 22 neurons from 4 mice. M, monosynaptic inputs. P, polysynaptic inputs. Icilin: 1 μM.

(G) Dose response curve of icilin (μM)-induced eEPSCs in CTB^+ SPB neurons in control and $Calb1^{Abl}$ mice. Control: 13 neurons from 5 mice; $Calb1^{Abl}$: 8 neurons from 4 mice; **** $p < 0.0001$; *** $p < 0.001$; ** $p < 0.01$; * $p < 0.05$; two-way ANOVA with Sidak post hoc analysis.

(H) Quantification of icilin-evoked EPSCs in CTB^+ SPB neurons at different concentrations in control and $Calb1^{Abl}$ mice. Control: 13 neurons from 5 mice; $Calb1^{Abl}$: 8 neurons from 4 mice; * $p < 0.05$; two-way ANOVA with Tukey post hoc analysis.

(I) Quantification of icilin-evoked APs in CTB^+ SPB neurons at different concentrations in Control and $Calb1^{Abl}$ mice. Control: 13 neurons from 5 mice; $Calb1^{Abl}$: 8 neurons from 4 mice; ** $p < 0.01$; * $p < 0.05$; two-way ANOVA with Tukey post hoc analysis.

(J) Schematic showing proposed neural pathways that transmits innocuous cool sensations and acute punctate mechanical pain. $Calb1^{Lbx1}$;SOM^- interneurons in laminae I-II_o receive monosynaptic inputs from $TRPM8^+$ primary sensory neurons and then innervate to cooling-sensitive SPB neurons via monosynaptic or polysynaptic connections; whereas $Calb1^+$;SOM^+ interneurons in lamina II are proposed to receive inputs from mechanosensitive C-nociceptors and then connect to unknown SPB neurons for acute punctate mechanical pain. However, whether $TRPM8^+$ fibers or C-nociceptor fibers synapse onto SPB neurons in lamina I remains unknown.

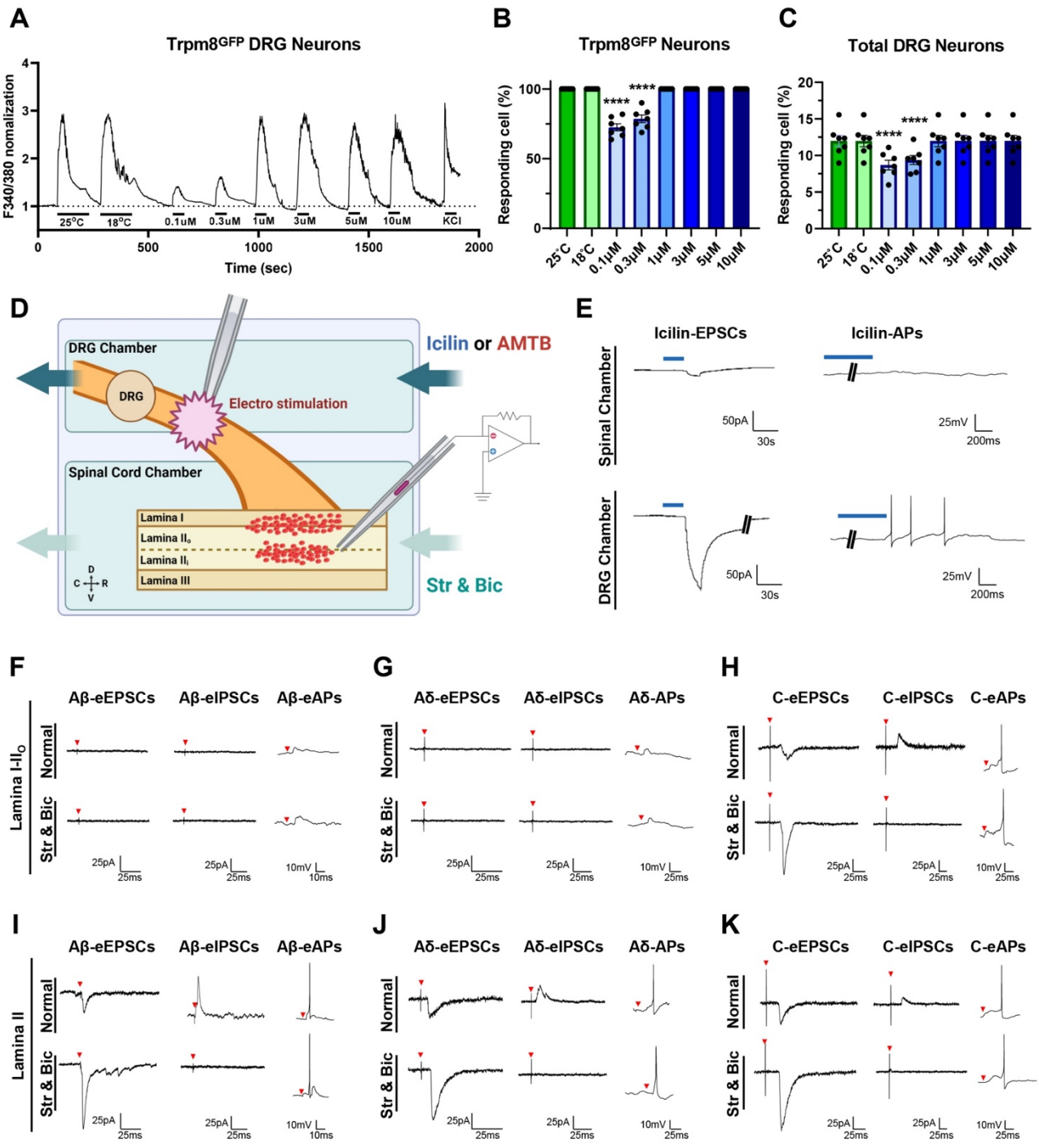
A
Trpm8GFP DRG Neurons
F340/380 nomalization
25°C
18°C
0.1uM
0.3uM
1uM
3uM
5uM
10uM
KCl
Time (sec)
B
Trpm8GFP Neurons
Responding cell (%)
C
Total DRG Neurons
Responding cell (%)
D
DRG Chamber
DRG
Electro stimulation
Spinal Cord Chamber
Lamina I
Lamina IIo
Lamina IIi
Lamina III
Icilin or AMTB
Str & Bic
E
Icilin-EPSCs
Icilin-APs
Spinal Chamber
DRG Chamber
50pA
30s
25mV
200ms
F
Aβ-eEPSCs
Aβ-eIPSCs
Aβ-eAPs
Lamina I-IIo
Normal
Str & Bic
G
Aδ-eEPSCs
Aδ-eIPSCs
Aδ-APs
H
C-eEPSCs
C-eIPSCs
C-eAPs
I
Lamina II
J
K

Figure 3.14. Activation of Superficial Calb1^{Lbx1} Neurons After Icilin Application to the DRG is Mediated by C-fiber Stimulation While Calb1^{Lbx1};SOM^{+} Neurons Receive Aβ, Aδ, and C Fiber Inputs

(A) Exemplar trace of calcium imaging change in fluorescence responses (F340/380) to various stimuli in cultured TRPM8^{GFP} DRG neurons. KCl: Potassium Chloride (50 mM). Icilin concentrations (μM): 0.1, 0.3, 1, 3, 5, and 10.

(B) Quantification of the percent of cells that respond to each stimulus in TRPM8^{GFP} cultured DRG neurons. TRPM8^{GFP} neurons: n = 103; icilin responding neurons: n = 84; **** $p < 0.0001$, two-way ANOVA with Tukey post hoc analysis. KCl: Potassium Chloride. Icilin concentrations (μM): 0.1, 0.3, 1, 3, 5, and 10.

(C) The total percentage of all DRG neurons that were responsive at various stimuli. DRG neurons: n = 697; icilin-responding neurons: n = 84; **** $p < 0.0001$, two-way ANOVA with Tukey post hoc analysis). KCl: Potassium Chloride. Icilin concentrations (μM): 0.1, 0.3, 1, 3, 5, and 10.

(D) Schematic demonstrating two-chamber apparatus that contains a DRG chamber and spinal cord chamber. Neurons are recorded in the spinal cord chamber while the attached DRG is separately housed to isolate stimulation application (electrical, icilin, and/or AMTB) (top). Glycine and $GABA_A$ receptor antagonists, strychnine and bicuculine respectively were administered to the spinal cord chamber (bottom) to block any inhibitory gating. Calb1^{Lbx1};SOM^{-} neurons were recorded in the superficial lamina I-II$_o$ whereas Calb1^{Lbx1};SOM^{+} neurons were recorded from lamina II. Red dots represent recorded neurons.

(E) Calb1^{Lbx1}-Tomato^{+} neurons recorded in lamina I-II$_o$ upon icilin administration to either the spinal cord chamber (top row) or DRG chamber (bottom row). A small icilin induced EPSCs (left column) and no APs (right column) responses were recorded from icilin application to the spinal cord chamber whereas icilin application to the DRG chamber evoked both EPSCs and APs. Blue line: 1 μM icilin application. n = 10.

(F-H) Exemplar traces of Aβ-evoked **(F)**, Aδ-evoked **(G)**, and C-evoked **(H)** EPSCs, IPSCs, APs recorded under normal conditions (top row) and under disinhibition condition (bottom row) in Calb1^{Lbx1};SOM^{-} neurons in lamina I-II$_o$. Str, strychnine. Bic, Bicuculline. Red arrowheads indicate stimulation artifacts.

(I-K) Exemplar traces of Aβ-evoked **(I)**, Aδ-evoked **(J)**, and C-evoked **(K)** EPSCs, IPSCs, APs recorded under normal conditions (top row) and under disinhibition condition (bottom row) in Calb1^{Lbx1};SOM^{+} neurons in lamina II. Str, strychnine. Bic, Bicuculline. Red arrowheads indicate stimulation artifacts.

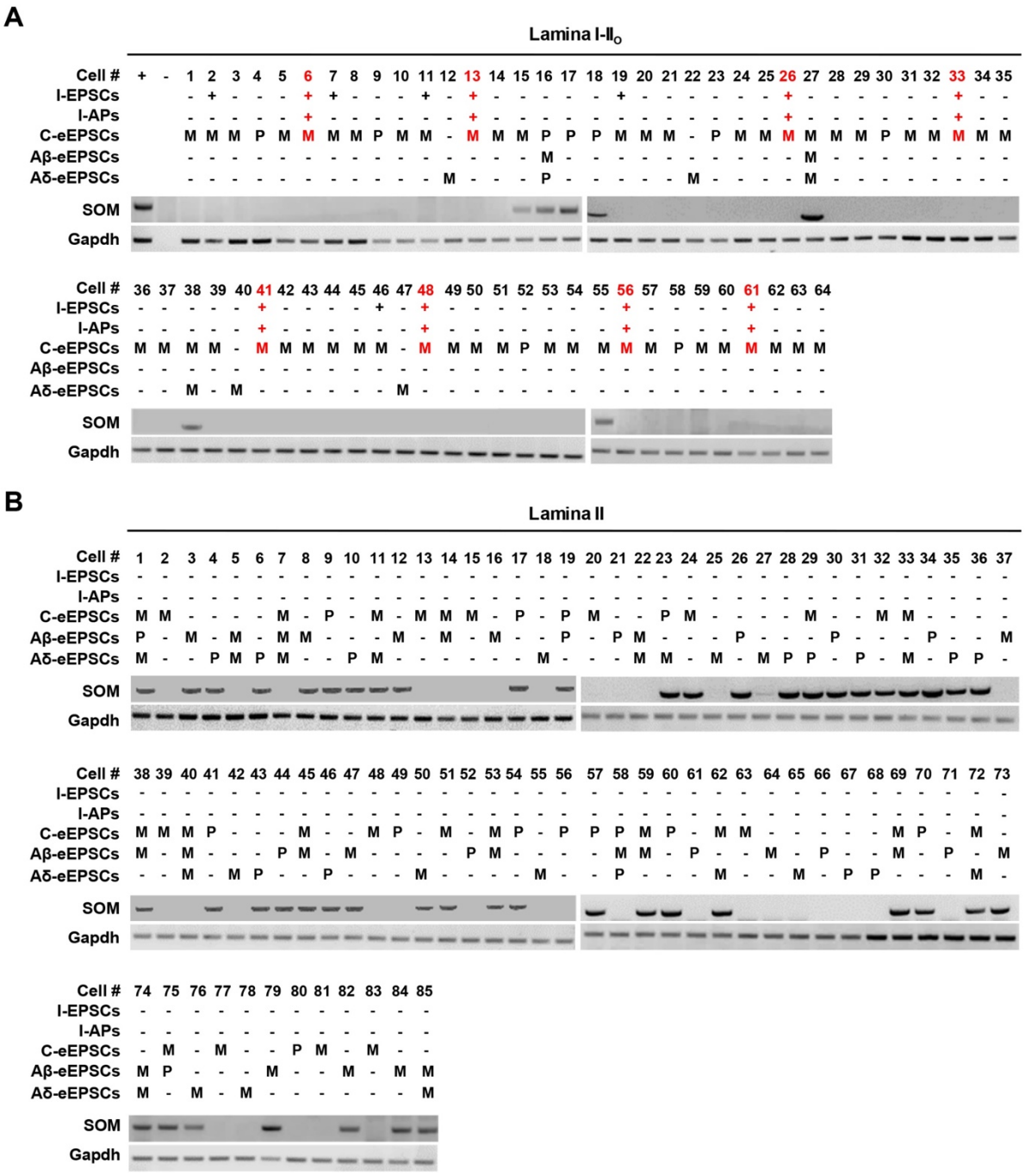
A
Lamina I-II$_o$
Cell #
I-EPSCs
I-APs
C-eEPSCs
Aβ-eEPSCs
Aδ-eEPSCs
SOM
Gapdh
B
Lamina II

Figure 3.15. RT-PCR Mediated Identification of Calb1^{Lbx1};SOM^{+} and Calb1^{Lbx1};SOM^{-} Neurons

(A) Following whole-cell patch clamp recordings, all recorded Calb1^{Lbx1};SOM^{-} neurons in lamina I-II$_o$ were identified by RT-PCR. SOM: Somatostatin; GAPDH: reference gene. M, monosynaptic inputs; P, polysynaptic inputs; +, positive control; -, negative control (mastermix without template DNA). Red highlights these neurons generating both Icilin-EPSCs and APs. Data were collected from 10 mice.

(B) Following whole-cell patch clamp recordings, all recorded Calb1^{Lbx1};SOM^{+} neurons in lamina II were identified by RT-PCR. SOM: Somatostatin; GAPDH: reference gene. M, monosynaptic inputs; P, polysynaptic inputs; +, positive control; -, negative control (mastermix without template DNA). Data were collected from 10 mice.

References

Andrew, D., and Craig, A.D. (2001). Spinothalamic lamina I neurones selectively responsive to cutaneous warming in cats. J Physiol 537, 489-495.

Bautista, D.M., Siemens, J., Glazer, J.M., Tsuruda, P.R., Basbaum, A.I., Stucky, C.L., Jordt, S.E., and Julius, D. (2007). The menthol receptor TRPM8 is the principal detector of environmental cold. Nature 448, 204-208.

Bester, H., Chapman, V., Besson, J.M., and Bernard, J.F. (2000). Physiological properties of the lamina I spinoparabrachial neurons in the rat. J Neurophysiol 83, 2239-2259.

Bourane, S., Duan, B., Koch, S.C., Dalet, A., Britz, O., Garcia-Campmany, L., Kim, E., Cheng, L., Ghosh, A., Ma, Q., and Goulding, M. (2015). Gate control of mechanical itch by a subpopulation of spinal cord interneurons. Science 350, 550-554.

Braz, J., Solorzano, C., Wang, X., and Basbaum, A.I. (2014). Transmitting pain and itch messages: a contemporary view of the spinal cord circuits that generate gate control. Neuron 82, 522-536.

Burton, H. (1975). Responses of spinal cord neurons to systematic changes in hindlimb skin temperatures in cats and primates. J Neurophysiol 38, 1060-1079.

Caterina, M.J., Leffler, A., Malmberg, A.B., Martin, W.J., Trafton, J., Petersen-Zeitz, K.R., Koltzenburg, M., Basbaum, A.I., and Julius, D. (2000). Impaired nociception and pain sensation in mice lacking the capsaicin receptor. Science 288, 306-313.

Caterina, M.J., Schumacher, M.A., Tominaga, M., Rosen, T.A., Levine, J.D., and Julius, D. (1997). The capsaicin receptor: a heat-activated ion channel in the pain pathway. Nature 389, 816-824.

Cavanaugh, D.J., Lee, H., Lo, L., Shields, S.D., Zylka, M.J., Basbaum, A.I., and Anderson, D.J. (2009). Distinct subsets of unmyelinated primary sensory fibers mediate behavioral responses to noxious thermal and mechanical stimuli. Proc Natl Acad Sci U S A 106, 9075-9080.

Chisholm, K.I., Lo Re, L., Polgar, E., Gutierrez-Mecinas, M., Todd, A.J., and McMahon, S.B. (2021). Encoding of cutaneous stimuli by lamina I projection neurons. Pain 162, 2405-2417.

Christensen, B.N., and Perl, E.R. (1970). Spinal neurons specifically excited by noxious or thermal stimuli: marginal zone of the dorsal horn. J Neurophysiol 33, 293-307.

Colburn, R.W., Lubin, M.L., Stone, D.J., Jr., Wang, Y., Lawrence, D., D'Andrea, M.R., Brandt, M.R., Liu, Y., Flores, C.M., and Qin, N. (2007). Attenuated cold sensitivity in TRPM8 null mice. Neuron 54, 379-386.

Craig, A.D., and Kniffki, K.D. (1985). Spinothalamic lumbosacral lamina I cells responsive to skin and muscle stimulation in the cat. J Physiol 365, 197-221.

Craig, A.D., Krout, K., and Andrew, D. (2001). Quantitative response characteristics of thermoreceptive and nociceptive lamina I spinothalamic neurons in the cat. J Neurophysiol 86, 1459-1480.

Dhaka, A., Earley, T.J., Watson, J., and Patapoutian, A. (2008). Visualizing cold spots: TRPM8-expressing sensory neurons and their projections. J Neurosci 28, 566-575.

Dhaka, A., Murray, A.N., Mathur, J., Earley, T.J., Petrus, M.J., and Patapoutian, A. (2007). TRPM8 is required for cold sensation in mice. Neuron 54, 371-378.

Duan, B., Cheng, L., Bourane, S., Britz, O., Padilla, C., Garcia-Campmany, L., Krashes, M., Knowlton, W., Velasquez, T., Ren, X.*, et al.* (2014). Identification of spinal circuits transmitting and gating mechanical pain. Cell 159, 1417-1432.

Gatto, G., Bourane, S., Ren, X., Di Costanzo, S., Fenton, P.K., Halder, P., Seal, R.P., and Goulding, M.D. (2021). A Functional Topographic Map for Spinal Sensorimotor Reflexes. Neuron 109, 91-104 e105.

Gong, J., Liu, J., Ronan, E.A., He, F., Cai, W., Fatima, M., Zhang, W., Lee, H., Li, Z., Kim, G.H.*, et al.* (2019). A Cold-Sensing Receptor Encoded by a Glutamate Receptor Gene. Cell 178, 1375-1386 e1311.

Grudt, T.J., and Perl, E.R. (2002). Correlations between neuronal morphology and electrophysiological features in the rodent superficial dorsal horn. J Physiol 540, 189-207.

Han, Z.S., Zhang, E.T., and Craig, A.D. (1998). Nociceptive and thermoreceptive lamina I neurons are anatomically distinct. Nat Neurosci 1, 218-225.

Haring, M., Zeisel, A., Hochgerner, H., Rinwa, P., Jakobsson, J.E.T., Lonnerberg, P., La Manno, G., Sharma, N., Borgius, L., Kiehn, O.*, et al.* (2018). Neuronal atlas of the dorsal horn defines its architecture and links sensory input to transcriptional cell types. Nat Neurosci 21, 869-880.

Luz, L.L., Szucs, P., Pinho, R., and Safronov, B.V. (2010). Monosynaptic excitatory inputs to spinal lamina I anterolateral-tract-projecting neurons from neighbouring lamina I neurons. J Physiol 588, 4489-4505.

McKemy, D.D., Neuhausser, W.M., and Julius, D. (2002). Identification of a cold receptor reveals a general role for TRP channels in thermosensation. Nature 416, 52-58.

Milenkovic, N., Zhao, W.J., Walcher, J., Albert, T., Siemens, J., Lewin, G.R., and Poulet, J.F. (2014). A somatosensory circuit for cooling perception in mice. Nat Neurosci 17, 1560-1566.

Montell, C., and Caterina, M.J. (2007). Thermoregulation: channels that are cool to the core. Curr Biol 17, R885-887.

Palkar, R., Lippoldt, E.K., and McKemy, D.D. (2015). The molecular and cellular basis of thermosensation in mammals. Curr Opin Neurobiol 34, 14-19.

Pan, H., Fatima, M., Li, A., Lee, H., Cai, W., Horwitz, L., Hor, C.C., Zaher, N., Cin, M., Slade, H.*, et al.* (2019). Identification of a Spinal Circuit for Mechanical and Persistent Spontaneous Itch. Neuron 103, 1135-1149 e1136.

Patapoutian, A., Peier, A.M., Story, G.M., and Viswanath, V. (2003). ThermoTRP channels and beyond: mechanisms of temperature sensation. Nat Rev Neurosci 4, 529-539.

Peier, A.M., Moqrich, A., Hergarden, A.C., Reeve, A.J., Andersson, D.A., Story, G.M., Earley, T.J., Dragoni, I., McIntyre, P., Bevan, S., and Patapoutian, A. (2002). A TRP channel that senses cold stimuli and menthol. Cell 108, 705-715.

Ran, C., Hoon, M.A., and Chen, X. (2016). The coding of cutaneous temperature in the spinal cord. Nat Neurosci 19, 1201-1209.

Russ, D.E., Cross, R.B.P., Li, L., Koch, S.C., Matson, K.J.E., Yadav, A., Alkaslasi, M.R., Lee, D.I., Le Pichon, C.E., Menon, V., and Levine, A.J. (2021). A harmonized atlas of mouse spinal cord cell types and their spatial organization. Nat Commun 12, 5722.

Sequier, J.M., Hunziker, W., Andressen, C., and Celio, M.R. (1990). Calbindin D-28k Protein and mRNA Localization in the Rat Brain. Eur J Neurosci 2, 1118-1126.

Shen, F.Y., Harrington, M.M., Walker, L.A., Cheng, H.P.J., Boyden, E.S., and Cai, D. (2020). Light microscopy based approach for mapping connectivity with molecular specificity. Nat Commun 11, 4632.

Todd, A.J. (2010). Neuronal circuitry for pain processing in the dorsal horn. Nat Rev Neurosci 11, 823-836.

Torsney, C., and MacDermott, A.B. (2006). Disinhibition opens the gate to pathological pain signaling in superficial neurokinin 1 receptor-expressing neurons in rat spinal cord. J Neurosci 26, 1833-1843.

Vandewauw, I., De Clercq, K., Mulier, M., Held, K., Pinto, S., Van Ranst, N., Segal, A., Voet, T., Vennekens, R., Zimmermann, K.*, et al.* (2018). A TRP channel trio mediates acute noxious heat sensing. Nature 555, 662-666.

Wang, H., and Zylka, M.J. (2009). Mrgprd-expressing polymodal nociceptive neurons innervate most known classes of substantia gelatinosa neurons. J Neurosci 29, 13202-13209.

Xiao, R., and Xu, X.Z.S. (2021). Temperature Sensation: From Molecular Thermosensors to Neural Circuits and Coding Principles. Annu Rev Physiol 83, 205-230.

Yoshimura, M., and Jessell, T. (1990). Amino acid-mediated EPSPs at primary afferent synapses with substantia gelatinosa neurones in the rat spinal cord. J Physiol 430, 315-335.

Zhang, J.H., Morita, Y., Hironaka, T., Emson, P.C., and Tohyama, M. (1990). Ontological study of calbindin-D28k-like and parvalbumin-like immunoreactivities in rat spinal cord and dorsal root ganglia. J Comp Neurol 302, 715-728.

Chapter 4

Noise-overexposure-induced Auditory and Nociceptive Sensitization[2]

Abstract

Noise exposure can result in cochlear damage, contributing to hearing loss, fullness in the ear, tinnitus, and hyperacusis. Hyperacusis is a debilitating auditory hypersensitivity disorder characterized by decreased tolerance to environmental sounds. Hyperacusis can therefore be classified into two different types, loudness hyperacusis (intensity coding issue) and affective hyperacusis (discomfort, aversion, and pain dysregulation). Patients with hyperacusis report widespread skin hypersensitivity (Fioretti et al., 2016). How pain sensitivity is altered following noise exposure is not well understood. This study examines changes in nociceptive sensitivity following acute noise exposure in mice.

Introduction

Nociception is an evolutionarily conserved mechanism to detect and appropriately respond to noxious thermal, mechanical, or chemical stimuli and is necessary for survival. Sensitization of the pain pathway can lead to chronic pain, including innocuous stimuli-induced pain (allodynia) or extreme responses to noxious

[2] Drs. Bo Duan and Susan E. Shore conceptualized and directed this project. Lorraine Horwitz performed all experiments. Lorraine Horwitz, Tin Long Rex Fung, and Ilma Rovcanin provided data analysis. Mitchel Cin generated the place aversion schematic. Lorraine Horwitz wrote the manuscript.

stimuli due to increases sensitivity (hyperalgesia). Chronic pain can persist for long periods after an acute injury.

Nociception begins upon activation of peripheral nerve fibers known as nociceptors. Nociceptors are pseudo-unipolar sensory neurons in which one axon splits into two branches, a peripheral branch that innervates target organs such as the skin, and a central branch that innervates the spinal cord. The cell bodies of nociceptors are housed in the dorsal root ganglia for the body and the trigeminal ganglion for the face. Noxious stimuli detected by nociceptors are processed in the spinal cord then transmitted to the brain through two major ascending pathways, the spinothalamic and spinoparabrachial tracts. The spinothalamic tract projects directly to the thalamus for the sensory-discriminative component of pain (i.e., intensity of stimuli, location, duration, etc). The spinoparabrachial tract synapses onto neurons of the parabrachial nucleus in the dorsolateral pons, containing outputs to the amygdala, insular cortex, anterior cingulate cortex, medial prefrontal cortex for the emotional component of pain (i.e. discomfort, aversion, distress) (Basbaum et al., 2009).

Auditory nociception is an essential mechanism for the protection of the auditory system as the basic sensory component for sound transduction, the hair cell, does not regenerate in mammals. Loud noise-overexposure can result in several auditory disorders such as hyperacusis, hearing loss, tinnitus, and inflammation of the external and internal regions of the ear (Schecklmann et a., 2014; Tyler et al., 2014; Sood and Coles 1998; Bartnik et al., 1999; Jastreboff and Jastreboff, 2000; Anari et al., 1999; Baguley 2003). Similar to chronic pain, hyperacusis is a loudness disorder in which innocuous auditory stimuli are perceived as too loud, uncomfortable, or even painful

(Tyler et al., 2014), but does not affect the threshold to detect sounds (Tyler and Conrad-Armes, 1983). Hyperacusis has been further classified as loudness hyperacusis (moderate-intensity sounds are perceived as too loud), avoidance hyperacusis (negative emotional reaction to sounds) and pain hyperacusis (sound-induced pain) (Baguley et al., 2011). Pain hyperacusis can be particularly traumatic as pain within and/or surrounding the ear and parts of the face can begin almost immediately after moderate-intensity noise exposure or develop slowly over several hours (Hayes et al., 2014). Loudness hyperacusis can be classified as an intensity coding issue and attributed to the intensity discrimination component of pain signaled through the thalamus and somatosensory cortex. Alternatively, avoidance and pain hyperacusis encompass the affective emotional component of pain and we refer to them cumulatively as affective hyperacusis to aid in our development of animal models of hyperacusis that reflect patient phenotypes.

The acoustic startle response is currently the most commonly used method to assess hyperacusis in animals, however in humans the acoustic startle does not produce fear, or avoidance of sounds, but rather changes in the perceived loudness of a sound (Knudson and Melcher 2016). Furthermore, the presentation of noxious stimuli in mice can produce a freezing response as would be expected with noise-induced pain and discomfort characteristic of affective hyperacusis, making the interpretation of results more difficult. The acoustic startle response therefore may be more accurate in detecting loudness hyperacusis rather than affective hyperacusis.

Hyperacusis is co-morbid with somatosensory disorders such as fibromyalgia, migraine, complex regional pain syndrome, and facial allodynia (Schecklmann et a.,

2014; Geisser et al., 2008; Gothelf et al., 2006; Ashkenazi et al., 2010; Irimia et al., 2008; de Klayer et al., 2007; Abouzari et al., 2020). Current animal models of hyperacusis do not accurately reflect the complex phenotypic diversity of hyperacusis patients by distinguishing between hyperacusis type or co-occurrence of somatosensory disorders.

In this study, we used a noise-overexposure paradigm that produced temporary changes in the ability to detect auditory stimuli, then assessed affective and somatic pain. Animals exhibited affective-hyperacusis behaviors across several assays but did not show neural correlates for central gain, suggesting divergent waveform signatures between loudness and affective hyperacusis. Furthermore, regardless of affective-hyperacusis-like status, noise-overexposure resulted mechanical allodynia. Taken together, these results suggest that additional animal behavioral models are necessary to differentiate between affective and loudness hyperacusis in animal studies of hyperacusis to represent patient experiences more accurately, and that auditory insult produced long lasting changes in both the auditory and somatosensory systems.

Results

Noise Overexposure-induced Affective Hyperacusis-Like Behaviors

In the present study, we aimed to assess the affective emotional component of hyperacusis and characterize somatosensory dysregulation often reported by patient, but not previously been described in mice. For this purpose, we exposed both male and female mice to acoustic overstimulation (8-16kHz, 100dB SPL, 1 h), while age- and gender- matched littermate control animals received a sham noise exposure. 2-4 weeks

after acoustic trauma we measured changes to thermal and mechanical sensitivity, and 4-6 weeks after noise injury tested for affective hyperacusis (Figure 4.1A). We analyzed the data from each mouse dependent upon the hyperacusis-like status determined in the affective hyperacusis behavioral assays.

To detect affective hyperacusis-like phenotypes (referred to as 'hyperacusis-like') in noise exposed animals, we adapted a conditioned place aversion assay (Cheng et al., 2017; Manohar et al., 2017) (Figure 4.1B and C). As a control experiment, a group of control mice were assessed to determine if innocuous noise presentation can induce aversion behaviors in animals that have no previous noise exposure. Control animals did not exhibit a significant difference in time spent in the light chamber post-conditioning compared to each animal's own baseline measurements (Figure 4.1D). Following noise-over exposure, a conditioned place aversion paradigm was used to detect moderate intensity noise-induced aversion characteristic of hyperacusis in mice (Figure 4.1E). A separate population of noise-exposed mice from the same batch did not demonstrate affective hyperacusis, suggesting not all noise-exposed mice develop affective hyperacusis (Figure 4.1E). Interestingly, the ratio of noise-exposed mice with and without affective hyperacusis is similar to that of noise-exposed mice with and without tinnitus (Koehler and Shore, 2013).

To confirm the presence of affective hyperacusis, we utilized the mouse grimace scale to detect facial metrics of pain and discomfort upon acute noise presentation (Figure 4.1F) (Langford et al., 2010). As the intensity of the noise stimulus increased, mean facial grimace scores became increasingly more distressed and painful. All animals previously identified as hyperacusis-like in the place aversion assay displayed

collapsed tolerance for innocuous sound presentation (Figure 4.1G), whereas no-hyperacusis animals were not significantly different from controls. These results suggest our novel animal behavioral paradigms are able to detect affective hyperacusis phenotypes in mice.

Characterization of Temporal Alterations in Auditory Functions

Temporary threshold shifts in auditory brainstem responses (ABR) were measured to detect permanent hearing loss that would affect hearing dependent behavior interpretations. All noise exposed mice regardless of hyperacusis-like status, displayed temporary hearing loss as indicated by a temporary ABR threshold shift at and above the noise-exposure frequencies. This ABR threshold shift return to baseline one week after the noise exposure and remained steady two weeks following the noise exposure (Figure 4.2A). Similarly, the distortion product otoacoustic emissions (DPOAE) threshold, a measure of outer hair cell health in the cochlea, was significantly shifted one day after noise exposure, which returned to control levels one week later and remained steady two weeks post-noise exposure (Figure 4.2B). ABR and DPOAE threshold was not significantly different from control groups after all behavior assays had been performed (data not shown)**.**

Characterization of Noise-Induced Somatosensory Sensitization

Noise-overexposure can affect not only the auditory but also the vestibular system. To measure any vestibular damage we first tested locomotor agility using the rotarod assay and found that locomotion ability remained intact (Figure 4.3A) in both

hyperacusis-like and no-hyperacusis animals compared to controls, suggesting the noise exposure paradigm did not significantly impair locomotor ability.

To detect skin sensitization often co-morbid with affective hyperacusis in humans, mechanical stimuli was applied to the face (cheek) or body (hindpaw). Starting at an innocuous level, von Frey fibers were applied to the check (0.008-2g) and nociceptive behavioral responses were recorded. Hyperacusis-like mice displayed a collapsed tolerance to mechanical stimulation exhibited by increased wiping, escape behaviors, vocalization, and facial pain indicators (Fig. 4.3B) compared to controls. Interestingly, no-hyperacusis animals exhibited sensitization to mechanical stimuli (0.04 and 0.07g) compared to controls, suggesting that noise-overexposure regardless of hyperacusis status, can produce mechanical allodynia (innocuous stimuli induced pain) (Figure 4.3B). Next, we assessed the threshold for mechanical pain using the up-down von Frey method (Figure 4.3C). We found that regardless of hyperacusis status, noise-exposed animals exhibited significant reductions in the threshold for punctate mechanical pain. As these behavior assays were assessed more than two weeks after the noise injury to allow for ABR and DPOAE physiological assays, these results suggest that noise-overexposure can produce chronic sensitization to mechanical stimuli.

Next, we evaluated changes in thermal nociception following noise-overexposure (Figure 4.3D-H). To test noxious heat nociceptive behavioral responses, we measured response latency to a hot plate (set at 46, 50, or 54°C) and the Hargreaves assay (Figure 4.3D-G). There was no difference in the latency to lick the hindpaw in the Hargreaves assay (Figure 4.3D). Concurrently, no significant difference

in the amount of time to respond (hindpaw lick) was observed between control, no-hyperacusis animals, or hyperacusis-like mice at any temperature (Figure 4.3E-G). These results suggest that noise exposure does not produce chronic nociceptive changes to noxious heat. To test changes in cold sensitivity, we again utilized the temperature plate, this time setting it to a noxious cold temperature (0°C). We found that the latency to lick the front paw was not significantly different between groups (control, no-hyperacusis, hyperacusis-like) (Figure 4.3H). Taken together, these results suggests that noise-overexposure does not produce sensitization to noxious hot or cold thermal stimuli.

Neural Correlates of Central Gain

It has been suggested that deafferentation due to noise injury results in compensatory hyperactivity in the central nervous system, described as “central gain” resulting in hyperacusis (Hickox and Liberman, 2014). The ABR waveform is comprised of seven waves, each corresponding to cumulative neuronal firing in nuclei across the canonical auditory pathway. Wave I corresponds to the auditory nerve, wave II to the cochlear nucleus, wave III to the superior olivary complex, wave iv to the lateral lemniscus, wave v and vi to the inferior collulcus, and wave vii to the medial geniculate and auditory cortex. Central gain could then be measured as a decrease in ABR wave I amplitudes (due to deafferentation) and a compensatory increase in the ABR wave V amplitude. To assess changes in neural correlates of central gain, we analyzed the wave I, wave II, and wave V amplitude changes across time. We found that one day after noise exposure, ABR wave I, wave II, and wave V amplitudes were significantly

decreased compared to controls and baseline measurements (Figure 4.4A, 4.4B, 4.5A, 4.5B, 4.6A, and 4.6B). There were more significant deficits in ABR wave I amplitudes at and above the frequency of noise exposure in no-hyperacusis animals (Figure 4.4C and 4.4D), mostly 14 days after noise exposure, although there were some significant differences between control and hyperacusis-like animals observed at 11.3 kHz and 16 kHz on 7 and 14 days after noise exposure respectively. 7 to 14 days after acoustic trauma, there were almost no significant differences between control, hyperacusis-like, and no-hyperacusis animals in ABR wave II (Figure 4.5C and D) or wave V (Figure 4.6C and D) amplitudes. Furthermore, we found no difference in ABR wave latencies (data not shown) at any timepoint. Overall, these results are not able to demonstrate neural correlates of central gain in affective hyperacusis-like animals.

Discussion

In the present study, we identified a noise-overexposure paradigm that can produce mechanical pain sensitization and affective hyperacusis. In particular, to identify affective hyperacusis, we adapted behavioral assays to detect the emotional component of pain by using an acute noise-induced facial grimace responses to noise and a conditioned place aversion assay to innocuous sound (Cheng et al., 2017; Manohar et al., 2017). To identify somatosensory sensitization, we employed nociceptive behavioral assays for mechanical and thermal pain (Duan et al., 2014; Pan et al., 2019). Our noise-overexposure paradigm was selected as it has previously been described to produced cochlear synaptopathy (Liberman et al., 2014; Fernandez et al., 2020), without producing long lasting affects to the hearing thresholds of the animal, which are necessary for the affective hyperacusis behavioral assays. Noise-

overexposed animals displayed ABR and DPOAE temporary threshold shifts that recovered one week after noise-overexposure. Similarly, overall there were very few long lasting changes to the mean ABR wave I, II, and V amplitudes in hyperacusis animals compared to controls. However, there was a decreasing trend in the wave I and II mean amplitudes at 16 kHz. Although there was no difference in ABR or DPOAE threshold taken after all behavior experiments were completed (data not shown), we do not exclude the possibility that amplitude decreases may compound overtime. Additional timepoints after 14 days would be beneficial in understanding this trend. Overall, our data suggests that neural amplification indicative of central gain is not present in animals with affective hyperacusis. In this study, we did not test for loudness hyperacusis. Future studies testing for affective and loudness hyperacusis in the same animal are necessary to delineate the relationship between different types of hyperacusis and central gain.

Although hyperacusis is comorbid with somatosensory disorders (Schecklmann et a., 2014; Geisser et al., 2008; Gothelf et al., 2006; Ashkenazi et al., 2010; Irimia et al., 2008; de Klayer et al., 2007; Abouzari et al., 2020), nociceptive changes after noise-overexposure have not been well studied in animals. Our results highlight the importance of developing animal models representative of the patient experience. By identifying a noise-overexposure paradigm that can produce mechanical pain sensitization, we can now better understand the interactions between the auditory and nociceptive systems. Pain is signaled through two pathways, the sensory discrimination (intensity, duration, etc.) and affective emotional (avoidance, discomfort, components of pain) through the thalamus and parabrachial nuclei receptively (Basbaum et al., 2009).

However, additional non-canonical pain pathways have been identified (Zhang et al., 2018; Zeng et al., 2011) that may be responsible for transmitting affective hyperacusis. The auditory to pain pathway for auditory nociception has not yet been identified, therefore the development of animal models will aid future studies. Our data indicates a previously undefined paradigm to induce mechanical allodynia in the face and body through noise-overexposure. The relationship between acoustic trauma and chronic sensitization to mechanical stimuli remains undefined. Future studies investigating the anatomical and physiological connectivity underlying auditory nociception are necessary to understand how noise is converted into pain under physiological conditions for auditory nociception, and pathological conditions resulting in hyperacusis.

Taken together, our present study has identified a novel auditory-nociception pathway involved in noise-overexposure-induce mechanical allodynia. Nociceptive tests were measured weeks after the noise trauma, therefore noise injury can result in chronic changes to the somatosensory system, similar to those seen in hyperacusis patients. Furthermore, by modeling the pain and discomfort aspect of hyperacusis seen in patients, we were able to develop novel methods to detect a subcategory of hyperacusis, affective hyperacusis. Through these experiments, we found that animals with affective hyperacusis do not display neural correlates of central gain, suggesting that central gain main be a component of loudness hyperacusis rather than affective hyperacusis.

Methods

Animals

All animal experiments were performed in accordance with protocols approved by the Institutional Animal Care and Use Committee at University of Michigan following NIH guidelines. Both male and female mice were used for all experiments. Mice were group housed at room temperature (25 °C) with *ad libitum* access to standard lab mouse pellet food and water on a 12-hour light/12-hour dark cycle. Animals with a mixed C57Bl6 x 129 background (Ouagazzal et al., 2006; Turner et al., 2012) were split into two groups and received either noise exposure (n=15, 7f, 8m), or sham exposure in age- and gender- matched littermate controls (n=15, 8f, 7m).

Noise Exposure

Mice were assigned at random into either a noise exposure or sham control group. Awake mice were individually placed within small mesh cages and then onto a rotating platform within a reverberant noise exposure chamber. The noise exposed group was exposed to an octave-band of noise (8-16kHz) at 100 dB SPL for 1 hour (Liberman et al., 2014; Fernandez et al., 2020). The sham control group was placed into the noise induction chamber in the same manner for an hour, but no sound was administered.

ABR and DPOAE Analysis

Auditory brainstem responses (ABRs) and distortion product otoacoustic emissions (DPOAEs) were performed and analyzed as previously described (Hashimoto et al., 2019; Wan et al., 2014), with the exception that ear pinna was not cut to avoid sensitization of the face due to trauma outside of the noise exposure.

Behavioral Testing

For all behavior tests the experimenter was blinded to the experimental condition. Baseline behavior testing began at the age of 8 weeks old. The behavioral and auditory physiological testing timeline was performed in the following order: baseline nociceptive behavior assays, baseline ABRs and DPOAEs, noise exposure, ABRs and DPOAEs measured 1, 7, and 14 days following noise exposure, post-noise-exposure nociceptive behavior assays, affective hyperacusis behavior assays. A final round of ABRs and DPOAEs was measured after all behavior experiments were completed. Overall, one hyperacusis-like male, two female controls, and three male control mice were excluded due to the following reasons: one hyperacusis-like male, one control female, and three control male mice were excluded from all experiments due to speaker malfunction during the conditioning period of the place aversion assay, as the place aversion assay was used to assess the hyperacusis-like status of the animal; one female control died during the experimental timeline and was removed; and two female controls were excluded from the facial grimace assay only due to corrupted data files.

Nociceptive Behavior Assays

After three to five ‘habituation’ sessions (20 minutes per day) in the behavior testing apparatus, acute somatosensory measures were recorded in the given order: rotarod, hind paw von Frey and Hargreaves (day 1), hot plate and cold plate (day 2). A cutoff of 60 seconds (46 °C), 30 seconds (50 °C), 20 seconds (54 °C), and 60 seconds (0 °C) was applied to prevent injury to the animal as previously described (Duan et al., 2014; Pan et al., 2019).

Affective Hyperacusis Behavior Assays

Place Aversion Assay

Adapted from Cheng et al., 2017, to measure the negative valence of an innocuous auditory sound presentation characteristic of affective hyperacusis, we used a biased compartment-assignment procedure in which we measured the amount of time spent in the dark compartment after conditioned association of the dark compartment to an innocuous 70 dB SPL octave band (8-16kHz) sound presentation. The place aversion apparatus consisted of two chambers, one dark side with a speaker located at the top of the compartment, and one bright, with a mesh floor underneath. A rectangular opening in the plastic divider separating the two compartments was closed during conditioning periods, restricting movement to just the conditioning chamber during for that trial. The divider was opened during the habituation sessions and recording period to allow the animal to travel freely between the two compartments. The amount of time the mouse spent in the light chamber was videorecorded on day 2 (baseline recording) and day 9 (post-conditioning recording). The total timeline for the place aversion assay consisted of 9 days. Each trial was 15 minutes. Days 1 and 2 were habituation periods in which the mice were allowed to freely travel between the two compartments. On the second habituation day the mice were recorded for 15 minutes and the time spent in the light chamber was calculates as the baseline value. On days 3, 5, and 7, mice were isolated to the bright chamber only, and on days 4, 6, and 8 mice were isolated to the dark chamber only and an innocuous 70 dB SPL octave band (8-16 kHz) sound was presented (FT17H Horn Super Tweeter, Fostex, Tokyo, Japan). On day 9, mice were allowed to freely move between the two chambers, no sound was presented, and the

time spent in the light chamber was recorded. The aversion score was measured as the difference in time spent in the light chamber (in minutes, seconds) after conditioning compared to before conditioning (post-conditioning in light chamber – pre-conditioning in light chamber).

Facial pain

The face was shaved at least 5-7 days before testing began. A gentle restraining device was used to restrict the movement of the mouse. Mice were habituated for two consecutive days for five minutes each day in the restraining device before testing began. On the day of testing, a von Frey hair of increasing force was applied to the mastoid region of the face at a 90° angle until bent randomly on either the left or right side of the face. 0.008, 0.02, 0.04, .07, 0.16, 0.4, 0.6, 1, 1.4, and 2 (g) von Frey hairs were applied individually, with 10 pokes per fiber. Recorded pain responses include unilateral or bilateral forepaw swipes across the face, vocalizations, continuous forepaw swipes, and/or aggression/biting of the probe following stimulus. No pain responses are indicated by light withdrawal or no response. The mice will be habituated to both the testing room and restraining device before the experiment, which will last no longer than 10 minutes for each animal (Kryzanowska et al., 2011).

Facial Grimace

The Mouse Grimace Scales (MGS) measures characteristic changes in facial expressions that are associated with pain (Langford et al., 2010). Changed in facial expressions of the eyes, nose, cheeks, whiskers, and ears positions upon sound

presentation ranging from 70 to 110 dB SPL increments (70, 75, 80, 85, 90, 95, 100, 105, 110 dB SPL) were videorecorded. A broadband noise at each sound intensity was presented randomly for each trial and each trial lasted less than 4 minutes each. The score represents the average mouse grimace score across three trials.

Quantification and Statistical Analysis

Results are expressed as mean ± SEM. Statistical analysis was performed in Prism 6 or 9 (GraphPad Software Inc., La Jolla, CA). A threshold of $p < 0.05$ was accepted as statistically different and $p > 0.05$ considered non-significant. For nociceptive experiments, locomotion coordination, hind paw von Frey, Hargreaves, and temperature data were subjected to two-way ANOVA with Sidak's post hoc analysis. For affective hyperacusis experiments, facial pain and facial grimace were subjected to two-way ANOVA with Tukey post hoc analysis. For place aversion experiments, control animals before and after conditioning were subjected to Student's paired t test; and place aversion comparison between all three groups was subjected to a one-way ANOVA with Tukey post host analysis. For all ABR and DPOAE analyses, two-way ANOVA with Tukey post hoc analysis was performed. No statistical methods were used to predetermine sample sizes, but our sample sizes are similar to those reported in previous publications (Duan et al., 2014; Pan et al., 2019).

Figures

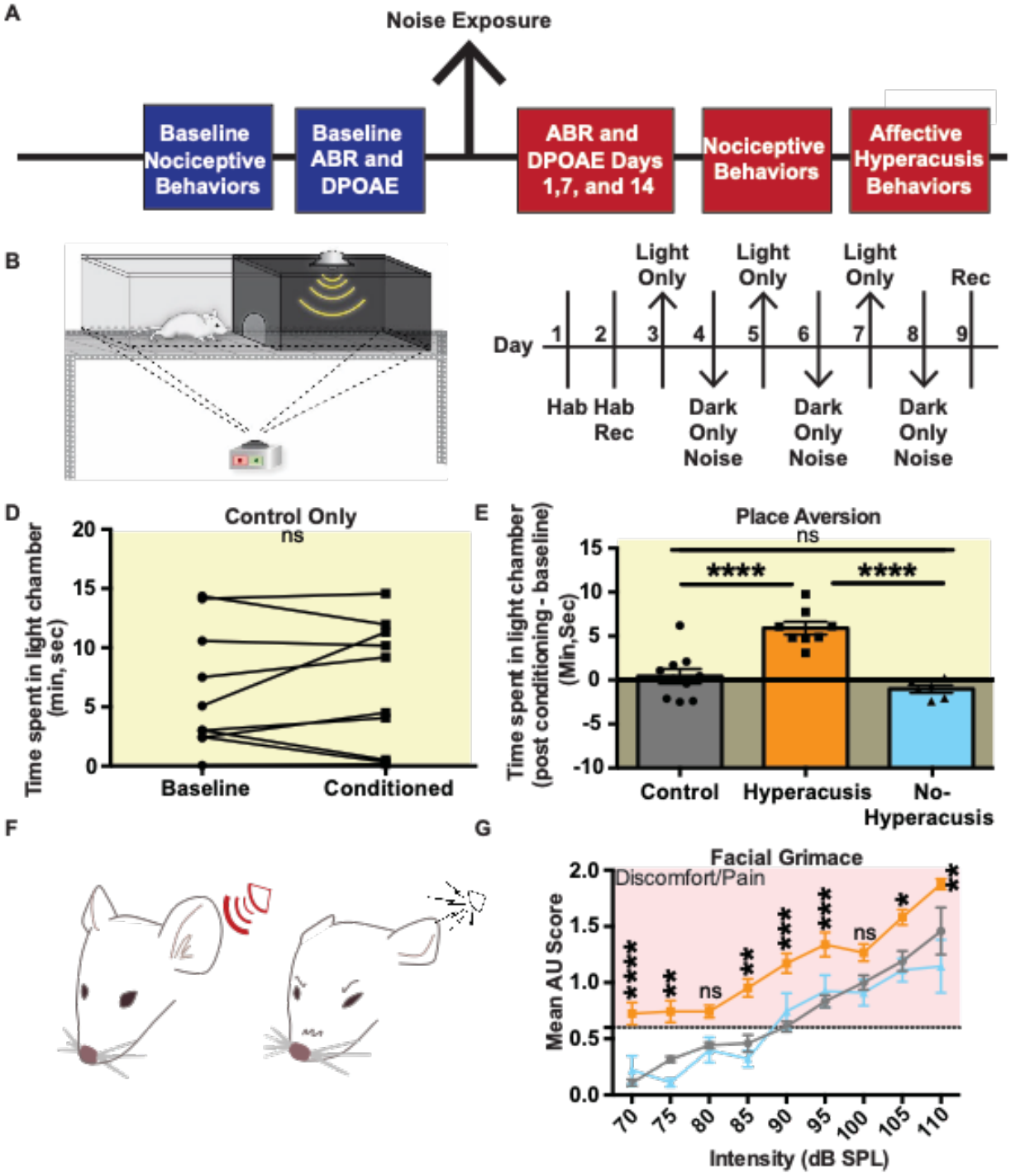

Figure 4.1 Classification of Affective Hyperacusis-like Animals

(A) Overview of Experimental Timeline

(B) Schematic of Adapted Place Aversion Assay

(C) Place Aversion Timeline. Rec: videorecording of time spent in light chamber. No barrier between the chambers or sound was presented on day of recording or habituation periods. Each trail was 15 minutes per session, one session per day.
(D) Time spent in the light chamber at baseline (habituation day 2) and post-conditioning in the place aversion apparatus in control animals only. Control: n = 10; ns, no significant difference; Student's paired t test.
(E) Place aversion assay in control and noise-exposed groups. Noise-exposed animals were split into 'hyperacusis-like' and 'no-hyperacusis' dependent upon their place preference (time spent in the light chamber). Bar graph represents the difference in time spent in the light chamber post-conditioning to baseline in minutes and seconds. Control (gray): n = 10; hyperacusis-like (orange): n = 8; no-hyperacusis (blue): n = 6; ns, no significant difference; **** $p < 0.0001$; two-way ANOVA with Tukey post hoc analysis.
(F) Schematic of mouse grimace response to noise, adapted from Langford et al., 2010.
(G) Facial grimace response to noise. AU: Action Score. Mean AU Score: the average of 3 trials at each intensity presented. Only clear images of the face were scored. AU Intensity rating is scored on a scale from 0 to 2, where 2 is the most severe. AU is scored across 5 metrics, orbital tightening, nose bulge, cheek bulge, ear position, and whisker changed. A broadband stimulis from 70 - 110 dB SPL was presented at random Control: n = 8; hyperacusis-like: n = 8; no-hyperacusis: n = 6; ns, no significant difference; * $p < 0.05$; ** $p < 0.01$; *** $p < 0.001$; **** $p < 0.0001$; two-way ANOVA with Tukey post hoc analysis.

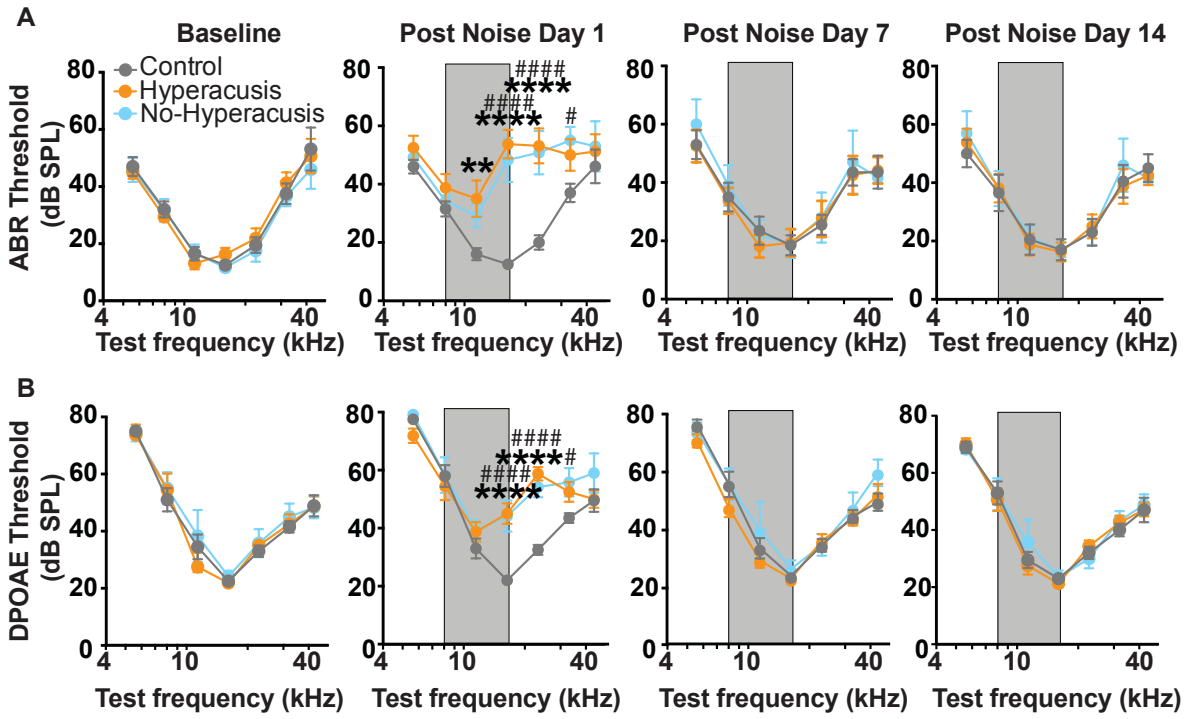

Figure 4.2 ABR and DPOAE Threshold Shifts Across Time

(A) Overview of Experimental Timeline ABR Threshold shift at baseline, and 1, 7, and 14 days after noise exposure. Frequencies of 5.6, 8, 11.3, 16, 22.6, 32, and 45.6 kHz were tested. Gray bar represents frequency of noise exposure (8 – 16 kHz, 100 dB SPL, 1hr). Control (gray): n = 10; hyperacusis-like (orange): n = 8; no-hyperacusis (blue): n = 6; * denotes statistics for the hyperacusis-like group. # denotes statistics for the no-hyperacusis group. ns, no significant difference; ** $p < 0.01$; **** $p < 0.0001$; two-way ANOVA with Tukey post hoc analysis.

(B) Overview of Experimental Timeline DPOAE Threshold shift at baseline, and 1, 7, and 14 days after noise exposure. Frequencies of 5.6, 8, 11.3, 16, 22.6, 32, and 45.6 kHz were tested. Gray bar represents frequency of noise exposure (8 – 16 kHz, 100 dB SPL, 1hr). Control (gray): n = 10; hyperacusis-like (orange): n = 8; no-hyperacusis

(blue): n = 6; * denotes statistics for the hyperacusis-like group. # denotes statistics for the no-hyperacusis group. ns, no significant difference; **** $p < 0.0001$; two-way ANOVA with Tukey post hoc analysis.

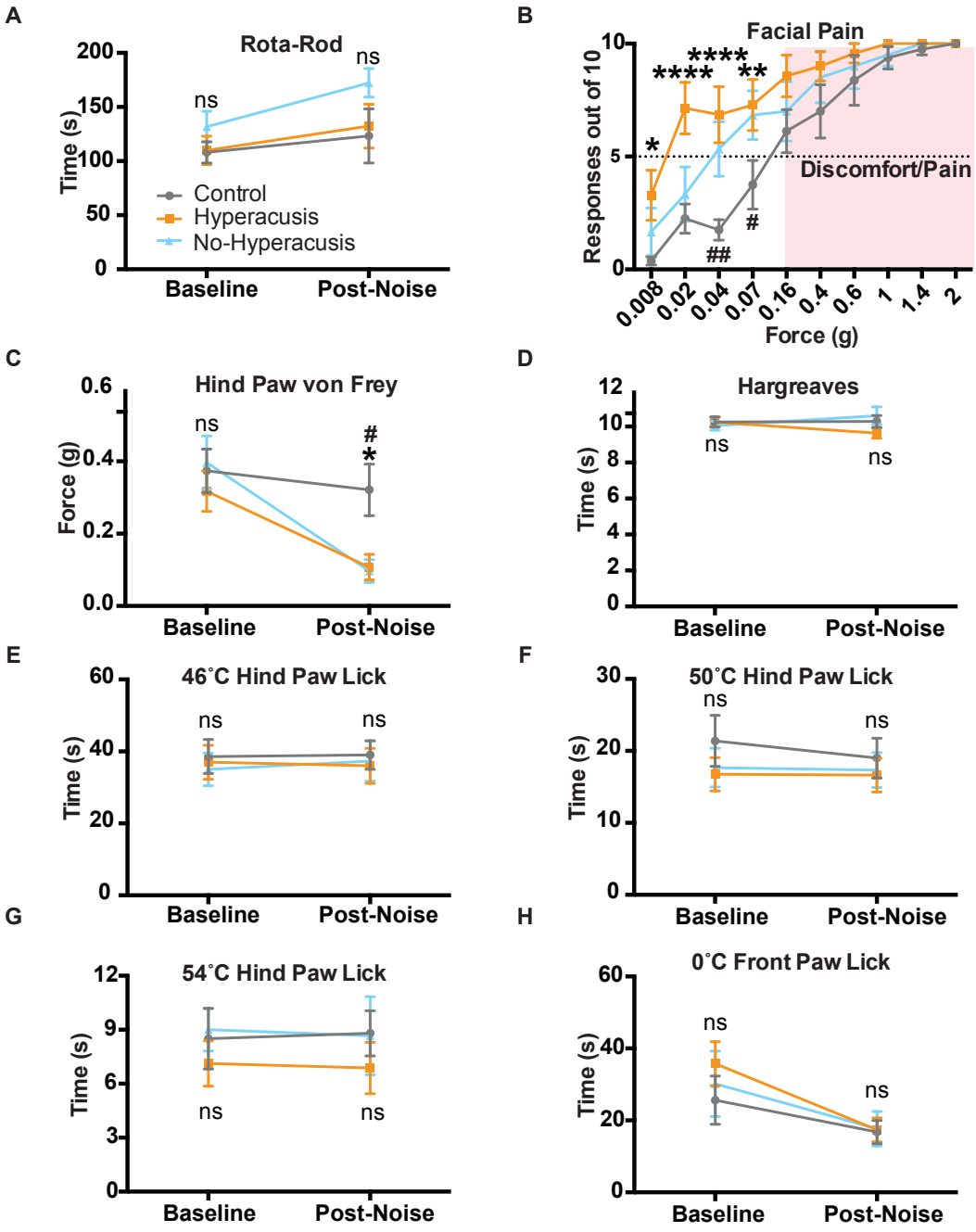

Figure 4.3 Behavioral Assessment of Locomotion, Touch, and Nociceptive Sensations After Acoustic Trauma

(A) Bar graph represents latency to fall in control, hyperacusis-like, and no-hyperacusis animals in the rotarod assay. No significant difference in the rotarod assay. Control: n =

10; hyperacusis-like: n = 8; no-hyperacusis: n = 6; ns, no significant difference; two-way ANOVA with Sidak post hoc analysis.

(B) Mechanical stimulation to the cheek of the face evoked nocifensive behavioral responses across increasing intensity of force. Noise-overexposed (hyperacusis-like and no-hyperacusis) animals exhibited significantly more nocifensive behavioral responses at a lower force compared to controls. Control: n = 10; hyperacusis-like: n = 8; no-hyperacusis: n = 6; ns, no significant difference; * denotes statistics for the hyperacusis-like group. # denotes statistics for the no-hyperacusis group. **** $p < 0.0001$; ** or ## $p < 0.01$; * or # $p < 0.05$; two-way ANOVA with Tukey post hoc analysis.

(C) Up-down von Frey threshold for mechanical pain in the hindpaw. Mechanical pain threshold was significantly reduced in noise-overexposed (hyperacusis-like and no-hyperacusis) animals compared to baseline and control. Control: n = 10; hyperacusis-like: n = 8; no-hyperacusis: n = 6; ns, no significant difference; * denotes statistics for the hyperacusis-like group. # denotes statistics for the no-hyperacusis group. * or #, $p < 0.05$; two-way ANOVA with Sidak post hoc analysis.

(D-G) Noxious heat thermosensation was measured through Hargreaves assay **(D)** and hot plate assay set to 46 °C, 50 °C, or 54 °C **(E-G)**. No significant difference in latency to lick the hindpaw between control, hyperacusis-like, or no-hyperacusis animals was observed. Control: n = 10; hyperacusis-like: n = 8; no-hyperacusis: n = 6; ns, no significant difference; two-way ANOVA with Sidak post hoc analysis.

(H) Noxious cold thermosensation was measured through cold plate assay set to 0 °C. No significant difference in latency to lick the front paw between control, hyperacusis-

like, or no-hyperacusis animals was observed. Control: n = 10; hyperacusis-like: n = 8; no-hyperacusis: n = 6; ns, no significant difference; two-way ANOVA with Sidak post hoc analysis.

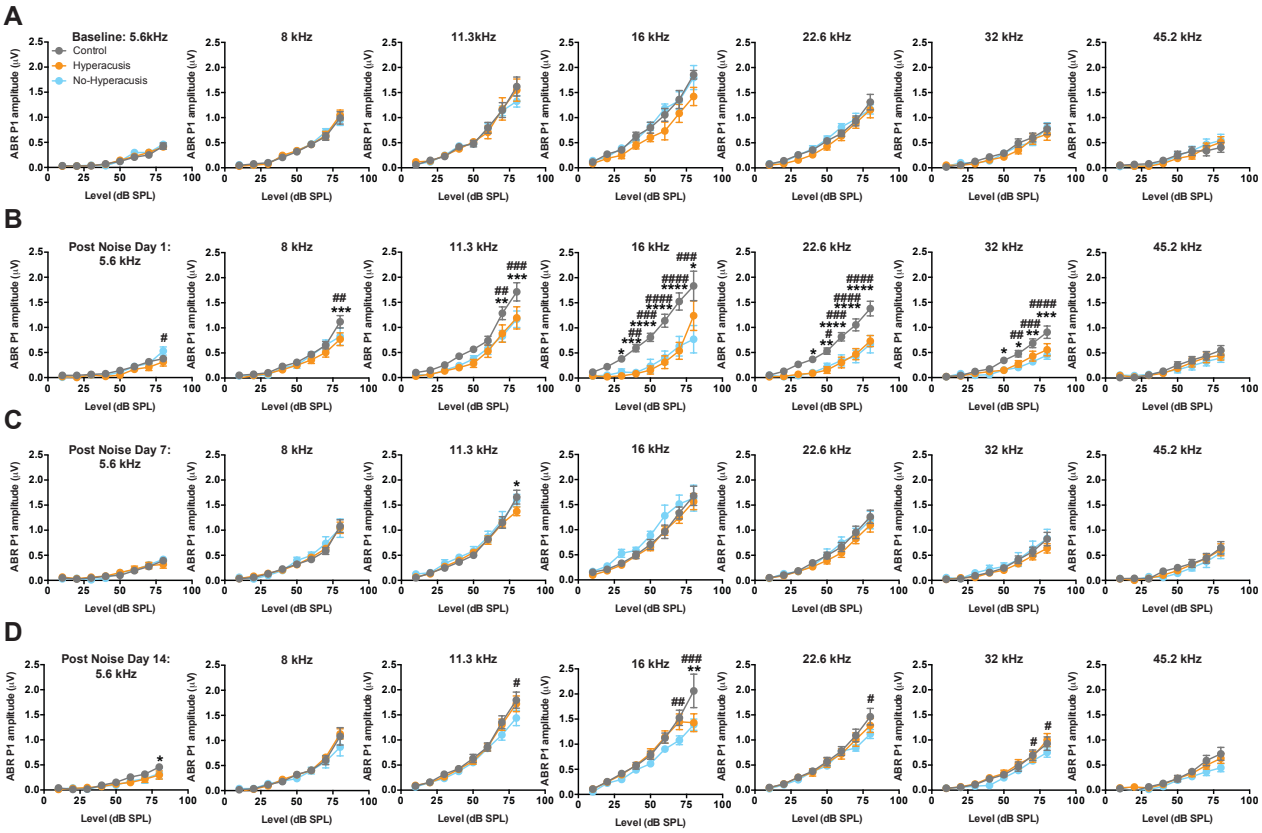

Figure 4.4 ABR Wave I Amplitudes Across Time

(A) No significant difference between control (gray), hyperacusis-like (orange), or no-hyperacusis (blue) mean wave I amplitudes to tone-pip stimuli at baseline were recorded. The test frequencies were presented at half-octave frequency intervals from 5.6 - 45.2 kHz starting at 10 dB SPL with 5 - dB steps and a maximum threshold of 80 dB SPL. Control: n = 10; hyperacusis-like: n = 8; no-hyperacusis: n = 6; two-way ANOVA with Tukey post hoc analysis.

(B) Animals that received an 8-16kHz 100 dB SPL 1hr noise exposure (hyperacusis-like, orange; no-hyperacusis, blue) had significant decreases in mean ABR wave I amplitudes one day post acoustic trauma compared to age- and gender-matched sham controls (gray). * denotes statistics for the hyperacusis-like group. # denotes statistics

for the no-hyperacusis group. Control: n = 10; hyperacusis-like: n = 8; no-hyperacusis: n = 6; * or # p < 0.05; ** or ## p < 0.01; *** or ### p < 0.001; **** or #### p < 0.0001; two-way ANOVA with Tukey post hoc analysis.

(C) Mean ABR wave I amplitude 7 days post-noise-exposure. No significant difference between control (gray), hyperacusis-like (orange), or no-hyperacusis (blue) at all test frequencies except 11.3 kHz (80 dB SPL only). * denotes statistics for the hyperacusis-like group. Control: n = 10; hyperacusis-like: n = 8; no-hyperacusis: n = 6; * p < 0.05; two-way ANOVA with Tukey post hoc analysis.

(D) Mean ABR wave I amplitude 14 days after acoustic overstimulation. No significant difference between control (gray) and hyperacusis-like (orange) animals at all test frequencies except 16 kHz and 5.6 kHz (80 dB SPL only). Significant differences between control and no-hyperacusis (blue) animals were recorded at several frequencies and intensities (11.3 kHz: 80 dB SPL; 16 kHz: 70 and 80 dB SPL; 22.6 kHz: 80 dB SPL; 32 kHz: 70 and 80 dB SPL). * denotes statistics for the hyperacusis-like group. # denotes statistics for the no-hyperacusis group. Control: n = 10; hyperacusis-like: n = 8; no-hyperacusis: n = 6; * or # p < 0.05; ** or ## p < 0.01; ### p < 0.001; two-way ANOVA with Tukey post hoc analysis.

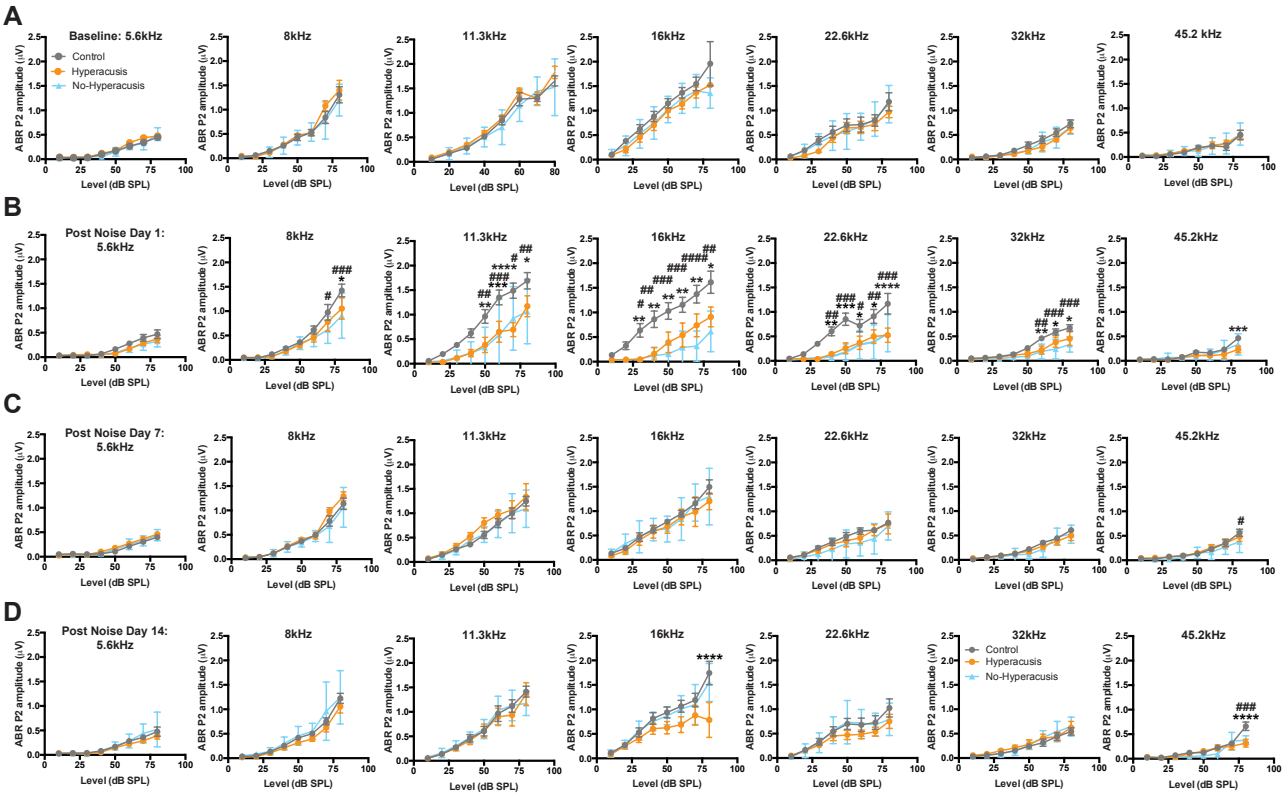

Figure 4.5 Mean ABR Wave II Amplitudes

(A) Mean wave II amplitudes to tone-pip stimuli showed no significant difference between control (gray), hyperacusis-like (orange), or no-hyperacusis (blue) at baseline. The test frequencies were presented at half-octave frequency intervals from 5.6 - 45.2 kHz starting at 10 dB SPL with 5 - dB steps and a maximum threshold of 80 dB SPL. Control: n = 10; hyperacusis-like: n = 8; no-hyperacusis: n = 6; two-way ANOVA with Tukey post hoc analysis.

(B) 8 - 16kHz 100 dB SPL 1hr noise exposure produced significantly decreased ABR wave II amplitude in hyperacusis-like (orange) and no-hyperacusis (blue) animals compared to sham-controls (gray). * denotes statistics for the hyperacusis-like group. # denotes statistics for the no-hyperacusis group. Control: n = 10; hyperacusis-like: n = 8;

no-hyperacusis: n = 6; * or # p < 0.05; ** or ## p < 0.01; *** or ### p < 0.001; **** or #### p < 0.0001; two-way ANOVA with Tukey post hoc analysis.

(C) Mean ABR wave I amplitude 7 days following sound injury. No significant difference between control (gray), hyperacusis-like (orange), and no-hyperacusis (blue) animals at any test frequency except at 45.2 kHz (80 dB SPL) in the no-hyperacusis group. # denotes statistics for the no-hyperacusis group. Control: n = 10; hyperacusis-like: n = 8; no-hyperacusis: n = 6; # p < 0.05; two-way ANOVA with Tukey post hoc analysis.

(D) Changes in mean ABR wave I amplitude 14 days after noise-overexposure. No significant difference between control (gray), hyperacusis-like (orange), or no-hyperacusis (blue) at any test frequencies except 16 kHz (80 dB SPL only) and 45.2 kHz (80 dB SPL only) in hyperacusis-like animals, and 45.2 kHz (80 dB SPL) in the no-hyperacusis group. * denotes statistics for the hyperacusis-like group. Control: n = 10; hyperacusis-like: n = 8; no-hyperacusis: n = 6; ### p < 0.001; **** p < 0.0001; two-way ANOVA with Tukey post hoc analysis.

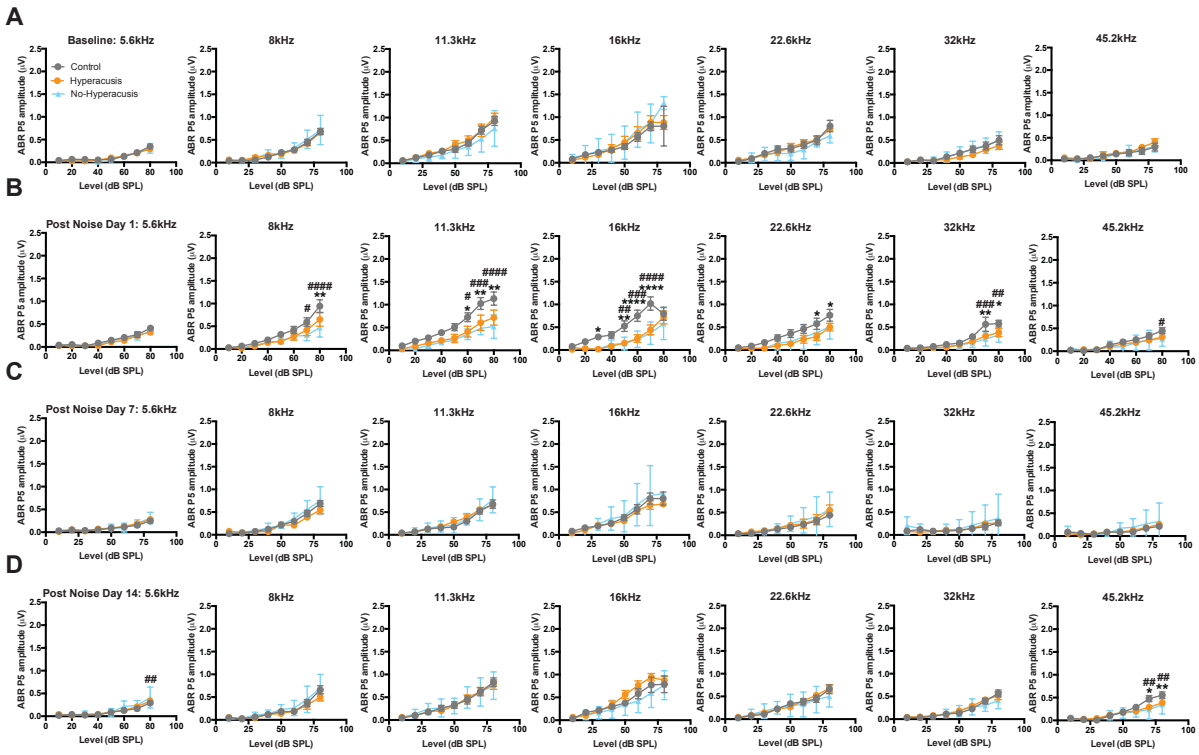

Figure 4.6 Mean ABR Wave V Amplitudes

(A) Mean wave V amplitudes to tone-pip stimuli showed no significant difference between control (gray), hyperacusis-like (orange), or no-hyperacusis (blue) at baseline. The test frequencies were presented at half-octave frequency intervals from 5.6 - 45.2 kHz starting at 10 dB SPL with 5 - dB steps and a maximum threshold of 80 dB SPL. Control: n = 10; hyperacusis-like: n = 8; no-hyperacusis: n = 6; two-way ANOVA with Tukey post hoc analysis.

(B) 8 - 16kHz 100 dB SPL 1hr noise exposure produced significantly decreased mean ABR wave V amplitudes in noise-exposed hyperacusis-like (orange) and no-hyperacusis (blue) animals compared to sham-controls (gray). * denotes statistics for the hyperacusis-like group. # denotes statistics for the no-hyperacusis group. Control: n

= 10; hyperacusis-like: n = 8; no-hyperacusis: n = 6; * or # p < 0.05; ** or ## p < 0.01; ### p < 0.001; **** or #### p < 0.0001; two-way ANOVA with Tukey post hoc analysis.

(C) Mean ABR wave I amplitude 7 days after noise-overexposure. No significant difference between control (gray), hyperacusis-like (orange), and no-hyperacusis (blue) animals at any test frequency. Control: n = 10; hyperacusis-like: n = 8; no-hyperacusis: n = 6; # p < 0.05; two-way ANOVA with Tukey post hoc analysis.

(D) Changes in mean ABR wave I amplitude 14 days post acoustic overstimulation. No significant difference between control (gray), hyperacusis-like (orange), or no-hyperacusis (blue) at any test frequencies except 45.2 kHz (70 and 80 dB SPL) in hyperacusis-like animals, and 5.6 kHz (80 dB SPL only) and 45.2 kHz (70 and 80 dB SPL) in the no-hyperacusis group. * denotes statistics for the hyperacusis-like group. # denotes statistics for the no-hyperacusis group. Control: n = 10; hyperacusis-like: n = 8; no-hyperacusis: n = 6; * p < 0.05; ** or ## p < 0.01; two-way ANOVA with Tukey post hoc analysis.

References

Abouzari, M., Tan, D., Sarna, B., et al., (2020). Efficacy of Multi-Modal Migraine Prophylaxis Therapy on Hyperacusis Patients. Ann Otol Phinol Laryngol. 129 (5), 421-427.

Anari, M., Axelsson, A., Eliasson, A., Magnusson, L. (1999). Hypersensitivity to sound. Questionnaire data, audiometry and classification. Scand Audiol. 28, 219–30.

Ashkenazi, A., Yang, I., Mushtaq, A., Oshinsky, M.L. (2010) Is phonophobia associated with cutaneous allodynia in migraine? J Neurol Neurosurg Psychiatry. 81(11),1256–1260.

Baguley, D.M. (2003). Hyperacusis. J R Soc Med. 96, 582-585.

Bartnik, G., Fabijanska, A., Rogowski, M. (1999). Our experience in treatment of patients with tinnitus and/or hyperacusis using the habituation method. In: Hazell, J W P. , ed. Proceedings of the Sixth International Tinnitus Seminar. London: The Tinnitus and Hyperacusis Centre. 416–17.

Basbaum, A. I., Bautista, D. M., Scherrer, G. & Julius, D. (2009). Cellular and molecular mechanisms of pain. Cell 139, 267–284.

Cheng, L., Duan, B., Huang, T., Zhang, Y., Chen, Y., Britz, O., Garcia-Campmany, L., Ren, X., Vong, L., Lowell, B.B., Goulding, M., Wang, Y., Ma, Q. (2017) Identification of spinal circuits involved in touch-evoked dynamic mechanical pain. Nat Neurosci. 20, 804-814.

de Klaver, M.J.M., van Rijn, M.A., Marinus. J., et al., (2007). Hyperacusis in patients with complex regional pain syndrome related dystonia. J Neurol, Neurosurg Psych. 78, 1310-1313.

Duan, B., Cheng, L., Bourange, S., Britz, O., Padilla, C., Garcia-Campmany, L., Krashes M., Knowlton W., Velasques T., Ren X., et al (2014). Identification of spinal circuits transmitting and gating mechanical pain. Cell 159, 1417-1432.

Fernandez, K.A., Guo, D., Micucci, S., De Gruttola, V., Liberman, C.M, Kujawa, S.G. Noise-induced Cochlear Synaptopathy with and Without Sensory Cell Loss. Neurosci. 47, 43-57.

Geisser, M.E., Glass, J.M., Rajcevska, L.D., Clauw, D.J., Williams, D.A., Kileny, P.R. et al., (2008). A psychophysical study of auditory and pressure sensitivity in patients with fibromyalgia and healthy controls. J Pain. 9(5), 417–422.

Gothelf, D., Farber, N., Raveh, E., Apter, A., Attias, J. (2006) Hyperacusis in Williams syndrome: characteristics and associated neuroaudiologic abnormalities. Neurology. 66(3), 390–395.

Hashimoto, K., Hickman, T.T., Suzuki, J., Ji, L., Kohrman, D.C., Corfas, G., Liberman, C.M. (2019). Protection from noise-induced cochlear synaptopathy by virally mediated overexpression of NT3. Scientifict Reports. 9, 15362.

Hickox, A.E. and Liberman, M.C. (2014) Is noise-induced cochlear neuropathy key to the generation of hyperacusis or tinnitus? J Neurophysiol. 111, 552-564.

Irimia, P., Cittadini, E., Paemeleire, K., Cohen, A.S., Goadsby, P.J. (2008). Unilateral photophobia or phonophobia in migraine compared with trigeminal autonomic cephalalgias. Cephalalgia. 28(6), 626–630.

Jastreboff, P.J. and Jastreboff, M.M. (2000). Tinnitus retraining therapy (TRT) as a method for treatment of tinnitus and hyperacusis patients. J Am Acad Audiol .11, 162–77.

Knudson, I.M., Melcher, J.R. (2016). Elevated acoustic startle responses in humans: relationship to reduced loudness discomfort level, but not self-report of hyperacusis. J. Assoc. Res. Otolaryngol. 17, 223e235.

Kryzanowska, A., Pittolo, S., Cabrerizo, M., Sanchez-Lopez, J., Krishnasamy, S., Venero, C., Avendano, C. (2011). Assessing nociceptive sensitivity in mouse models of inflammatory neuropathic trigeminal pain. J Neurosci Methods 201(1), 46-54.

Langford D, Bailey A, Chanda M, Clarke S, Drummond T, Echols S, Glick S, Ingrao J, Klassen-Ross T, Lacroix-Fralish M, Matsumiya L, Sorge R, Sotocinal S, Tabaka J, Wong D, van den Maagdenberg A, Ferrari M, Craig K, Mogil J (2010) Coding of facial expressions of pain in the laboratory mouse. *Nat Methods* 7(6):447-9

Koehler, S.D., Shore, S.E. (2013) Stimulus timing-dependent plasticity in dorsal cochlear nucleus is altered in tinnitus. J Neurosci 33, 19647–19656.

Manohar, S. Spoth, J., Radziwon, K., Auerbach, B.D., Salvi, R. (2017). Noise-induced hearing loss induces loudness intolerance in a rat Active Sound Avoidance Paradigm (ASAP). Hearing Research. 353, 197-203.

Ouagazzal, A.M.,Reiss, D.,Romand, B. (2006). Effects of age-related hearing loss on startle reflex and prepulse inhibition in mice on pure and mixed C57Bl and 129 genetic background. Behav Brain Res. 172, 307– 315.

Pan, H., Fatima, M., Li, A., Lee, H., Cai, W., Horwitz, L., Hor, C.C., Zaher, N., Cin, M., Slade, H.*, et al.* (2019). Identification of a Spinal Circuit for Mechanical and Persistent Spontaneous Itch. Neuron 103, 1135-1149 e1136.

Schecklmann, M., Landgrebe, M., Langguth, B., (2014). Phenotypic characteristics of hyperacusis in tinnitus. PLoS One. 9(1), e86944.

Sood, S.K., Coles, R.R.A. (1998). Hyperacusis and phonophobia in tinnitus patients. Br J Audiol. 22, 228.

Turner, J., Larsen, D., Hughes, L., Moechars, D., Shore, S. (2012). Time course of tinnitus development following noise exposure in mice. J Neurosci Research. 90(7), 1480-1488.

Tyler, R.S. and Conrad-Armes, D. (1983). The determination of tinnitus loudness considering the effects of recruitment. J Speech Hear Res. 26, 59-72.

Tyler, R.S., Pienkowski, M., Roncancio, E.R., Jun, H.J., Brozoski, T., Dauman, N., Dauman, N., Andersson, G., Keiner, A.J., Cacace, A.T., Martin, N., Moore, B.C. (2014). A review of hyperacusis and future directions: part I. Definitions and manifestations. Am J Audiol. 23, 402-419.

Wang, G., Gomez-Casati, M.E., Gigliello, A.R., Liberman, C.M., Corfas, G. (2014). Neurotrophin-3 regulates ribbon synapse density in the cochlea and induces synapse regeneration after acoustic trauma. eLife. https://doi.org/10.7554/eLife.03564.001.

Chapter 5

Discussion

5.1 Sensory Coding of Innocuous Stimuli in the Dorsal Horn of the Spinal Cord

While thermal heat seems to be coded in a clearly graded manner, meaning more heat-sensitive neurons are activated at an individual and population level as the thermal signal becomes stronger (i.e., increasingly hot); cool/cold temperatures are more complex. Instead, distinct populations are responsive to either narrow or broad ranges of cool/cold temperatures in a combinatorial coding scheme (Wang et al., 2018). Under this paradigm it is then possible that distinct spinal populations for cold sensing exist, in particular, a spinal population specific for innocuous cool sensing, a separate spinal population of unimodal (cold only) neurons, and a spinal population of polymodal (combination of cold, mechanical pain, and/or heat pain) neurons. In support of this hypothesis, ablation of TRPM8^{+} DRG neurons significantly reduced the number of spinal neurons responding to cool but not noxious cold (Ran et al 2016) stimuli. In agreeance, TRPM8 KO and TRPM8^{+} neuron ablated mice display deficits within the cool range (15-25 °C) in the two-temperature place preference test, but are still able to avoid noxious cold surfaces (<15 °C), suggesting the presence of an additional noxious cold sensor. GLR-3/GluK2 is an evolutionarily conserved cold sensor. GLR-3 is required for cold sensitivity and cold-induced avoidance responses in *C.elegans* and siRNA

knockdown of GuK2 in cultured DRG neurons specifically suppressed noxious cold but not innocuous-cool-temperature-induced calcium responses (Xiao and Xu 2021; Gong et al., 2019). Thus, there may be three populations of cold encoding neurons in the spinal cord: polymodal cold neurons, noxious/innocuous cold neurons, and innocuous cool neurons which are inhibited by the noxious and polymodal populations. We suggest that the Calb1^{+} spinal neuron is responsible for innocuous cool transmission, and the spinal neuron responsible for noxious cold transmission remains unknown.

5.2 Calb1 Amplification Interneurons in Innocuous Cool Coding

Lamina I spinothalamic and spinoparabrachial project neurons (PNs) in the dorsal horn of the spinal cord have been classified into three different types: nociceptive-specific (NS), polymodal nociceptive noxious heat, pinch, and noxious cold (HPC) neurons, and innocuous cool thermo-sensitive neurons (COOL) (Craig et al., in 2001; Dostrovsky and Craig 1996; Andrew and Craig 2001**;** Chisholm et al., 2021**;** Hachisuka et al., 2020). PNs in lamina I receive monosynaptic connections from the DRG (Grudt and Perl, 2002) from interneurons in lamina I and II (Luz et al., 2010), although the precise identity (NS, HPC, or COOL) of these PNs was not characterized. Studies in NS PNs have begun to investigate the input-output characteristics of NS PNs in the dorsal spinal cord (Agashkoy et al., 2019; Bester et al., 2000; Andrew 2009; Andrew and Craig 2002; Andrew 2010; Allard 209); however, few studies have addressed the direct and indirect inputs onto cool PNs or the coding mechanisms by which innocuous cool/warm information is transmitted to the brain.

Our study revealed a feed-forward microcircuit that transmits innocuous cool sensations in the superficial dorsal horn of the spinal cord. In this circuit, a small subpopulation of lamina I-II$_o$ Calb1^{Lbx1};SOM$^-$ neurons receive monosynaptic inputs from TRPM8$^+$ cooling-sensitive peripheral sensory neurons. Activation of TRPM8$^+$ neurons evokes action potential firing in Calb1^{Lbx1};SOM$^-$ neurons, which display an initial bursting firing pattern. Ablation of Calb1^{Lbx1} lineage neurons results in decreased activity in cool-sensitive spinoparabrachial PNs, suggesting that the subgroup of Calb1^{Lbx1};SOM$^-$ neurons provide excitatory input onto spinoparabrachial PNs, perhaps acting as an amplifier of cool afferent outputs to cool-sensitive spinoparabrachial PNs. Further studies characterizing the synaptic connections from Calb1^{Lbx1};SOM$^-$ neurons to cooling-sensitive spinoparabrachail and spinothalamic PNs will advance our understanding of the role of lamina I-II$_o$ Calb1^{Lbx1};SOM$^-$ neurons in cool transmission.

5.3 Projecting the Role of Cool-sensitive Projection Neurons

Neurokinin 1 receptor (NK1R) is a marker for spinothalamic and spinoparabrachial ascending projection neurons in lamina I of the dorsal horn of the spinal cord (Marshall et al., 1996; Ding et al., 1995). Lamina I cool-responsive neurons were shown to have a distinct pyramidal morphology (Han et al., 1998). NK1R positive spinothalamic projection neurons were mostly fusiform or multipolar neurons not pyramidal (Yu et a., 2005). In our study, we found a small population of Calb1^{Lbx1} lineage neurons were located in the lamina I (~10.5%), and that very few Calb1^{Lbx1} lineage neurons colocalized with NK1R (~1.5%). We then considered the possibility that Calb1^{Lbx1} lineage neurons were NK1R$^-$ pyramidal spinothalamic and/or

spinoparabrachial ascending projection neurons in lamina I of the dorsal horn of the spinal cord. However we found that no Calb1^{Lbx1} lineage neurons were labeled as cool spinoparabrachial projection neurons, and the Calb1 population could not be distinctly defined by a particular morphology. Preliminary experiments performed in Calb1^{Cre}-Tomato reporter animals showed a similar number of projection neurons in the dorsal spinal cord were labeled when the thalamus or lateral parabrachial nucleus was injected with CTB. This is consistent with other studies which show that spinoparabrachial projection neurons co-lateralize to send projections to other regions such as the thalamus or pariaqueductal gray. Al-Khater and Todd reported as high as 99% of C7-8, and 97% of L3-5 spinothalamic neurons were also lateral parabrachial projection neurons (Al-Khater and Todd, 2009). Therefore, while our present study only addressed spinoparabrachial Calb1^{Lbx1} lineage projection neurons it is very unlikely that there is a separate population of Calb1^{Lbx1} lineage projection neurons that exclusively target the thalamus for innocuous cool sensory discrimination. Future studies of cool-spinothalamic projection neurons would be useful to confirm the role of Calb1^{Lbx1} lineage neurons as interneurons and not cool-projection neurons.

Lamina I spinoparabrachial and spinothalamic nociceptive-specific and polymodal noxious heat, pinch, noxious cold responsive projection neurons have been identified (Chisholm et al., 2021; Hachisuka et al., 2020; Craig et al., 2001; Bester et al., 2000) but are highly heterogenous (Allard 2019). Recenlty, a subpopulation of spinoparabrachial projection neurons that exclusively respond to innocuous cool stimuli has been identified (Chisholm et al., 2021). The precise molecular, morphological, and physiological identity of spinal thermosensitive ascending circuits remain unknown.

Future studies are necessary to elucidate the functional characteristics of these temperature-sensitive pathways in the development of chronic pain (such as for cold allodynia).

5.4 Looking Towards the Future: Innocuous Cool Sensing Under Pathological Conditions

Our study showed that Calb1 interneurons are key for the transmission of innocuous cool temperature sensations in the dorsal horn of the spinal cord under physiological conditions. Under pathological conditions, normally innocuous cool temperatures are perceived as painful, a disorder known as cold allodynia that is often seen in patients with neuropathic pain (MacDonald et al., 2020). Injury to primary sensory neurons, such as spared nerve injury (SNI), spinal nerve ligation (SNL), and chronic constriction injury (CCI) can induce cold allodynia in rodent models (Allchorne et al., 2005; Proudfoot et al., 2006). TRPM8, which is presynaptic to Calb1 neurons, is involved in neuropathic cold allodynia (Proudfoot et al., 2006; Kayama et al., 2018). Ablation of Calb1^{Lbx1} lineage neurons in preliminary experiments, resulted in deficits in acetone-induced nocifensive responses, suggesting that Calb1^{Lbx1} lineage neurons are required for the development of cold allodynia under neuropathic conditions. Future studies are necessary to define the role of Calb1^{Lbx1} lineage neurons in the induction and transmission of cold allodynia.

5.5 Multisensory Integration Across Sensory Systems

Multisensory integration is the mechanism by which information from different sensory modalities (such as sight, sound, touch, smell, self-motion, and taste) is integrated by the nervous system. Pain is an evolutionarily conserved mechanism to detect noxious stimuli and engage in appropriate protective behaviors and avoid future life-threatening or dangerous situations. Although pain is an essential component of distinct sensory systems, alternations to the pain system can lead to chronic and debilitating aberrant signaling to innocuous stimulus. Chronic pain may play a role in the healing process, to promote guarding of the injured area for a prolonged period of time. However, in some cases the pain does not resolve resulting in extended periods of psychological and physiological distress. Chronic pain can be induced or maintained at both the peripheral and central divisions of the nervous system (Basbaum et al., 2009), therefore understanding the basic mechanisms of sensory transmission (such as innocuous cool-sensing) is important to understand the same system under pathological conditions (i.e. cold allodynia). For example, identification of a spinal circuit for mechanical pain revealed the presence of a population of inhibitory gating neurons, predicted in the gate-control theory of pain (Duan et al., 2014). Under pathological conditions, disinhibition (reduced inhibitory signaling from the inhibitory interneurons) results in the manifestation of mechanical allodynia. Similar mechanisms may be present in other sensory systems, therefore studies investigating how diverse sensory systems transmit pain may be useful in understand other sensory systems under pathological conditions.

Audition is an evolutionarily conserved sensory perception that allows for sound waves in the environment to be transduced into electrical signals that can be interpreted by the brain. Dysregulation of the auditory system due to noise-overexposure can lead to hyperacusis, a decreased tolerance to environmental sounds. Loudness hyperacusis can be classified as a sensory discrimination issue, whereas the negative emotional and painful perceptions of affective hyperacusis are more similar to the affective emotional component of pain transmitted through the medial thalamus and parabrachial nucleus in the canonical pain pathway (Figure 1.1) (Basbaum et al., 2009). The cochlear nucleus is similar to the dorsal horn of the spinal cord as it is the first relay station in the auditory pathway and receives primary sensory information from the auditory nerve fiber as well as the trigeminal ganglia and trigeminal nuclei. The CN is thus a major site of multisensory integration and may play an essential role in the pathophysiology of hyperacusis (Aries et al., 2017; Zeng et al., 2011). How auditory signals activate the pain pathway remain unknown.

5.6 Widening the Scope of Animals Models of Hyperacusis

Our current study introduced novel behavioral models for affective hyperacusis and noise-induced mechanical allodynia, a comorbid somatosensory disorder seen in hyperacusis patients (Ashkenazi et al., 2010; Abouzari et al., 2020). Future studies that combine current animal models for loudness hyperacusis (acoustic startle response input-output functions, operant conditioning, reaction intensity, etc.), tinnitus testing (gap pre-pulse inhibition of the acoustic startle response, two-choice operant conditioning, lick or lever pressing suppression etc.), affective hyperacusis testing (place aversion

assay, facial grimace in response to noise assay), and somatosensory testing (facial and hinpaw von Frey), would be useful in beginning to understand the underlying mechanisms of hyperacusis, the relationship between hyperacusis and tinnitus, and the processing of pain in multiple sensory systems (somatic and auditory) (Zhang et al., 2014; Chen et al., 2014; Radziwon and Salvi, 2020; Lauer and Dooling, 2007; Ison et al., 2007; Turner and Parrish, 2008; Sun et al., 2009; Sun et al., 2012; Pace and Zhang, 2013; Hickox and Liberman, 2014; Chen et al., 2013; Hayes et al., 2014; Jastreboff et al., 1988; Bauer et al., 1999; Ruttiger et al., 2003; Lobarinas et al., 2013; Heffner and Koay, 2005; Heffner and Harrington, 2002; Sederholm and Swedberg, 2013; Stolzberg et al., 2013; Turner et al., 2006; Turner et al., 2012). From these studies, the co-incidence of tinnitus, affective hyperacusis, loudness of hyperacusis, and mechanical allodynia in the same animal could be determines, and the prevalence could be compared to that of humans.

The behavioral timeline for our study included 1 week of baseline nociceptive behavior testing, 2 weeks of post-noise exposure ABR and DPOAE data collection, then 3 weeks of post-noise exposure affective hyperacusis and nociceptive behavior testing. One major limitation of tinnitus testing in particular is the weeks of behavioral testing to establish a GPIAS baseline (4 weeks), and post-noise exposure GPIAS testing (4 weeks, starting 4 weeks after noise exposure) (Wu et al., 2016a). Testing for both tinnitus, affective hyperacusis, and loudness hyperacusis would require multiple weeks of animal handling, even before noise exposure, which could result in additional stress and anxiety in the animals and unreliable responses in post-noise exposure tests. Acute behavioral test such as the facial grimace response to noise and nociceptive

somatosensory tests are useful because they limit the experimental timeline and prevent excessive stress and anxiety for the subjects. Future studies utilizing these new animal models to investigate the neuronal mechanisms underlying hyperacusis would be useful with the eventual goal of developing therapeutics in humans.

5.7 Theoretical Models of Hyperacusis

The Central Gain Model of hyperacusis suggests that hyperacusis results from compensatory increases in gain or neural amplification of the central auditory system as a result of decreased sensory input from the cochlea (Auerbach et al., 2014). The Acoustic Startle Response (ASR) is commonly used to assess (loudness) hyperacusis in animals, however changes in ASR input/output functions usually occur at high stimulus intensities (greater than 90 dB SPL) rather than at moderate sound stimulus levels characteristic of hyperacusis (Sun et al., 2009; Sun et al., 2012; Chen et al., 2014). Additionally, the attribution of increased startle amplitudes to hyperacusis may be confounded by the presence of loudness recruitment (Sun et al., 2009). Therefore, the ascription of central gain to animals determined to have hyperacusis by using the acoustic startle response may be incorrect. A recent study by Mohrle et al., suggests that enhanced central gain does not correlate with loudness hyperacusis but rather compensates for acoustic trauma in general. In this study, an operant conditioning model was utilized to detect loudness hyperacusis and found that ABR and DPOAE thresholds were not significantly different between groups, however noise-exposed symptom-free animals that did not display behavioral evidence of hyperacusis as well

as sham controls animals instead displayed increased ABR amplitude ratios and decreased latencies indicative of central gain (Mohrle et al., 2019).

In our study, mean ABR wave I, II, and V amplitude analysis showed very little change after noise-overexposure in hyperacusis-like animals compared to controls. While the central gain model may ultimately prove useful for understanding loudness hyperacusis, it fails to address the avoidance, discomfort, and painful components of affective hyperacusis. Therefore, our results may be attributed to the presence of affective hyperacusis without loudness hyperacusis. Ultimately, the central gain model of hyperacusis is in need of more rigorous testing with additional models of loudness and affective hyperacusis, as well as additional studies that precisely define the relationship between ABR amplitudes and hyperacusis-status.

Affective hyperacusis is defined by the affective emotional pain pathway. The canonical and non-canonical (i.e., the reticular-limbic (Zhang et al., 2018) or trigeminal nerve (Zeng et al., 2011)) pain pathways have not been investigated or defined as outputs of the auditory systems in hyperacusis. In our study, we introduced a new animal model for affective hyperacusis detection, based on acute measures of noise-induced pain and discomfort in combination with a conditioned place aversion paradigm. Furthermore, our results demonstrate that noise-overexposure can produce sensitization of the face and body to mechanical stimuli indicative of mechanical allodynia. Future studies investigating the anatomical connections between the auditory and nociceptive systems in conjunction with our novel behavioral assays would be useful in demonstrating the relationship between the pain and auditory pathways.

5.8 Concluding Remarks and Future Directions

Allodynia, innocuous stimuli induced pain, exists across sensory systems including sound-induced pain (affective hyperacusis), and innocuous cool-induced pain (cold allodynia). There are three major mechanisms by which chronic pain can be generated: sensitization, disinhibition, or a novel nociceptive pathway. Sensitization occurs as a result of increased activity in excitatory pain transmission neurons due to a variety of reasons such as increased plasticity of the presynaptic neuronal inputs, or changes to the intrinsic firing properties of the excitatory pain transmission neurons. Chronic pain can also be generated through disinhibition or decreased neuronal firing of inhibitory neurons. A decrease in inhibitory input onto excitatory pain transmission neurons allows for pain transmission even at innocuous stimulus intensity levels and ultimately spontaneous and/or chronic pain. Lastly, under pathological conditions, normally silent parallel nociceptive pathways may be unmasked leading to chronic pain. Multiple sensory systems must integrate to form a cohesive living experience that prioritizes the most important stimuli, the process of which is called multisensory integration. For example, the somatosensory and auditory systems communicate to identify internal-evoked sounds such as chewing or blood rushing through veins, as unimportant to prioritize external sounds such as animal predators. While the auditory and somatosensory interactions are important, a disease state in the auditory systems may then lead to a disordered somatosensory system due to cross-talk between the two pathways.

In the first part of this thesis, I described a feed-forward microcircuit that transmits innocuous cool sensations in the superficial dorsal horn of the spinal cord. In

this circuit, TRPM8^{+} cooling-sensitive peripheral sensory neurons form monosynaptic connections with a subpopulation of lamina I-II$_o$ Calb1^{Lbx1};SOM^{-} interneurons, which are functionally relevant. Although our study suggests that cool-sensitive Calb1^{Lbx1} neurons are not projection neurons, future studies that characterize the proportion of lamina I-II$_o$ Calb1^{Lbx1};SOM^{-} neurons that are spinothalamic projection neurons would delineate the canonical pain pathway that is activated in cold allodynia. Additional studies identifying innocuous cool, noxious cold, and warmth subpopulations would be helpful in understanding the coding mechanisms controlling the thermal heat grill illusion. Lastly, the conversion from innocuous cool sensations to cold allodynia is unclear, however future studies investigating the role of Calb1^{Lbx1};SOM^{-} neurons in the pathogenesis of cold allodynia under the three major mechanisms previously characterized would greatly aid in our ability to develop therapeutics for patients.

In the second part of this thesis, I described several novel animal models to identify sound induced pain and discomfort characteristic of affective hyperacusis. Future studies further modeling hyperacusis patient phenotypes in animals would be useful in beginning to understand the underlying neural circuitry of affective hyperacusis. For example, patients with hyperacusis experience comorbid tinnitus. Is the prevalence of hyperacusis and tinnitus in animal models similar to those in humans? Refinements to animal models would be aided by concurrent improved identification of affective hyperacusis in patients and thorough documentation of hyperacusis patient experiences. Lastly, by focusing on patient reported phenotypes, our study revealed cross-talk between the auditory and somatosensory systems that has not previously been described. Future studies further characterizing the interactions between the

auditory and somatosensory system, for example by using a mouse model for migraine to induce hyperacusis rather than noise exposure, would greatly aid in our understanding affective hyperacusis.

Taken together, these two thesis projects have worked towards understanding how sensory systems identify and transmit distinct sensory stimuli, such as temperature and sound to activate the nociceptive systems under physiological and pathological conditions.

References

Abouzari, M., Tan, D., Sarna, B., et al., (2020). Efficacy of Multi-Modal Migraine Prophylaxis Therapy on Hyperacusis Patients. Ann Otol Phinol Laryngol. 129 (5), 421-427.

Agashkov, K., Krotov, V., Krasniakova, M., Shevchuk, D., Andrianov, Y., Zabenko, Y., Safronov, B.V., Voitenko,N., Belan, P. (2019). Distinct mechanisms of signal processing by lamina I spino-parabrachial neurons. Sci Rep. 9, 19231. https://doi.org/10.1038/s41598-019-55462-7.

Allard, J. (2019). Physiological properties of lamina I spinoparabrachial neurons in the mouse. J Physiol. 597(7), 2097-2113.

Allchorne, A.J., Broom, D.C., Woolf, C.J. (2005). Detection of Cold Pain, Cold Allodynia and Cold Hyperalgesia in Freely Behaviing Rats. Molecular Pain. 1(36). oi: 10.1186/1744-8069-1-36.

Andrew, D. and Craig, A.D. (2001). Spinothalamic lamina I neurons selectively responsive to cutaneous warming in cats. J. Physiol. (Lond.) 537, 489–495.

Andrew, D. and Craig, A. D. B. (2002). Quantitative responses of spinothalamic lamina I neurones to graded mechanical stimulation in the cat. J. Physiol. 545, 913–31.

Andrew, D. (2009). Sensitization of lamina I spinoparabrachial neurons parallels heat hyperalgesia in the chronic constriction injury model of neuropathic pain. J Physiol. 587, 2005–2017.

Andrew, D. (2010). Quantitative characterization of low-threshold mechanoreceptor inputs to lamina I spinoparabrachial neurons in the rat. J Physiol. 588, 117–124.

Aries, P.S., Finch, P.M., and Drummond, P.D. (2017). Hyperacusis in chronic pain: neural interactions between the auditory and nociceptive systems. International Journal of Audiology. 56(11), 801-809.

Auerbach, B.D., Rodrigues, P.V., Salvi, R.J. (2014). Central Gain Control in Tinnitus and Hyperacusis. Front Neurol. 5,206.

Bester, H., Chapman, V., Besson, J.M. and Bernard, J.F. (2000).Physiological properties of the lamina I spinoparabrachial neurons in the rat. J. Neurophysiol. 83, 2239–2259.

Bauer, C.A., Brozoski, T.J., Rojas, R., Boley, J., Wyder, M. (1999). Behavioral model of chronic tinnitus in rats. Otolaryngol Head Neck Surg. 121(4):457–62. doi:10.1016/S0194-5998(99)70237-8.

Chen, G., Lee, C., Sandridge, S.A., Butler, H.M., Manzoor, N.F., Kaltenbach, J.A. (2013). Behavioral evidence for possible simultaneous induction of hyperacusis and tinnitus following intense sound exposure. J Assoc Res Otolaryngol. 14, 413–24. doi:10.1007/s10162-013-0375-2.

Chen, G.D., Radziwon, K.E., Kashanian, N. (2013) Salicylate-induced auditory perceptual disorders and plastic changes in nonclassical auditory centers in rats. Neural plasticity. 2014, 658741.

Chen, G.-D., Radziwon, K.E., Kashanian, N., Manohar, S., Salvi, R., (2014). Salicylated-induced auditory perceptual disorders and plastic changes in non-classical auditory centers in rats. Neural Plast. doi: 10.1155/2014/658741.

Chisholm, K.I., Lo Re, L., Polgár, E., Gutierrez-Mecinas, M., Todd, A. J., McMahon, S. B. (2021). Encoding of cutaneous stimuli by lamina I projection neurons. Pain. 162(9), 2405-2417.

Craig, A.D., Krout, K., and Andrew, D. (2001). Quantitative response characteristics of thermoreceptive and nociceptive lamina I spinothalamic neurons in the cat. J. Neurophysiol. 86, 1459–1480.

Ding, Y.Q., Takada, M., Shigemoto, R., Mizuno, N. (1995). Spinoparabrachial tract neurons showing substance P receptor-like immunoreactivity in the lumbar spinal cord of the rat. Brain Res. 647, 336-340.

Dostrovsky, J.O. and Craig, A.D. (1996). Cooling-specific spinothalamic neurons in the monkey J Neurophysiol, 76, 3656-3665.

Duan B., Cheng L., Bourange S., Britz O., Padilla C., Garcia-Campmany L., Krashes M., Knowlton W., Velasques T., Ren X., et al (2014). Identification of spinal circuits transmitting and gating mechanical pain. Cell 159, 1417-1432.

Gong, J., Liu, J., Ronan, E.A., He, F., Cai, W., et al. (2019). A cold-sensing receptor encoded by a glutamate receptor gene. Cell 178, 1375–86.e11.

Grudt, T.J., and Perl, E.R. (2002). Correlations between neuronal morphology and electrophysiological features in the rodent superficial dorsal horn. J Physiol 540, 189-207.

Hachisuka, J., Koerber, H.R., Ross, S.E. (2020). Selective-cold output through a distinct subset of lamina I spinoparabrachial neurons. Pain. 161, 185–94.

Han, Z.S., Zhang, E.T., and Craig, A. (1998). Nociceptive and thermoreceptive lamina I neurons are anatomically distinct. Nat Neurosci. 1, 218–225.https://doi.org/10.1038/665.

Hayes, S., Radziqon, K., Stolzberg, D., Salvi, R. (2014). Behavioral Models of Tinnitus and Hyperacusis in Animals. Front Neurol. 5:179.

Heffner, H.E. and Harrington, I.A. (2002). Tinnitus in hamsters following exposure to intense sound. Hear Res. 170(1–2), 83–95. doi:10.1016/S0378-5955(02)00343-X.

Heffner, H.E. and Koay, G. (2005). Tinnitus and hearing loss in hamsters (*Mesocricetus auratus*) exposed to loud sound. Behav Neurosci. 119(3),734–42. doi:10.1037/0735-7044.119.3.734.

Hickox, A.E. and Liberman, C.M. (2014). Is noise-induced cochlear neuropathy key to the generation of hyperacusis or tinnitus? J. Neurophysiology. 111(3), 552-564.

Ison, J.R., Allen, P.D., O'Neill, W.E. (2007). Age-related hearing loss in C57BL/6J mice has both frequency-specific and non-frequency-specific components that produce a hyperacusis-like exaggeration of the acoustic startle reflex. J Assoc Res Otolaryngol. 8, 539–50. doi:10.1007/s10162-007-0098-3.

Jastreboff, P.J., Brennan, J.F., Coleman, J.K., Sasaki, C.T. (1988). Phantom auditory sensation in rats: an animal model for tinnitus. Behav Neurosci. 102(6),811–22. doi:10.1037/0735-7044.102.6.811

Kayama, Y., Shibata, M., Takizawa, T., Ibata, K., Shimizu, T., Ebine, T., Toriumi, H., Yuzaki, M., Suzuki, N. (2018). Functional interactions between transient receptor potential M8 and transeint receptor potential V1 in the trigeminal system: relevance to migraine pathophysiology. Cephalalgia. 38, 833-845.

Lauer, A.M. and Dooling, R.J. (2007). Evidence of hyperacusis in canaries with permanent hereditary high-frequency hearing loss. Semin Hear. 28, 319-326.

Lobarinas, E., Hayes, S.H., Allman, B.L. (2013). The gap-startle paradigm for tinnitus screening in animal models: limitations and optimization. Hear Res. 295, 150–60. doi:10.1016/j.heares.2012.06.001.

Luz, L.L., Szucs, P., Pinho, R., and Safronov, B.V. (2010). Monosynaptic excitatory inputs to spinal lamina I anterolateral-tract-projecting neurons from neighbouring lamina I neurons. J Physiol 588, 4489-4505.

MacDonald, D.I., Wood, J.N., Emery, E.C. (2020). Molecular mechanisms of cold pain. Neurobiol Pain. 7, 100044. https://doi.org/10.1016/j.ynpai.2020.100044.

Marshall, G.E. Shehab, S.A.S., Spike, R.C., Todd, A.J. (1996). Neurokinin-1 receptors on lumbar spinothalamic neurons in the rat. Neuroscience. 72, 255-263.

Mohrle, D., Hofmeier, B., Amend, M., Wolpert, S., Ni, K., Bing, D., Klose, U., Pichler, B., Knipper, M., Ruttiger, L. (2019). Enhanced Central Neural Gain Compensates Acoustic Trauma-induced Cochlear Impairment, but Unlikely Correlates with Tinnitus and Hyperacusis. Neurosci. 407, 146-169.

Pace, E. and Zhang, J. (2013). Noise-induced tinnitus using individualized gap detection analysis and its relationship with hyperacusis, anxiety, and spatial cognition. PLoS One. 8, e75011. doi:10.1371/journal.pone.0075011.

Proudfoot, C.J., Garry, E.M., Cottrell, D.F., Rosie, R., Anderson, H., Robertson, D.C., Fleetwood-Walker, S.M., Mitchell, R. (2006). Analgesia Mediated by the TRPM8 Cold Receptor in Chronic Neuropathic Pain. Curr Biol. 16, 1591-1605.

Radziwon, K.E. and Salvi, R. (2020) Using auditory reaction time to measure loudness growth in rats. Hearing Research. 395, 108026.

Ran, C., Hoon, M.A., Chen, X. (2016). The coding of cutaneous temperature in the spinal cord. Nat Neurosci 19,1201-1209.

Rüttiger, L., Ciuffani, J., Zenner, H.P., Knipper, M. (2003). A behavioral paradigm to judge acute sodium salicylate-induced sound experience in rats: a new approach for an animal model on tinnitus. Hear Res. 180(1–2), 39–50. doi:10.1016/S0378-5955(03)00075-3.

Sederholm, F. and Swedberg, M.D. (2013). Establishment of auditory discrimination and detection of tinnitus induced by salicylic acid and intense tone exposure in the rat. Brain Res. 1510, 48–62. doi:10.1016/j.brainres.2013.03.013.

Stolzberg, D., Hayes, S.H., Kashanian, N., Radziwon, K., Salvi, R.J., Allman, B.L. (2013). A novel behavioral assay for the assessment of acute tinnitus in rats optimized for simultaneous recording of oscillatory neural activity. J Neurosci Methods. 219(2), 224–32. doi:10.1016/j.jneumeth.2013.07.021.

Sun, W., Lu, J., Stolzberg, D., Gray, L., Deng, A., Lobarinas, E., Salvi, R.J. (2009). Salicylate increases the gain of the central auditory system**.** Neuroscience. 159, 325-334.

Sun, W., Deng, A., Jayaram, A., Gibson, B. (2012). Noise exposure enhances auditory cortex responses related to hyperacusis behavior**.** Brain Res. 1485, 108-116.

Turner, J.G., Brozoski T.J., Bauer, C.A., Parrish, J.L., Myers, K., Hughes, L.F., et al. (2006). Gap detection deficits in rats with tinnitus: a potential novel screening tool. Behav Neurosci 20(1), 188–95. doi:10.1037/0735-7044.120.1.188.

Turner, J. and Parrish, J. (2008). Gap detection methods for assessing salicylate-induced tinnitus and hyperacusis in rats. Am. J. Audiol. 17, S185-S192.

Turner, J., Larsen, D., Hughes, L., Moechars, D., Shore, S. (2012). Time course of tinnitus development following noise exposure in mice. J Neurosci Research. 90(7), 1480-1488.

Xiao, R. and Xu, S.X.Z. (2021). Temperature Sensation: From Molecular Thermosensors to Neural Circuits and Coding Principles. Annu. Rev Physiol. 83, 205-230.

Wang, F., Bélanger, E., Côté, S.L., Desrosiers, P., Prescott, S.A., Côté, D.C., De Koninck Y. (2018). Sensory afferents use different coding strategies for heat and cold Cell Rep. 23, 2001-2013.

Yu, X.H., da Silva, A.R., De Koninck, Y. (2005) Morphology and neurokinin 1 receptor expression of spinothalamic lamina I neurons in the rat spinal cord. J Compar Neurol. 491, 56-68.

Zeng, C., Shroff, H., Shore, S. (2011). Cuneate and Spinal Trigeminal Nucleus Projections to the Cochlear Nucleus are Differentially Associated with Vesicular Glutamate Transporter. Neuroscience. 176, 142–151.

Zhang, C., Flowers, E., Li, J-X., Wang, Q., Sun, W. (2014). Loudness perception affected by high doeses of salicylate- A behavioral model of hyperacusis. Beh Brain Research. 2271, 16-22.

Zhang, G., Sun, W., Zingg, B., Shen, L., He, J., Xiong, Y., Tao, H. W., Zhang, L. (2018). A Non-canonical reticular-limbic central auditory pathway via medial speptum contributes to fear conditioning. Neuron. 97, 406-417.

Wu, C., Martel, D.T., Shore, S.E.(2016a). Increased synchrony and bursting of dorsal cochlear nucleus fusiform cells correlate with tinnitus. J Neurosci. 36, 2068-2073.